A Lateral Control Solution for Cooperative Vehicle Platooning Applications

D.G. van den Berg

Master of Science Thesis

TU Delft Delft University of Technology

Delft Center for Systems and Control

A Lateral Control Solution for Cooperative Vehicle Platooning Applications

Master of Science Thesis

For the degree of Master of Science in Systems and Control at Delft University of Technology

D.G. van den Berg

June 8, 2020

Faculty of Mechanical, Maritime and Materials Engineering (3mE) · Delft University of Technology

The work in this thesis was supported by TNO. Their cooperation is hereby gratefully acknowledged.

Delft University of Technology
Department of
Delft Center for Systems and Control (dcsc)

The undersigned hereby certify that they have read and recommend to the Faculty of Mechanical, Maritime and Materials Engineering (3mE) for acceptance a thesis entitled

A Lateral Control Solution for Cooperative Vehicle Platooning Applications

by

D.G. van den Berg

in partial fulfillment of the requirements for the degree of

Master of Science Systems and Control

Dated: June 8, 2020

Supervisor(s):

Dr.ir. R. Ferrari

Dr.ir. M.Alirezaei

ir. C. J. van der Ploeg

Reader(s):

prof.Dr.ir. N. van de Wouw

prof.Dr.ir. T. Keviczky

Abstract

Over the past 20 years road usage has increased by over 50%. Although the road network is being expanded, it is a costly and short-term solution for the issue of traffic congestion. Related to this are the environmental issues partially caused by the large amount of road traffic. The societal demand for smart solutions to these problems, has accelerated the research and development of vehicle platooning solutions. By allowing vehicles to drive closer to one another road capacity can be used more efficiently, and fuel consumption will also be reduced. Moreover, it reduces the mental load on the drivers in the trailing vehicles. Driving safely at close intervehicular distances, however, requires automation of the lateral and longitudinal motion of the vehicle.

The automation of longitudinal motion for vehicle platooning is a well researched problem and experimentally verified solutions exist. Lateral platooning has received considerably less attention. One of the main motivations of this work is to develop a lateral control strategy, designed for easy and robust deployment in real-world platooning applications. Most lateral platooning solutions nowadays rely on path information. In platooning applications path reconstruction is often inaccurate, mostly due to the low visibility for the camera's when vehicles are driving close to each other. Alternative approaches whereby the path is reconstructed heavily rely on the availability of signals with high signal to noise ratio to have accurate reconstruction of the path. Because sensors in road vehicles are often of average quality, this can not be guaranteed. The main alternative is the direct vehicle following approach. Although much simpler to implement than path following, it suffers from the fact that in transient and steady state cornering each of the vehicles in platoon will undercut the path of the preceding vehicle, something which is deemed undesirable as it could lead to dangerous situations. The main motivation for the work in this thesis, is to find a vehicle following method that has the accessibility of direct vehicle following, but the accuracy of path following.

In this thesis work a new vehicle following strategy is proposed that combines the strengths of the direct vehicle following approach and the path following approach. In this work, a novel approach to calculate the road induced error is proposed, allowing a trailing vehicle to use direct vehicle following in order to deduce a combined measurement of the actual road error states. This measurement can be used in combination with an observer to asymptotically

reconstruct the individual road error states. For the controller and observer a linear vehicle model is used, in which the error dynamics with respect to a path are included as function of the vehicle dynamics.

An H_∞ controller optimization is used to developed a feedforward-feedback control structure. The choice for H_∞ is motivated by the requirement for having string stability as string stability for linear systems is defined using an H_∞ norm. In this work it is shown that given the error definitions of the system, the string stability complementary sensitivity function is identical to the complementary sensitivity function for a feedback system. Using Bode's integral theorem it is proven that string stability for a system with only a feedback controller is impossible to achieve. In the case of a feedforward feedback structure it can be shown that string stability requires infeasible high gain on the feedback controllers to achieve string stability. Given that such a control solution can only be used in noiseless situations that solution is regarded as a theoretical solution. From this analysis it is concluded that for the feedback case string stability is impossible to achieve, and in the case of feedback-feedforward deemed infeasible.

The control algorithm, in combination with the observer, has been implemented and tested in a simulation environment. A typical highway lane changing or overtaking manoeuvre was chosen for testing, as well as a simulation to show how the state evolution when the system is subjected to initial condition errors. The latter is chosen to highlight the functionality of the observer. The simulation results show that using the new measurement approach in combination with an observer works equally well to a system that has direct access to the road error states. The initial condition error simulation also shows that the individual error states can be successfully reconstructed.

Although the work in this thesis showcases a new method, and proves it to work within a simulation environment, a few open questions remained at the end of the thesis. Achieving string stability proved to be impossible with the chosen controller architecture. Research showed that this could be put down to fundamental limits on the string stability complementary sensitivity function. Nevertheless, a conclusive proof is not yet given and it is recommended that this is researched before attempting any further control design. Although string stability was not achieved, the new vehicle following method did achieve the desired requirements, and it shows that it is possible to combine the two vehicle following methods using the road-error and observer.

Table of Contents

List of Figures

Nomenclature

List of Symbols

Greek Symbols

α_f	Front tyre slip angle [rad].
α_r	Rear tyre slip angle [rad].
β	Body slip angle [rad].
δ	Front wheel steering angle [rad].
$\dot{\theta}_s$	Rate of change of curvature of road [rad/s].
Γ	String stability complenetary sensitivity function.
ν	Class $\mathcal{K}$ function.
ω_n	Natural frequency steering system [rad/s].
ψ	Yaw angle of the vehicle [rad].
$\psi_{e,i}$	Heading Error [rad].
σ	Class $\mathcal{K}$ function.
ε_i	Measured road error [m].
ζ	Steering system damping [-].

Lower Case Latin Alphabet

a	Distance front axle CoG [m].
b	Distance rear axle CoG [m].
d_i	Following distance between two vehicles [m].
e	Error signal.
h_i	Headway time [s].
j	Imaginary number.
s	Laplace variable.
v	Local vehicle velocity [m/s].
x	Local vehicle x-axis.

y	Local vehicle y-axis.
y_e	Lateral offset error [m].
z	Local vehicle z-axis.

Mathematical Symbols

Δ	Denotes a difference between two variables.
$\|\|.\|\|_\infty$	Infinity norm.
$\mathcal{K}$	Class $\mathcal{K}$ function.
$\mathcal{L}_p$	$\mathcal{L}_p$ function space.
$\mathcal{O}$	Origin of axis system.
$\mathcal{R}$	Clockwise rotation matrix.
$\mathcal{S}_m$	Set containing m amount of vehicles.
$\vec{e}$	Unit vector for axis system $\mathcal{O}$.
$\vec{V}$	Velocity vector.
H_∞	H_∞ norm.
lim	Limit function.
min	Minimization function.

Subscripts

f	Front of the vehicle.
g	Denotes variable defined in the Global axis system; gravitational acceleration.
i	Vehicle index in platoon.
r	Denotes variable defined in the road axis system
r	Rear of the vehicle.

Upper Case Latin Alphabet

C_{α_f}	Front tyre cornering stiffness [N/rad].
C_{α_r}	Rear tyre cornering stiffness [N/rad].
A	State Space Dynamics matrix.
B	State Space Input matrix.
C	State Space Output matrix ; Curvature of path.
D	State Space Direct throughput matrix.
E	Disturbance input matrix state space system.
F_x	Longitduinal Force [N].
F_y	Lateral Force [N].
I_z	Vehicle inertia [kgm^2].
K	Feedback controller.
K_f	Feedforward controller.
L	Vehicle wheelbase [m].
N	Lower fractional expansion.
P	Transfer function; Point in Global axis system; Generalized Plant
S	Sensitivity function.
T	Complementary sensitivity function.

W	Weighting transfer function
X	Global x-axis.
Y	Global y-axis.

Acknowledgements

This thesis marks the end of almost 8 years as a student at the TU Delft. I believe that the work in this thesis perfectly summarizes what any engineer should strive for: to use the knowledge gained to try and improve society where and whenever possible. It is for this reason that I am also grateful for being given the opportunity to do my work at TNO. Although testing fell through due to the COVID-19 outbreak, it was one of the main motivations that kept me going.

I would like to further extend my thanks to my daily supervisors, Mohsen Alirezaei and Chris van der Ploeg. Mohsen thank you for the many insightful discussions we had at TNO, in the train and later at Eindhoven University. Chris I would like to thank you for always trying to make time, even though you yourself had just started working at TNO. Having the opinion of someone from the same field of study greatly helped me get back on track, when I was lost for ideas. I think we would have both been rather surprised when someone told us, back in September 2014, that one day you would supervise my thesis. I also would like to extend my special thanks to Nathan van de Wouw. Without your critical, yet extremely helpful, feedback on my work this thesis would have been of much less quality. I rank the monthly meetings as highest in terms of usefulness when it comes to the work presented in this thesis.

Special thanks goes to my family, who have supported me throughout my study, and allowed me to do what I wanted to do. I would also like to thank all my friends from both my studies as well as Formula Student team Delft, especially Oscar, with whom I spent many an hour in the DCSC laboratory working on both our theses.

Finally I would like to thank my girlfriend Sara for her love and support and giving me energy to finish this graduation research.

Delft, University of Technology — D.G. van den Berg
June 8, 2020

"We choose to go to the Moon! We choose to go to the Moon...We choose to go to the Moon in this decade and do the other things, not because they are easy, but because they are hard."

— *United States President John F. Kennedy*

Chapter 1

Introduction

1-1 Platooning

Since the 1990's road usage in the Netherlands has increased by over 50% [1]. The main cause for this rise in road usage comes from an increase in road freight and passenger car traffic. In the same time the road capacity has increased, but not by nearly as much as the amount of traffic. As a result the amount and also average length of traffic jams has steadily increased [2]. A simple way to negate the increased pressure on the road network would be to simply increase the size of the road network by either expanding existing highways or constructing new ones. This, however, is often a costly short-term solution [3]. Furthermore, the increase in road traffic is also an issue with respect to environmental concerns and the desire to increase road safety.

An alternative solution is to increase road usage efficiency. In the Netherlands, a general rule of thumb is to have a spacing of 2 seconds between vehicles. At normal highway velocities of 100 km/h, it gives an average spacing of 56 metres between two vehicles. This is enough space for roughly ten average sized vehicles (Based on a VW Golf, the most common car in the Netherlands [4]). Unfortunately, tighter spacing than this can not be met if the vehicles are human operated as the "human controller" is simply not accurate or fast enough to react to changes when the spacing time is significantly lower than 2 seconds [5]. This has led to a desire to automate the task of driving and has led to the emergence of the Intelligent Transport System, or ITS for short.

1-1-1 Vehicle Platooning

One of the applications of the ITS is vehicle platooning. At its core a platoon of vehicles is a group of vehicles driving closely together with a hardware or software implementation allowing them to drive closely together while maintaining safety. An illustration of such a platoon can be seen in Figure 1-1. Such a platoon of vehicles can be led by a human operated vehicle or a host vehicle travelling along a predetermined path. An important aspect of vehicle platooning

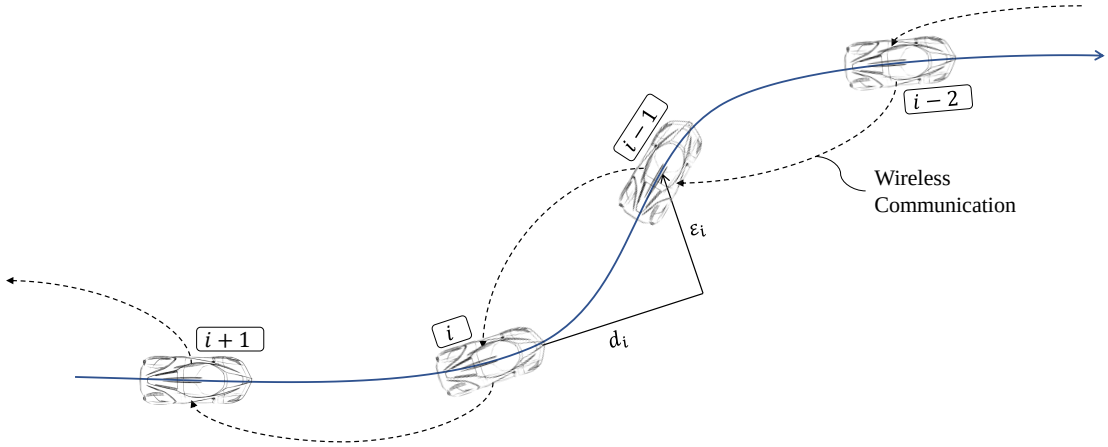

Figure 1-1: Illustration of a (lateral) vehicle platoon

is the ability for the vehicles to communicate with one another. This communication can be used to transmit vehicles states, and has shown to improve platooning safety [6]. It should, however, also be possible to platoon without any form of communication. For longitudinal platooning the challenge is to have vehicles driving closely together in a safe manner whilst keeping inter-vehicular velocities and accelerations at the same rate. For a human-operated platoon, if following distances are short, the acceleration of the first vehicle will be amplified by the human controller due to the long reaction time and/or a poor lack of judgement of the intended acceleration of the preceding vehicle [5]. The propagation of this amplification throughout the string of vehicles is similar to the effect of a shock wave travelling through the string of vehicles. It is this shock wave that is often the cause of a traffic jam [7]. The shock wave effect that causes traffic jams also exists in a similar form for the lateral case.

For lateral platooning the challenge is to follow the preceding vehicle on a curved path while guaranteeing safety. In this case, safety is defined as the ability to stay within the road-lane boundaries. For a large number of vehicles in a platoon this practically means that deviation in lateral direction from the original path may not be amplified through the string of vehicles. To illustrate this, consider a homogeneous platoon of vehicles, where homogeneous means that each of the vehicles has identical dynamics and controllers. Say that the lead vehicle undertakes a lane change because it wants to, for example , overtake a different platoon of vehicles. If the first following vehicle overshoots the lateral movement of the host vehicle, the second following vehicle will overshoot the overshoot of that vehicle. At one point the lateral overshoot will cause one of the vehicles in the platoon to venture into an undesirable location. For this reason string stability in lateral direction is required.

Several control solutions that guarantee string stability for the longitudinal platooning problem already exist, and can be found in [6, 8, 9]. In the cited research lateral control is often also implemented, but in such a way that it is not interactive with other vehicles, i.e., each

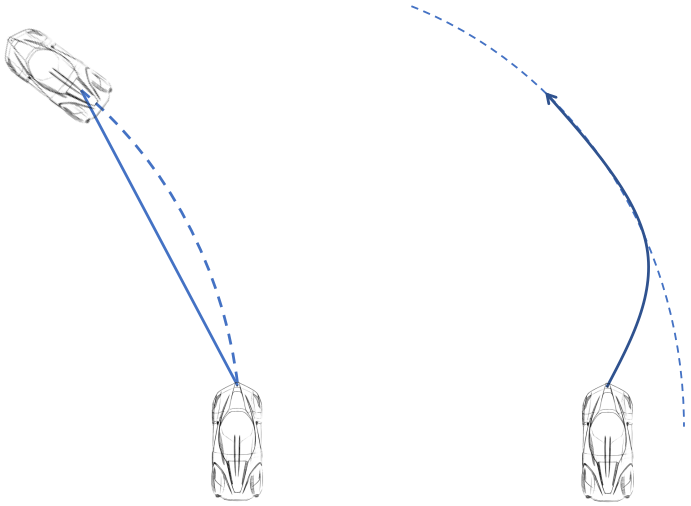

Figure 1-2: Two vehicle following solutions illustrated. On the left, point or direct vehicle following is shown and on the right, path following.

participant determines and follows its own path (e.g., the lane center). Here the goal is to keep the vehicles driving along the centre-line of the lane. Research on lateral control in platooning applications is not extensively researched, or is restricted to two-vehicle platoons. A few examples of existing solutions can be found in the following literature [8, 9, 10, 11, 12, 13]. However, all of the solutions presented use path following and not direct vehicle following. The main goal of this thesis is to find a vehicle following method that unifies both methods, using the strengths of both whilst counteracting the downsides of both. What these strengths and downsides are will now be explained in the following section.

1-2 Lateral Control for Cooperative Driving

In literature a wide variety of control solutions can be found with respect to lateral control of a vehicle. In most cases lateral control is implemented using path following, where the path is derived from lane markings [14, 15, 16]. In lane keeping the vehicle generates control action based on a deviation from a path. This path can either be predetermined, or reconstructed using sensory data. Sensors commonly used for this are radar and cameras. Using information from road markings the vehicle is able to deduce its location with respect to the lane. LiDARs or radar are commonly employed to measure the position with respect to other objects (vehicles)[17]. The two commonly used methods for vehicle following will now be elaborated, see Figure 1-2.

1-2-1 Path Following in Platooning

In the context of platooning path following can also be employed, but rather than following the middle of the lane or following a predetermined path, the path is reconstructed based on sensory data in combination with data received from the preceding vehicle. Based on this information the trailing vehicle is then able to deduce both its heading error and lateral offset error with respect to the path. Each error can be controlled using two independent controllers. Path following in a vehicle platoon is often more challenging than lane following for a single vehicle. Due to the close following distances desired when the vehicles are driving in a platoon, lane markings are often obstructed, and path reconstruction is unreliable. This can partly be solved using information transmitted by the preceding vehicle, but this is subjected to delays, packet losses and noise. [18].

1-2-2 Point Following Solutions

An alternative solution to the vehicle following problem, is the direct vehicle following approach. In the direct vehicle following approach the trailing vehicle tries to minimize the offset distance between its heading and a point it has to follow. Control action generated on this measured distance then steers the vehicle back to the desired heading. For the platooning application this point is often on the back of the preceding vehicle in the platoon. Although it is a relatively simple solution, it suffers a well known drawback of corner cutting [10]. If, in Figure 1-2 in the left situation, the trailing vehicle orients itself along the solid line it will undercut the path driven by the preceding vehicle. This behaviour is undesired as each further trailing vehicle in the platoon will undercut a path that already undercuts the original path. Nevertheless, in certain situations corner cutting is accepted in the end result, or it can be mitigated, and direct vehicle following is used as solution to the vehicle following problem [13, 10, 12, 19].

1-3 Problem Statement

The aim of this research is to develop a controller and vehicle following method that is suitable for lateral control platooning in highway applications. The lateral control solution should be based on the errors defined as in the path-following approach to vehicle following such that it does not have the issue of corner cutting. Furthermore, the lateral behaviour should be string stable. It will be shown in Chapter 3 that the latter requirement is, in some cases fundamentally, impossible to achieve with the path following approach. Because of this the string stability requirement was relaxed, and the goal was set to minimize the lateral overshoot. This minimization requirement calls for an optimization-based control solution. Finally the controllers should be implementable on actual vehicles for practical experimentation. This requires the chosen control solution to also account for practical aspects such as the presence of noise, actuator limits, vehicle limits etc.

Vehicle platooning limits itself to regular or normal driving conditions, i.e., the vehicles are operated well within the linear regime. By assuming constant forward velocity the longitudinal and lateral vehicle dynamics can be decoupled. In this work the focus lies solely on the

development of a lateral control solution, and assume that the longitudinal behaviour of the platoon is controlled through a proven CACC solution as can be found in [20].

1-4 Research Approach and Requirements

This section describes the steps to be taken to solve the problems posed in the previous section. Firstly, a model describing the lateral vehicle dynamics is required. Secondly the dynamics of the errors will be based on previous solutions developed at TNO [11, 13, 21]. In this literature the relative position and heading error are described as function of the vehicle dynamics of the trailing vehicle, and as function of the preceding vehicle dynamics. These two errors need to be driven back to zero by the control design. A novel approach to deducing the road errors will also be developed, such that the strengths of both the direct vehicle following and path following approaches.

Finally, because string stability seems infeasible to achieve in practical conditions, the control design should be such that the amount of overshoot that can occur is minimized. This calls for an optimization-based control solution. On a road vehicle the tyres dampen out a large part of the response of the vehicle, especially when the excitation of the system is of high frequency. This damping is not captured in the linear model due to the way how the tyres are modelled. However, this knowledge that there exists a frequency range in which the vehicle will not respond to steering inputs can be used when designing the controllers. By designing the controllers such that they show string stable behaviour in the frequency range of interest, it might be possible to have the overshoot in a frequency range where the vehicle is not expected to be excited. Because string stability requirements can easily be formulated using system norms, an H_∞ based control solution is proposed for the development of the controller. An added benefit of this method is that it allows penalization of the control action, which is desired from a practical perspective.

Throughout the thesis it is assumed that each vehicle is able to communicate with the vehicles directly neighbouring it, and that there are no delays present in the communication. This has no effect on the string stability analysis of the system [21]. Next to the problem statement, the following requirements are added to the problem statement. The requirements are listed below:

- The vehicle must track the path of the preceding vehicle without steady-state error.
- Following distance shorter than achieved with human-controlled string. (Achieved with a headway time of ≈ 1 second with V2V).
- Platoon must be as close as possible to being laterally string stable.
- Rejection of initial condition errors.
- Controller must be real world implementable, as in, it must be robust against noise and disturbances.
- Controller is designed for highway driving situations. This means velocities in the region of 80 to 100 km/h.

Each of the requirements will now be discussed to explain, where necessary, why they are included.

No Steady-State Error

It is desired that each of the vehicles eventually ends up on the same path as the preceding vehicle. During transients the trailing vehicle is allowed to veer off the path. In steady state cornering or straight line driving the vehicle should converge to the path of the preceding vehicle.

Headway time of approximately 1 second

The following distance is defined by the velocity multiplied by the headway time between two vehicles. The target is chosen such that the average distance between vehicles is half of what is the minimal requirement in the Netherlands. This target is based on practical results from CACC experiments found in [6].

Lateral String Stability Requirement

The string stability requirement will be formulated to allow as many vehicles as possible to drive in a single platoon without the effect of the string instability becoming too large.

Initial Condition Error Rejection

It is possible to design controllers that achieve the goal of path tracking, but any initial condition error (or steady state offset) will not be solved. This is undesired and hence the controllers should also be capable of acting on initial condition errors.

Real World Application

The controller will be designed such that they are not sensitive to high frequency noise and external disturbances. Originally other aspects such as computation time were going to be taken into account, but the lack of testing due to the COVID-19 outbreak prevented that.

Highway Driving Situations

There are two reasons why the driving environment is chosen to represent highway driving. Firstly manoeuvres during regular highway driving are lower frequency. This keeps the vehicle well within the linear dynamics regime, allowing for a linear dynamic model. Secondly, the chosen CACC solution was also developed for highway use. The absence of traffic lights and/or pedestrians, combined with predictable vehicle flow also makes it an easier environment to develop for, as one has to take less safety-related disturbances into account.

1-5 Thesis Outline

The rest of the thesis is organized as follows. Chapter 2 covers the equations of motion describing the lateral vehicle dynamics as well as the derivation of the vehicle-road errors. Finally, the platoon dynamics are also given. These are required for string stability analysis.

Chapter 3 will give a mathematical background on the string stability requirement. It will also cover the string stability requirement for the platoon dynamics from Chapter 2. It will also include the proof and analysis on the string stability properties of the system. Chapter 4 will cover the control design, given these limitations. Chapter 5 will show simulation results with a comparison of the proposed controller to the one implemented currently. Chapters 6 and 7 will form respectively the discussion and conclusion. In the discussion a potential solution to the string stability issue is proposed. There are also two appendices added to this thesis. Appendix A goes into detail on signal and system norms, and how they can be computed. Appendix B gives the derivation of Bode's Integral, a well known integral relation in feedback control design.

Chapter 2

Vehicle Theory

In this chapter, the equations of motion for a vehicle will be derived. The derivation is based on a vehicle representation called the bicycle model and is based on the work found in [22]. Section 2-1 will derive the lateral, longitudinal and yaw dynamics as function of steering and longitudinal force input. These dynamics will then be used to derive the road error dynamics, which is done in section 2-2. In section 2-1, the dynamics of the power steering system will also be covered and incorporated into the model. Section 2-3 will cover how a platoon of interconnected vehicles can be modelled and their dynamics can be linked. Finally, section 2-4 will cover a way of deriving the error induced by the curvature of the road.

2-1 Lateral Vehicle Dynamics Modelling

The dynamics of a vehicle can be modelled with a varying degree of complexity. The type of model is mainly dependant on the complexity of the tyre model as well as the chosen amount of degrees of freedom. Based on requirements the designer has for the design, an appropriate model can be chosen. For this thesis the primary goal is to follow the path of a preceding vehicle. In turn, this requires us to be able to influence the motions and rotations of each of vehicles in the platoon. A further simplification of the dynamics comes from only considering the motion of the vehicle in the $x-y$ plane and its rotation among the z-axis. Figure 2-1 shows the SAE J670 standard axis system for a vehicle. Any displacement in the z-direction as well as rotations around the x (roll) and y (pitch) axis are disregarded in the analysis. This can be done because the expected lateral accelerations during highway driving are low enough such that load transfer plays no major role in the dynamics of the vehicle.

2-1-1 The Bicycle Model

The bicycle model is a model that describes the longitudinal, lateral and the yaw motion of the vehicle, and can easily be adapted to a linear model. In this model the tyre on the front and rear axle are grouped together to one tyre attached to the centre line of the vehicle. The

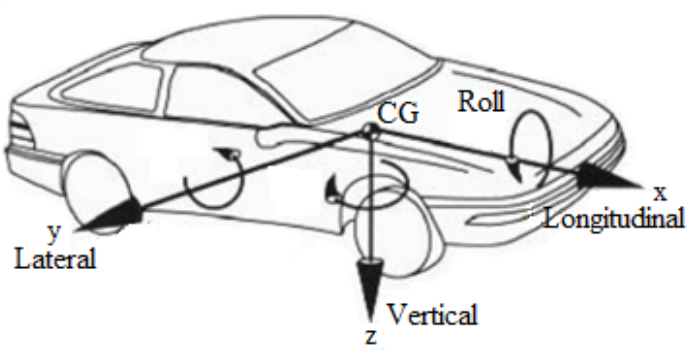

Figure 2-1: SAE vehicle axis definitions [23]

front tyre can be steered. Figure 2-2 shows a free body diagram in which all relevant vectors, angles and distances required for the derivation are labelled.

In Figure 2-2, the motion of the vehicle can be described by the coordinates X_1,Y_1 and ψ in the global reference frame, with origin $\mathcal{O}^g$. Coordinates X_1 and Y_1 are global location coordinates of the centre of gravity of the vehicle. The angle ψ is the rotation of the vehicle with respect to this inertial frame. It is assumed that only the front wheel has a rotational degree of freedom, and its angle with respect to the vehicle longitudinal axis is denoted by δ. The vehicle has wheelbase $L = a + b$, where a is the distance from the front wheel to the centre of gravity and b is the distance from the rear wheel to the centre of gravity. Each of the tyres is capable of producing both lateral and longitudinal forces, denoted as vectors in the vehicle axis system. The lateral forces are denoted by $F_{y,f}$ and $F_{y,r}$ for the front and rear tyres, and likewise for the longitudinal forces $F_{x,f}$ and $F_{x,r}$ for the front and rear tyres. The vector $\vec{V}$ denotes the magnitude and direction of the velocity of the vehicle.

The vehicle itself also has a local coordinate system of which the origin, denoted by $\mathcal{O}^i$, lies on the centre of gravity. The unit vector $\vec{e}_x^i$ is aligned parallel to the centreline of the vehicle and the unit vector $\vec{e}_y^i$, perpendicular to the vehicle centreline. The velocity vector, $\vec{V}$, can be constructed from the local velocities, denoted by $\vec{v}_y$ and $\vec{v}_x$, see Figure 2-2. In the vehicle coordinate frame, the tyres also have their own local velocities, denoted by $\vec{v}_f$ and $\vec{v}_r$ for front and rear respectively. The angle between these velocity vectors and the centreline of the tyres is called the slip angle, α_f and α_r for front and rear, respectively, and plays an important part in the force generation of a tyre. The angle of the velocity vector $\vec{V}$ with respect to the vehicle centre-line is called the body slip angle, denoted by β. Finally, when the vehicle is cornering, it is rotating around its own centre of gravity. This rotational velocity is commonly referred to as the yaw rate of the vehicle, and is denoted by $\dot{\psi}$. In other literature the yaw rate of the vehicle is also often denoted by r. However to keep uniformity throughout the thesis the notation of the yaw rate was chosen to be $\dot{\psi}$.

2-1-2 Bicycle Model Equations of Motion

In this section the equations of motion for the bicycle model, using the definitions in Figure 2-2, will be derived. The derivation given in this thesis is based on [22]. Alternate ways of arriving at the same set of equations exist, but the author found this the most insightful method.

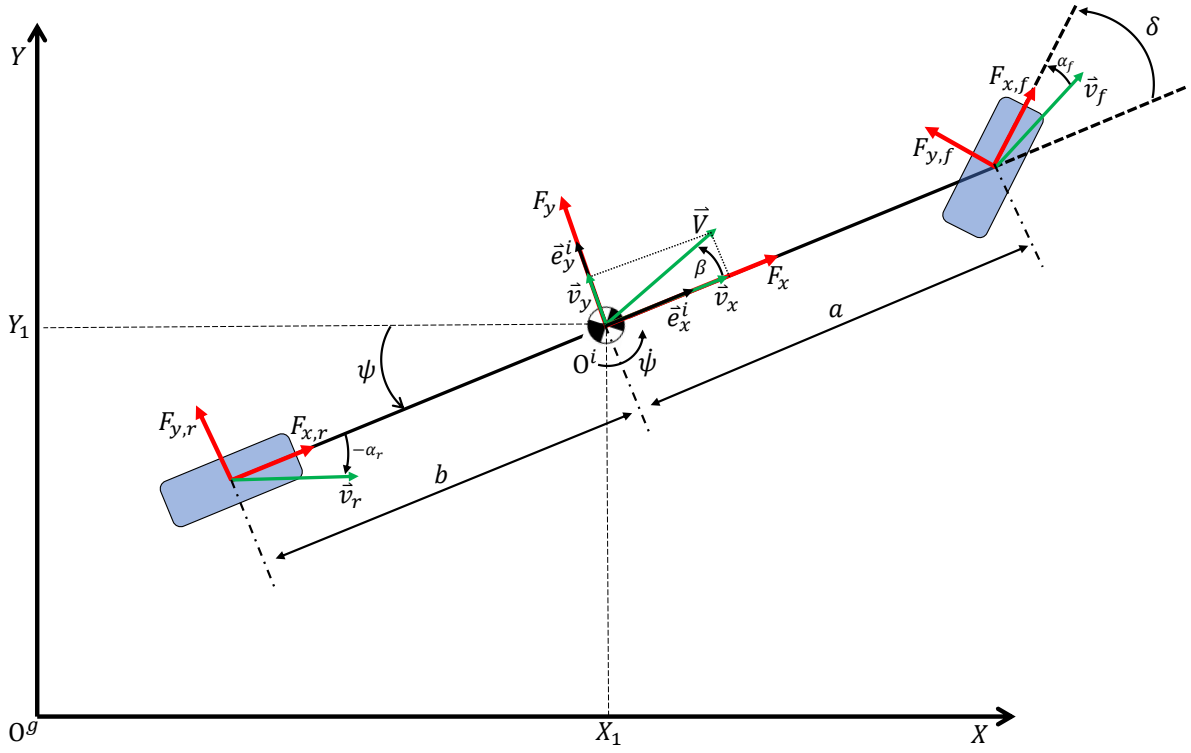

Figure 2-2: Bicycle model with all variables defined.

The method uses Lagranges theorem for mechanics to derive the equations of motion. For a system with n degrees of freedom, n generalised coordinates q_i are selected. These coordinates completely describe the motion of the vehicle whilst kinematic constraints are satisfied. In general the system possesses kinetic energy T, potential energy U and is subjected to external generalized forces, Q_i, which act on the system. The Lagrange equations for generalized coordinate q_i reads

$$\frac{d}{dt}\frac{\partial T}{\partial \dot{q}_i} - \frac{\partial T}{\partial q_i} + \frac{\partial U}{\partial q_i} = Q_i. \tag{2-1}$$

The generalized coordinates for the bicycle model in Figure 2-2 are given by $q_i = \begin{bmatrix} X_1 & Y_1 & \psi \end{bmatrix}$. When the vehicle is driving under normal conditions it has no potential energy and only kinetic energy. The total kinetic energy of the vehicle is given by

$$T = \frac{1}{2}m\left(\dot{X}_1^2 + \dot{Y}_1^2\right) + \frac{1}{2}I_z\dot{\psi}^2, \tag{2-2}$$

where $\dot{X}_1$ and $\dot{Y}_1$ are the velocities in the global coordinate system and $\dot{\psi}$ the rotation in the same coordinate system. Substituting Equation 2-2 for each of the generalized coordinates, q_i, in the Lagrange Equation 2-1 yields

$$\frac{d}{dt}\frac{\partial T}{\partial \dot{X}_1} = m\ddot{X}_1 = Q_X, \tag{2-3a}$$

$$\frac{d}{dt}\frac{\partial T}{\partial \dot{Y}_1} = m\ddot{Y}_1 = Q_Y, \tag{2-3b}$$

$$\frac{d}{dt}\frac{\partial T}{\partial \dot{\psi}} = I_z\ddot{\psi} = Q_\psi. \tag{2-3c}$$

Because it is desired to describe the motion of the vehicle in its own local velocities rather than global velocities, the Lagrangian equations of Equation 2-3 need to be translated from global to local coordinates. By using rotation matrix $R(\psi)$ it possible to write $\dot{X}_1$ and $\dot{Y}_1$ in local vehicle velocities v_x and v_y, and vice versa. This relation is given by

$$\begin{bmatrix} \dot{X}_1 \\ \dot{Y}_1 \end{bmatrix} = \begin{bmatrix} \cos(\psi) & -\sin(\psi) \\ \sin(\psi) & \cos(\psi) \end{bmatrix} \begin{bmatrix} v_x \\ v_y \end{bmatrix}. \tag{2-4}$$

Writing out $\ddot{X}_1$ and $\ddot{Y}_1$ using the definitions in Equation 2-4 yields

$$\begin{bmatrix} \ddot{X}_1 \\ \ddot{Y}_1 \end{bmatrix} = \dot{\psi}\begin{bmatrix} 0 & -1 \\ 1 & 0 \end{bmatrix}\begin{bmatrix} \cos(\psi) & -\sin(\psi) \\ \sin(\psi) & \cos(\psi) \end{bmatrix}\begin{bmatrix} v_x \\ v_y \end{bmatrix} + \begin{bmatrix} \cos(\psi) & -\sin(\psi) \\ \sin(\psi) & \cos(\psi) \end{bmatrix}\begin{bmatrix} \dot{v}_x \\ \dot{v}_y \end{bmatrix}. \tag{2-5}$$

Under the assumption that angle ψ is small, such that $\cos(\cdot) \approx 1$ and $\sin(\cdot) \approx 0$, Equation 2-5 can be written as

$$\ddot{X}_1 = \dot{v}_x - \dot{\psi}v_y, \tag{2-6a}$$

$$\ddot{Y}_1 = \dot{v}_y + \dot{\psi}v_x. \tag{2-6b}$$

Replacing $\ddot{X}_1$ and $\ddot{Y}_1$ in Equation 2-3 with the definitions of Equations 2-6, a set of equations from which it is possible to describe the motion of the vehicle in its local coordinates is

derived. These equations are given by:

$$m\ddot{X}_1 = m\left(\dot{v}_x - v_y\dot{\psi}\right) = Q_X, \tag{2-7a}$$

$$m\ddot{Y}_1 = m\left(\dot{v}_y + v_x\dot{\psi}\right) = Q_Y, \tag{2-7b}$$

$$I_z\ddot{\psi} = Q_\psi, \tag{2-7c}$$

or, solving for the accelerations of v_x, v_y and $\dot{\psi}$

$$\dot{v}_x = \frac{Q_X}{m} + \frac{v_y\dot{\psi}}{m}, \tag{2-8a}$$

$$\dot{v}_y = \frac{Q_Y}{m} - \frac{v_x\dot{\psi}}{m}, \tag{2-8b}$$

$$\ddot{\psi} = \frac{Q_\psi}{I_z}. \tag{2-8c}$$

Generalised Forces

Having derived a set of dynamics equations for the motion of the vehicle in both global and local coordinates, the generalized forces Q_X, Q_Y and Q_ψ as function of these local coordinates needs to be found. This can be done by assuming the vehicle undergoes a movement in the direction of generalized coordinates q_i. Then the generalised forces can be found from the virtual work they exert on the vehicle. These are given by

$$\partial W = \sum_{i=1}^{3} Q_i \partial q_i, \tag{2-9}$$

where the total work done is the force multiplied by the direction it is pointing in, defined by the generalized coordinates q_i. Let us now assume that the vehicle in Figure 2-2 undergoes a virtual displacement in the ∂x, ∂y and $\partial\psi$ direction, where x and y are local vehicle coordinates in the $\mathcal{O}^i$ frame, then the virtual work is given by

$$\partial W = \sum_{i=1}^{3} Q_i \partial q_i = \sum F_x \partial x + \sum F_y \partial y + \sum M_z \partial\psi. \tag{2-10}$$

From Equation 2-10 the generalized forces Q_X, Q_Y and Q_ψ can be derived as

$$Q_X = \sum F_x = F_{x,f}\cos(\delta) + F_{y,f}\sin(\delta) + F_{x,r}, \tag{2-11a}$$

$$Q_Y = \sum F_y = F_{x,f}\sin(\delta) + F_{y,f}\cos(\delta) + F_{y,r}, \tag{2-11b}$$

$$Q_\psi = \sum M_z = aF_{x,f}\sin(\delta) + aF_{y,f}\cos(\delta) - bF_{y,r}, \tag{2-11c}$$

which becomes, after a small angle approximation,

$$Q_X = \sum F_x = F_{x,f} + F_{x,r}, \tag{2-12a}$$

$$Q_Y = \sum F_y = F_{y,f} + F_{y,r}, \tag{2-12b}$$

$$Q_\psi = \sum M_z = aF_{y,f} - bF_{y,r}. \tag{2-12c}$$

The set of equations in (2-12), combined with Equation 2-7, give us a set of equations for describing the lateral, longitudinal and yaw motion of a vehicle. Writing out the equations yields

$$m\ddot{X}_1 = m\left(\dot{v}_x - v_y\dot{\psi}\right) = F_{x,f} + F_{x,r}, \tag{2-13a}$$

$$m\ddot{Y}_1 = m\left(\dot{v}_y + v_x\dot{\psi}\right) = F_{y,f} + F_{y,r}, \tag{2-13b}$$

$$I_z\ddot{\psi} = aF_{y,f} - bF_{y,r}. \tag{2-13c}$$

Writing out the equations in 2-13 for each of the generalized accelerations yields

$$\dot{v}_x = \frac{F_{x,f} + F_{x,r}}{m} + v_y\dot{\psi} \tag{2-14a}$$

$$\dot{v}_y = \frac{F_{y,f} + F_{y,r}}{m} - v_x\dot{\psi} \tag{2-14b}$$

$$\ddot{\psi} = \frac{aF_{y,f} - bF_{y,r}}{I_z} \tag{2-14c}$$

Inclusion of Lateral Tyre Dynamics

The forces $F_{x,i}$ and $F_{y,i}$ are produced by the tyres. As the goal is to arrive at a lateral vehicle model, only the lateral tyre dynamics will be explored in detail. Further on in the derivation, the longitudinal forces $F_{x,i}$ will also be removed from the equations. In the literature [22] various ways of mathematically describing how a tyre produces a force are presented. As the model being developed in this thesis aims to arrive at a linear description of the vehicle dynamics, a linear tyre model will be used to model the forces they generate. In the linear tyre model the amount of force a tyre generates is linearly dependant on the amount of slip angle the tyre has. The forces for the front and rear tyres are given by

$$\begin{aligned} F_{y,f} &= C_{\alpha_f}\alpha_f, \\ F_{y,r} &= C_{\alpha_r}\alpha_r. \end{aligned} \tag{2-15}$$

where C_{α_f} is the front tyre cornering stiffness and C_{α_r} the rear tyre cornering stiffness. The cornering stiffness of a tyre is a measure of how much lateral force a tyre produces per radian of rotation. In turn it is possible to write the slip angles as function of vehicle states. Using the angles as defined in Figure 2-2, α_f and α_r can be written as

$$\begin{aligned} \alpha_f &= \delta - \frac{v_y + a\dot{\psi}}{v_x}, \\ \alpha_r &= -\frac{v_y - b\dot{\psi}}{v_x}, \end{aligned} \tag{2-16}$$

Combining Equations 2-13, 2-15 and 2-16 results in a non linear description of the vehicle motion in longitudinal, lateral and yaw direction.

$$\dot{v}_x = \frac{F_{x,f} + F_{x,r}}{m} + v_y\dot{\psi} \tag{2-17a}$$

$$\dot{v}_y = \frac{C_{\alpha_f}}{m}\left(\delta - \frac{v_y + a\dot{\psi}}{v_x}\right) - \frac{C_{\alpha_r}}{m}\left(\frac{v_y - b\dot{\psi}}{v_x}\right) - v_x\dot{\psi}, \tag{2-17b}$$

$$\ddot{\psi} = \frac{aC_{\alpha_f}}{I_z}\left(\delta - \frac{v_y + a\dot{\psi}}{v_x}\right) + \frac{bC_{\alpha_r}}{I_z}\left(\frac{v_y - b\dot{\psi}}{v_x}\right). \tag{2-17c}$$

Lateral Vehicle Dynamics

The model in Equation 2-17 completely describes the longitudinal, lateral and yaw dynamics of the vehicle. However, in this form the model is still non-linear, where a linear description is required. It turns out that including the longitudinal dynamics and, as such longitudinal velocity v_x in the description, complicates matters as it appears in non-linear fashion in the tyre slip angle. This can be circumvented by assuming that the vehicle drives at a constant forward velocity. In turn this means that $\dot{v}_x = 0$. As such it is possible to arrive at a linear description of the lateral vehicle dynamics for v_y and $\dot{\psi}$. By assuming $\dot{v}_x = 0$, Equation 2-17 reduces to

$$\begin{aligned} \dot{v}_y &= \frac{C_{\alpha_f}}{m}\left(\delta - \frac{v_y + a\dot{\psi}}{v_x}\right) - \frac{C_{\alpha_r}}{m}\left(\frac{v_y - b\dot{\psi}}{v_x}\right) - v_x\dot{\psi}, \\ \ddot{\psi} &= \frac{aC_{\alpha_f}}{I_z}\left(\delta - \frac{v_y + a\dot{\psi}}{v_x}\right) + \frac{bC_{\alpha_r}}{I_z}\left(\frac{v_y - b\dot{\psi}}{v_x}\right). \end{aligned} \tag{2-18}$$

The assumption that the forward velocity, v_x, is constant holds for all other derivations in this thesis. As such, v_x is no longer a state but a parameter of the system.

2-1-3 State-Space Model Description

By setting $\dot{v}_x = 0$, it is possible to put the Equations of 2-18 into a linear state-space description. By taking v_y and $\dot{\psi}$ as vehicle states, (2-18) can also be written as

$$\dot{v}_y = \left(-\frac{C_{\alpha_f} + C_{\alpha_r}}{mv_x}\right)v_y + \left(-v_x + \frac{-aC_{\alpha_f} + bC_{\alpha_r}}{mv_x}\right)\dot{\psi} + \frac{C_{\alpha_f}}{m}\delta, \tag{2-19}$$

for the state v_y and for $\dot{\psi}$ we can write

$$\ddot{\psi} = \left(\frac{-aC_{\alpha_f} + bC_{\alpha_r}}{I_z v_x}\right)v_y + \left(\frac{a^2C_{\alpha_f} - b^2C_{\alpha_r}}{I_z v_x}\right)\dot{\psi} + \frac{aC_{\alpha_f}}{I_z}\delta. \tag{2-20}$$

Using equations 2-19 and 2-20 a state space description of the form $\dot{x} = Ax + Bu$, with output $y = Cx + Du$ is given in (2-21) and (2-22). This description is given by:

$$\begin{bmatrix} \dot{v}_y \\ \ddot{\psi} \end{bmatrix} = \begin{bmatrix} \left(-\frac{C_{\alpha_f}+C_{\alpha_r}}{mv_x}\right) & \left(-v_x + \frac{-aC_{\alpha_f}+bC_{\alpha_r}}{mv_x}\right) \\ \left(\frac{-aC_{\alpha_f}+bC_{\alpha_r}}{I_z v_x}\right) & \left(\frac{a^2C_{\alpha_f}-b^2C_{\alpha_r}}{I_z v_x}\right) \end{bmatrix}\begin{bmatrix} v_y \\ \dot{\psi} \end{bmatrix} + \begin{bmatrix} \frac{C_{\alpha_f}}{m} \\ \frac{bC_{\alpha_r}}{I_z} \end{bmatrix}\delta. \tag{2-21}$$

Typical outputs of the system are given in Equation 2-22

$$\begin{bmatrix} \dot{v}_y \\ \dot{\psi} \\ \beta \end{bmatrix} = \begin{bmatrix} \left(-\frac{C_{\alpha_f}+C_{\alpha_r}}{mv_x}\right) & \left(\frac{-aC_{\alpha_f}+bC_{\alpha_r}}{I_z v_x}\right) \\ 0 & 1 \\ -\frac{1}{v_x} & 0 \end{bmatrix}\begin{bmatrix} v_y \\ \dot{\psi} \end{bmatrix} + \begin{bmatrix} \frac{C_{\alpha_f}}{m} \\ 0 \\ 0 \end{bmatrix}\delta, \tag{2-22}$$

where $\dot{v}_y$ is also the lateral acceleration of the vehicle and β is the body slip angle of the vehicle under a small angle approximation.

2-1-4 Steering Dynamics

The system in Equation 2-21 uses the tyre steering angle as system input. However, since the steering wheel of the vehicle will be actuated using the power steering it is beneficial to include the the dynamics in the state space. The steering system is described by a second order system of the form [24]

$$\ddot{\delta} = -2\zeta\omega_n\dot{\delta} + \omega_n^2\left(\delta_{ref} - \delta\right) \tag{2-23}$$

In Equation 2-23 ζ is the damping of the power steering, ω_n its natural frequency and δ_{ref} the desired steering wheel angle. Expanding the state space description of the vehicle given in Equation 2-21 yields

$$\begin{bmatrix} \dot{v}_y \\ \ddot{\psi} \\ \dot{\delta} \\ \ddot{\delta} \end{bmatrix} = \begin{bmatrix} \left(-\frac{C_{\alpha_f}+C_{\alpha_r}}{mv_x}\right) & \left(-v_x + \frac{-aC_{\alpha_f}+bC_{\alpha_r}}{mv_x}\right) & \frac{C_{\alpha_f}}{m} & 0 \\ \left(\frac{-aC_{\alpha_f}+bC_{\alpha_r}}{I_z v_x}\right) & \left(\frac{a^2C_{\alpha_f}-b^2C_{\alpha_r}}{I_z v_x}\right) & \frac{bC_{\alpha_r}}{I_z} & 0 \\ 0 & 0 & 0 & 1 \\ 0 & 0 & -\omega_n^2 & -2\zeta\omega_n \end{bmatrix} \begin{bmatrix} v_y \\ \dot{\psi} \\ \delta \\ \dot{\delta} \end{bmatrix} + \begin{bmatrix} 0 \\ 0 \\ 0 \\ \omega_n^2 \end{bmatrix} \delta_{ref}. \tag{2-24}$$

2-2 Error Dynamics

Having established the vehicle dynamics, the error dynamics of a vehicle i in the platoon with respect to a reference path will be derived. Figure 2-3 will be used as reference for this derivation. Note that since the errors are vehicle specific, the subscript i has been added to states of vehicle i. If this subscript is lacking it means that that state is independant of vehicle i. In Figure 2-3 the reference path is denoted as a curve, C. Furthermore, three different frames of reference are denoted, namely, $\mathcal{O}^g$ as origin for the global coordinate system, $\mathcal{O}^r$ as origin for an axis system located on curve C and $\mathcal{O}^i$ as origin for the frame of reference for vehicle i. The axis system with origin $\mathcal{O}^r$ is an orthogonal projection of $\mathcal{O}^i$ on the curve C. The origins $\mathcal{O}^g$ and $\mathcal{O}^i$ are defined in Figure 2-2.

The frame of reference with origin $\mathcal{O}^r$ has unit vector $\vec{e}_x^r$, which is tangential to the curve C. This unit vector has angle θ_s with respect to the global X-axis. Vector $\vec{y}_{e,i}$ connects the origins $\mathcal{O}^r$ and $\mathcal{O}^i$, and is the shortest distance between the centre of the vehicle and the curve C. It is calculated by the inner product of the vector $\vec{y}_{e,i}$, and unit vector $\vec{e}_y^r$,

$$y_{e,i} = \vec{y}_{e,i} \cdot \vec{e}_y^r \tag{2-25}$$

The angle ψ_i is the angle between the vector $\vec{e}_x^i$ and the global X-axis. Angle β_i is the angle between the vector $\vec{e}_x^i$, and the velocity vector $\vec{V}_i$, as defined in Figure 2-2. This angle can be calculated using the local velocities $v_{y,i}$ and $v_{x,i}$ as

$$\beta_i = \arctan\left(\frac{v_{y,i}}{v_{x,i}}\right), \tag{2-26}$$

or approximated by

$$\beta_i = \frac{v_{y,i}}{v_{x,i}}, \tag{2-27}$$

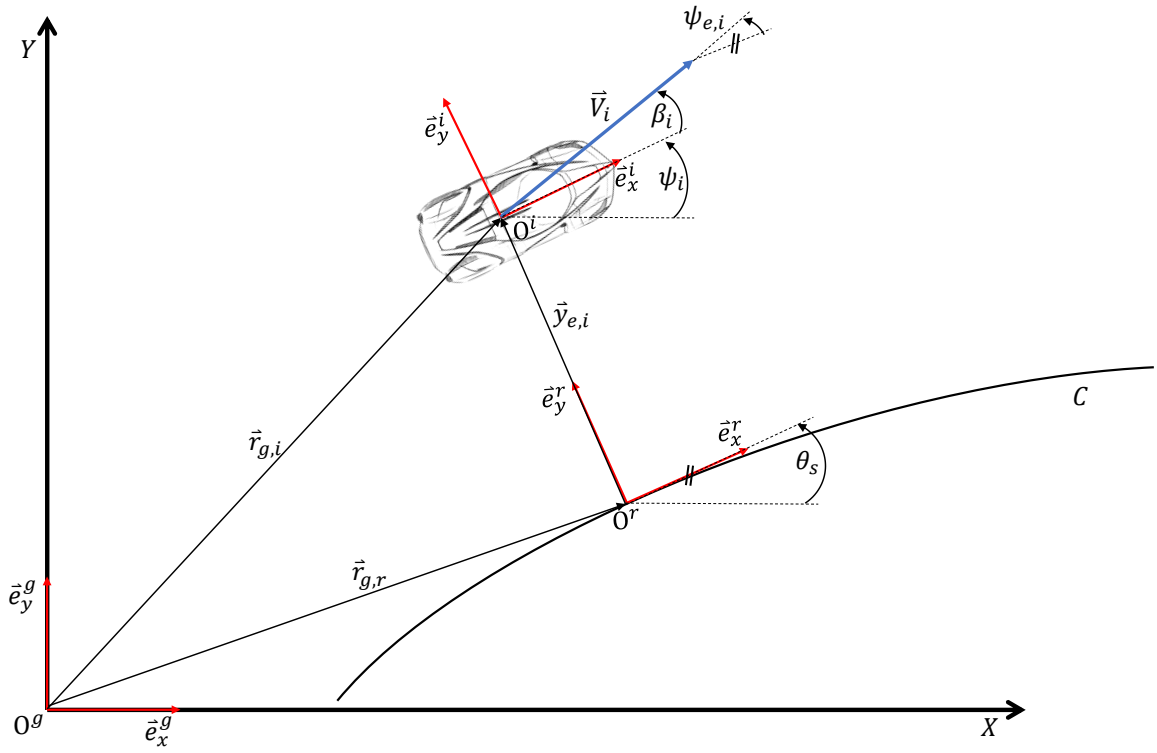

Figure 2-3: Error model with all variables defined.

when using a small angle approximation. Finally the heading error $\psi_{e,i}$ is considered. The heading error is defined as the difference in angle between the vector $\vec{e}_x^r$, tangent to the curve C and the velocity vector V_i

$$\psi_{e,i} = \beta_i + \psi_i - \theta_s. \tag{2-28}$$

In literature the heading error is often also defined as the error between the tangent $\vec{e}_x^r$ and the vehicle centreline, or $\vec{e}_x^i$ [13]. When the error as defined in Equation 2-28 is brought to zero, it will align the velocity vector of the vehicle with the tangent of the curve, and the vehicle will be moving along the tangent. The alternate definition does not necessarily force this upon the vehicle.

Having defined the errors, their time derivatives are required to describe their dynamics. First the dynamics for $\psi_{e,i}$ will be derived in section 2-2-1, after which the dynamics for $y_{e,i}$ are derived in section 2-2-2 Finally, in section 2-3 the error definitions will be included in the state space description of Equation 2-24.

2-2-1 Error Dynamics for $\dot{\psi}_{e,i}$

Let us now derive the error dynamics $\dot{\psi}_{e,i}$. Taking the time derivative of Equation 2-28 yields

$$\dot{\psi}_{e,i} = \dot{\beta}_i + \dot{\psi}_i - \dot{\theta}_s. \tag{2-29}$$

Using the approximation for the body slip angle as given in Equation 2-27, writing out the time derivative yields

$$\dot{\psi}_{e,i} = \frac{\dot{v}_{y,i}v_{x,i} - v_{y,i}\dot{v}_{x,i}}{{v_{x,i}}^2} + \dot{\psi}_i - \dot{\theta}_s = \frac{\dot{v}_{y,i}}{v_{x,i}} - \frac{v_{y,i}\dot{v}_{x,i}}{{v_{x,i}}^2} + \dot{\psi}_i - \dot{\theta}_s. \tag{2-30}$$

One of the requirements for arriving at a linear vehicle model was that $\dot{v}_{x,i} = 0$, therefore there is no inclusion of longitudinal dynamics into the vehicle model. Applying this to the error definition of (2-30) results in

$$\dot{\psi}_{e,i} = \frac{\dot{v}_{y,i}}{v_{x,i}} + \dot{\psi}_i - \dot{\theta}_s. \tag{2-31}$$

In Equation 2-31 $\dot{\psi}_i$ is the yaw rate of vehicle i, $\dot{\theta}_s$ is the rotation of the curvature of the road and $\frac{\dot{v}_{y,i}}{v_{x,i}}$ is the change in body slip angle due to change in lateral velocity. Using the definition in (2-19), and substituting it in (2-31) gives

$$\begin{aligned}\dot{\psi}_{e,i} &= \left(-\frac{C_{\alpha_f} + C_{\alpha_r}}{mv_{x,i}^2}\right) v_{y,i} + \left(-1 + \frac{-aC_{\alpha_f} + bC_{\alpha_r}}{mv_{x,i}^2}\right)\dot{\psi}_i + \frac{1}{v_{x,i}}\frac{C_{\alpha_f}}{m}\delta_i + \dot{\psi}_i - \dot{\theta}_s \\ &= \left(-\frac{C_{\alpha_f} + C_{\alpha_r}}{mv_{x,i}^2}\right) v_{y,i} + \left(\frac{-aC_{\alpha_f} + bC_{\alpha_r}}{mv_{x,i}^2}\right)\dot{\psi}_i + \frac{1}{v_{x,i}}\frac{C_{\alpha_f}}{m}\delta_i - \dot{\theta}_s.\end{aligned} \tag{2-32}$$

For sake of brevity (2-32) is written as

$$\dot{\psi}_{e,i} = p_1 v_{y,i} + p_2\dot{\psi}_i + p_3\delta_i - \dot{\theta}_s, \tag{2-33}$$

with

$$p_1 = \left(-\frac{C_{\alpha_f} + C_{\alpha_r}}{mv_{x,i}^2}\right) \tag{2-34a}$$

$$p_2 = \left(\frac{-aC_{\alpha_f} + bC_{\alpha_r}}{mv_{x,i}^2}\right) \tag{2-34b}$$

$$p_3 = \frac{1}{v_{x,i}}\frac{C_{\alpha_f}}{m} \tag{2-34c}$$

2-2-2 Error Dynamics for $\dot{y}_{e,i}$

Having derived the dynamics for $\psi_{e,i}$ as a function of vehicle states for vehicle i and road curvature C, the error dynamics for $y_{e,i}$ will be derived. Using (2-25), its time derivative can be written as

$$\dot{y}_{e,i} = \dot{\vec{y}}_{e,i} \cdot \vec{e}_y^r + \dot{\vec{e}}_y^r \cdot \vec{y}_{e,i}. \tag{2-35}$$

As the frame of reference spanned by vectors $\vec{e}_x^r$ and $\vec{e}_y^r$ is defined as being tangential to the curve, it is moving purely in the $\vec{e}_x^r$ direction, hence $\dot{\vec{e}}_y^r = 0$. Thus

$$\dot{y}_{e,i} = \dot{\vec{y}}_{e,i} \cdot \vec{e}_y^r. \tag{2-36}$$

The time derivative of vector $\vec{y}_{e,i}$ can also be written as

$$\dot{\vec{y}}_{e,i} = \dot{\vec{r}}_{g,i} - \dot{\vec{r}}_{g,r}, \tag{2-37}$$

with vectors $\vec{r}_{g,i}$ and $\vec{r}_{g,r}$ as in Figure 2-3. Using the local vehicle velocities $v_{x,i}$ and $v_{y,i}$, $\dot{\vec{r}}_{g,i}$ can be written as

$$\dot{\vec{r}}_{g,i} = \begin{bmatrix} v_{x,i} & v_{y,i} \end{bmatrix} \begin{bmatrix} \vec{e}_x^i \\ \vec{e}_y^i \end{bmatrix} \tag{2-38}$$

Using the fact that the frame $\mathcal{O}^r$ is an orthogonal projection of the frame $\mathcal{O}^i$, and using rotation matrix $\mathcal{R}(\psi_i - \theta_s)$, defined as

$$\mathcal{R}(\psi_i - \theta_s) = \begin{bmatrix} \cos(\psi_i - \theta_s) & -\sin(\psi_i - \theta_s) \\ \sin(\psi_i - \theta_s) & \cos(\psi_i - \theta_s) \end{bmatrix} \tag{2-39}$$

Equation 2-38 can be written as

$$\dot{\vec{r}}_{g,i} = \begin{bmatrix} v_{x,i} & v_{y,i} \end{bmatrix} \mathcal{R}(\psi_i - \theta_s)^T \begin{bmatrix} \vec{e}_x^r \\ \vec{e}_y^r \end{bmatrix}, \tag{2-40}$$

which equals

$$\dot{\vec{r}}_{g,i} = \begin{bmatrix} v_{x,i}\cos(\psi_i - \theta_s) - v_{y,i}\sin(\psi_i - \theta_s) & v_{x,i}\sin(\psi_i - \theta_s) + v_{y,i}\cos(\psi_i - \theta_s) \end{bmatrix} \begin{bmatrix} \vec{e}_x^r \\ \vec{e}_y^r \end{bmatrix}. \tag{2-41}$$

Furthermore, as $\mathcal{O}^r$ can only move in the direction tangent to the curve C, then with slight abuse of notation

$$\dot{\vec{r}}_{g,r} = \dot{\vec{r}}^{r}_{g,r} \cdot \vec{e}_x^r, \tag{2-42}$$

where $\dot{\vec{r}}^{r}_{g,r}$ is the velocity of the vector $\vec{r}_{g,r}$ system among the curve C. Combining Equations 2-41 and 2-42 into Equation 2-37 it then yields

$$\dot{\vec{y}}_{e,i} = \begin{bmatrix} v_{x,i}\cos(\psi_i - \theta_s) - v_{y,i}\sin(\psi_i - \theta_s) - \dot{\mathcal{O}}^r & v_{x,i}\sin(\psi_i - \theta_s) + v_{y,i}\cos(\psi_i - \theta_s) \end{bmatrix} \begin{bmatrix} \vec{e}_x^r \\ \vec{e}_y^r \end{bmatrix}. \tag{2-43}$$

With $\dot{y}_{e,i} = \dot{\vec{y}}_{e,i} \cdot \vec{e}_y^r$ (2-43) becomes

$$\dot{y}_{e,i} = v_{x,i}\sin(\psi_i - \theta_s) + v_{y,i}\cos(\psi_i - \theta_s) \tag{2-44}$$

Using Equation 2-28 it is possible to write $\psi_i - \theta_s = \psi_{e,i} - \beta_i$, such that (2-44) can be written as

$$\dot{y}_{e,i} = v_{x,i}\sin(\psi_{e,i} - \beta_i) + v_{y,i}\cos(\psi_{e,i} - \beta_i). \tag{2-45}$$

Using the small angle approximation in Equation 2-27 for β_i, Equation 2-45 can be rewritten to

$$\begin{aligned} \dot{y}_{e,i} &= v_{x,i}\left(\psi_{e,i} - \frac{v_{y,i}}{v_{x,i}}\right) + v_{y,i}, \\ &= v_{x,i}\psi_{e,i} \end{aligned} \tag{2-46}$$

2-3 Full State-Space Model Description and Platoon Model

Having derived the dynamic equations for the road errors in (2-33) and (2-46) as a function of vehicle states and an external input $\dot{\theta}_s$ the following linear state space system can be defined:

$$\begin{bmatrix} \dot{v}_{y,i} \\ \ddot{\psi}_i \\ \dot{y}_{e,i} \\ \dot{\psi}_{e,i} \\ \dot{\delta}_i \\ \ddot{\delta}_i \end{bmatrix} = \begin{bmatrix} -\left(\frac{C_{\alpha_f}+C_{\alpha_r}}{mv_{x,i}}\right) & \left(-v_{x,i}+\frac{bC_{\alpha_r}-aC_{\alpha_f}}{mv_{x,i}}\right) & 0 & 0 & \frac{C_{\alpha_f}}{m} & 0 \\ \left(\frac{bC_{\alpha_r}-aC_{\alpha_f}}{I_z v_{x,i}}\right) & \left(-\frac{a^2C_{\alpha_f}+b^2C_{\alpha_r}}{I_z v_{x,i}}\right) & 0 & 0 & \frac{aC_{\alpha_f}}{I_z} & 0 \\ 0 & 0 & 0 & v_{x,i} & 0 & 0 \\ -\left(\frac{C_{\alpha_f}+C_{\alpha_r}}{mv_{x,i}^2}\right) & \left(\frac{bC_{\alpha_r}-aC_{\alpha_f}}{mv_{x,i}^2}\right) & 0 & 0 & \frac{C_{\alpha_f}}{mv_{x,i}^2} & 0 \\ 0 & 0 & 0 & 0 & 0 & 1 \\ 0 & 0 & 0 & 0 & -\omega_n^2 & -2\zeta\omega_n \end{bmatrix} \begin{bmatrix} v_{y,i} \\ \dot{\psi}_i \\ y_{e,i} \\ \psi_{e,i} \\ \delta_i \\ \dot{\delta}_i \end{bmatrix} + \begin{bmatrix} 0 \\ 0 \\ 0 \\ 0 \\ 0 \\ \omega_n^2 \end{bmatrix} \delta_{i,ref} + \begin{bmatrix} 0 \\ 0 \\ 0 \\ -1 \\ 0 \\ 0 \end{bmatrix} \dot{\theta}_s. \tag{2-47}$$

In shorthand notation this system is written as

$$\dot{x}_i = Ax_i + B\delta_{i,ref} + E\dot{\theta}_s, \tag{2-48}$$

$$y_i = Cx_i, \tag{2-49}$$

where C is an output matrix of choice. The state space description given in Equation 2-47 fully describes how a change in road curvature leads to accumulation of heading error $\psi_{e,i}$, and when left untreated leads to lateral offset error $y_{e,i}$. Heading error $y_{e,i}$ is wholly dependant on heading error $\psi_{e,i}$, which in turn is affected by a disturbance input $\dot{\theta}_s$ and vehicle steering angle δ_i. The control input $\delta_{i,ref}$ will be generated by a controller as function of the heading and lateral offset error. Correction of any accumulated heading error leads to correction of lateral offset error.

From the model in (2-47) it is not yet apparent how the dynamics of the preceding vehicle can be connected to that of the trailing vehicle. To arrive at this consider a homogeneous platoon of vehicles of n vehicles long. The path vehicle i now has to drive is defined by the path driven by its preceding vehicle, vehicle $i-1$. The rate of change of the path, $\dot{\theta}_s$, sensed by vehicle i is induced by vehicle $i-1$. This rate of change $\dot{\theta}_s$ can be written as function of the states of vehicle $i-1$. Define Δt as the time it takes vehicle i to travel following distance d_i, then

$$\dot{\theta}_{s,i-1} = \dot{\psi}_{i-1}(t-\Delta t) + \dot{\beta}_{i-1}(t-\Delta t) \tag{2-50}$$

Using the definitions for $\dot{\psi}_i$ and $\dot{\beta}_i$ as developed earlier in this chapter, Equation 2-50 can then be written as

$$\begin{aligned} \dot{\theta}_{s,i-1} = \left(-\frac{C_{\alpha_f}+C_{\alpha_r}}{mv_{x,i-1}^2}\right) v_{y,i-1}(t-\Delta t) + \left(\frac{-aC_{\alpha_f}+bC_{\alpha_r}}{mv_{x,i-1}^2}\right) \dot{\psi}_{i-1}(t-\Delta t) \\ + \frac{1}{v_{x,i-1}} \frac{C_{\alpha_f}}{m} \delta_{i-1}(t-\Delta t), \end{aligned} \tag{2-51}$$

Rewriting $E\dot{\theta}_s$ to

$$\begin{bmatrix} 0 \\ 0 \\ 0 \\ -1 \\ 0 \\ 0 \end{bmatrix} \dot{\theta}_s = \begin{bmatrix} 0 & 0 & 0 & 0 & 0 & 0 \\ 0 & 0 & 0 & 0 & 0 & 0 \\ 0 & 0 & 0 & 0 & 0 & 0 \\ -\left(\frac{C_{\alpha_f}+C_{\alpha_r}}{mv_{x,i}^2}\right) & \left(\frac{bC_{\alpha_r}-aC_{\alpha_f}}{mv_{x,i}^2}\right) & 0 & 0 & \frac{C_{\alpha_f}}{mv_{x,i}^2} & 0 \\ 0 & 0 & 0 & 0 & 0 & 0 \\ 0 & 0 & 0 & 0 & 0 & 0 \end{bmatrix} \begin{bmatrix} v_{y,i-1}\left(t-\Delta t\right) \\ \dot{\psi}_{i-1}\left(t-\Delta t\right) \\ y_{e,i-1}\left(t-\Delta t\right) \\ \psi_{e,i-1}\left(t-\Delta t\right) \\ \delta_{i-1}\left(t-\Delta t\right) \\ \dot{\delta}_{i-1}\left(t-\Delta t\right) \end{bmatrix}, \tag{2-52}$$

which, when substituted in (2-47), leads to

$$\begin{aligned} \begin{bmatrix} \dot{v}_{y,i} \\ \ddot{\psi}_i \\ \dot{y}_{e,i} \\ \dot{\psi}_{e,i} \\ \dot{\delta}_i \\ \ddot{\delta}_i \end{bmatrix} &= \begin{bmatrix} -\left(\frac{C_{\alpha_f}+C_{\alpha_r}}{mv_{x,i}}\right) & \left(-v_{x,i}+\frac{bC_{\alpha_r}-aC_{\alpha_f}}{mv_{x,i}}\right) & 0 & 0 & \frac{C_{\alpha_f}}{m} & 0 \\ \left(\frac{bC_{\alpha_r}-aC_{\alpha_f}}{I_z v_{x,i}}\right) & \left(-\frac{a^2C_{\alpha_f}+b^2C_{\alpha_r}}{I_z v_{x,i}}\right) & 0 & 0 & \frac{aC_{\alpha_f}}{I_z} & 0 \\ 0 & 0 & 0 & v_{x,i} & 0 & 0 \\ -\left(\frac{C_{\alpha_f}+C_{\alpha_r}}{mv_{x,i}^2}\right) & \left(\frac{bC_{\alpha_r}-aC_{\alpha_f}}{mv_{x,i}^2}\right) & 0 & 0 & \frac{C_{\alpha_f}}{mv_{x,i}^2} & 0 \\ 0 & 0 & 0 & 0 & 0 & 1 \\ 0 & 0 & 0 & 0 & -\omega_n^2 & -2\zeta\omega_n \end{bmatrix} \begin{bmatrix} v_{y,i} \\ \dot{\psi}_i \\ y_{e,i} \\ \psi_{e,i} \\ \delta_i \\ \dot{\delta}_i \end{bmatrix} \\ &+ \begin{bmatrix} 0 \\ 0 \\ 0 \\ 0 \\ 0 \\ \omega_n^2 \end{bmatrix} \delta_{i,ref} + \begin{bmatrix} 0 & 0 & 0 & 0 & 0 & 0 \\ 0 & 0 & 0 & 0 & 0 & 0 \\ 0 & 0 & 0 & 0 & 0 & 0 \\ -\left(\frac{C_{\alpha_f}+C_{\alpha_r}}{mv_{x,i}^2}\right) & \left(\frac{bC_{\alpha_r}-aC_{\alpha_f}}{mv_{x,i}^2}\right) & 0 & 0 & \frac{C_{\alpha_f}}{mv_{x,i}^2} & 0 \\ 0 & 0 & 0 & 0 & 0 & 0 \\ 0 & 0 & 0 & 0 & 0 & 0 \end{bmatrix} \begin{bmatrix} v_{y,i-1}\left(t-\Delta t\right) \\ \dot{\psi}_{i-1}\left(t-\Delta t\right) \\ y_{e,i-1}\left(t-\Delta t\right) \\ \psi_{e,i-1}\left(t-\Delta t\right) \\ \delta_{i-1}\left(t-\Delta t\right) \\ \dot{\delta}_{i-1}\left(t-\Delta t\right) \end{bmatrix}. \end{aligned} \tag{2-53}$$

or in shorthand notation

$$\dot{x}_i = A_i x_i + B\delta_{i,ref} + A_{i-1}x_{i-1}\left(t-\Delta t\right). \tag{2-54}$$

This interconnection between two vehicles in the platoon will be used when analyzing the string stability properties of the platoon. This analysis can be found in Chapter 3.

2-4 The Road Error

In section 2-2 the road error definitions were defined. This was done through projecting the vehicle axis system, rotated such that it is tangential with the path and defining a heading and offset error around the global axis system, and two local axis systems. Figure 2-4 shows a similar scenario to that posed in Figure 2-3, here; however, the vehicle measures a total distance off-set $y_{tot,i}$. This distance is measured by using images captured with a camera. In this image there will be two points, one is defined as the tracking point and the other is the location where the vehicle will end if it travels a certain distance with this heading. The tracking point is normally located on the back of the preceding vehicle, whereas the heading

point is defined by the look-ahead distance d_i. The distance error between the two points is the measurement $y_{tot,i}$ This error comprises the two errors seen in section 2-2, but also a distance denoted by ε_i,

$$y_{tot,i} = y_{e,i} + d_i\psi_{e,i} + \varepsilon_i. \tag{2-55}$$

When vehicle following based on direct vehicle following is used, the control action is generated on the measurement of $y_{tot,i}$. From 2-4 it is clear that this measurement contains a superposition of both the road errors, and a distance ε_i from the fact that the vehicle in front has moved away. When this distance ε_i is left unaccounted for, the vehicle will undercut the path of the preceding vehicle; namely, making $y_{tot,i}$ zero does not imply making $y_{e,i} + d_i\psi_{e,i}$ zero.

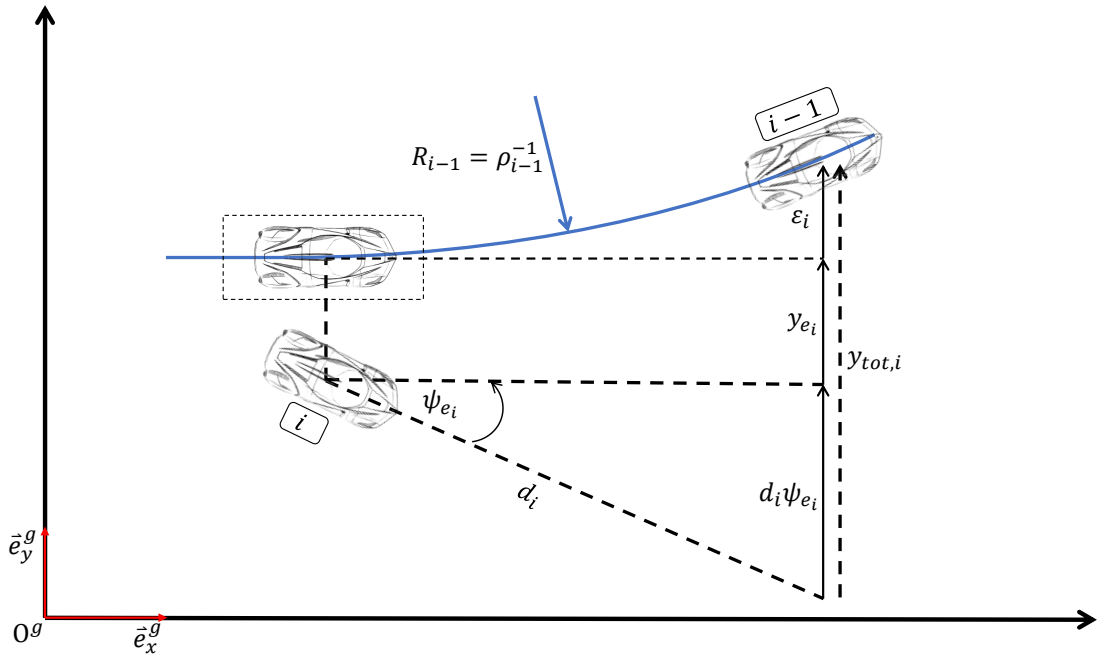

Figure 2-4: Platoon with lateral errors defined.

This distance ε_i can be calculated by vehicle $i-1$. Taking the situation as depicted in Figure 2-4 where the platoon drives perpendicular to the x-axis with $Y = 0$ then when vehicle $i-1$ starts following the path from point A to point B, ε_i is calculated as

$$\varepsilon_i = \int_{t-t_{la}}^{t} \dot{Y}dt = \int_{t-t_{la}}^{t} v_x \sin\left(\psi_{i-1}(t)\right) + v_{y,i-1}(t)\cos\left(\psi_{i-1}(t)\right)dt, \tag{2-56}$$

where t_{la} is the time it takes for vehicle $i-1$ to drive following distance d_i. This time is almost equal to the time it takes vehicle $i-1$ to drive from point A to B. Using the small angle approximation for the integral in (2-56) yields

$$\varepsilon_i \approx \int_{t-t_{la}}^{t} v_{x,i-1}\left(\psi_{i-1}(t)\right) + v_{y,i-1}(t)dt. \tag{2-57}$$

Taking the time derivative of Equation 2-57 yields a formulation for ε_i that can be used by a vehicle to approximate ε_i. The time derivative is given by

$$\dot{\varepsilon}_i = v_{x,i-1}\left(\psi_{i-1}(t) - \psi_{i-1}(t - t_{la})\right) + v_{y,i-1}(t) - v_{y,i-1}(t - t_{la}). \tag{2-58}$$

As highway manoeuvring is considered, it holds that when $v_{x,i-1} >> v_{y,i-1}$ in all cases considered, Equation 2-58 can be approximated as

$$\dot{\varepsilon}_i \approx v_{x,i-1}\left(\psi_{i-1}(t) - \psi_{i-1}(t - t_{la})\right). \tag{2-59}$$

Using this approximation vehicle $i-1$ can use its own velocity measurement and yaw rate measurement to give an approximation for the error distance induced by the road curvature that is measured when using a direct vehicle following method. Adding this measurement to the communication between the two vehicles, allows the trailing vehicle to deduce the error

$$e_i = y_{e,i} + d_i\psi_{e,i}. \tag{2-60}$$

This measurement of the superposition of the two individual errors described in section 2-2 opens up the possibility to reconstruct the individual error states. This is done by using an observer designed for the state space system in (2-47). For this system, if the output matrix is taken as

$$C = \begin{bmatrix} 0 & 0 & 1 & d_i & 0 & 0 \end{bmatrix}, \tag{2-61}$$

it turns out that the system's observability matrix is full rank. This means that the system is observable. The error measurement in (2-60) as described in this section open up the possibility of having vehicles use the direct vehicle following method, and also be able to follow the path without corner cutting. Furthermore, it opens up the possibility to develop individual feedback controllers for the error states. The biggest advantage however comes from the fact that direct vehicle following is relatively easy to implement, and that if communication fails, the control strategy remains the same, only with the downside that corner cutting will now occur, as ε_i is unknown in that case.

Chapter 3

String Stability Analysis

A platoon of vehicles can be interpreted as a set of interconnected systems. The performance of the platoon of vehicles can be assessed by their string stability property. As for any other system, connected or not, the notion of internal stability is also important. Such conventional stability for a closed-loop feedback system considers the evolution of system states over time.

In contrast, string stability concerns itself with the propagation of a state over the platoon as a function of vehicle index. Recall the examples given in the introduction, where string instability was described by either an amplification of longitudinal or lateral acceleration, depending on the manoeuvre. The human operator for a car in vehicle following scenarios can be described as a stable system as seen in [25]. Obviously, there are exceptions where this is not necessarily true (drunk driving for example). However, the occurrence of, for example, a ghost traffic jam is a practical indication that the system is not string stable.

In [26] string stability, or lack thereof, is described for the development of a longitudinal vehicle following controller. In this paper the authors describe a so-called slinky effect of the platoon. In [27] Swaroop and Hendrick formally define string stability as uniform boundedness in all states. In their paper they go on to show that string stability is the critical requirement for vehicle platooning.

The first formal definition of string stability can be found in the the work of Swaroop and Hedrick [27]. In [20] a mathematical framework is developed with which string stability is defined using linear system analysis. This makes it well suited for interconnected systems analysis. The mathematical framework of [20] is based on the development of controllers for longitudinal platooning. It will be covered in section 3-1. In section 3-2 the analysis used in [20] will be used with slight adaptation for the connected vehicle model as developed in section 2-3. At the end of section 2-3 a definition for lateral string stability will be given. Finally, section 3-4 will give a proof, showing that given the system model as in section 2-3, string stability can never be achieved with only feedback control, and is infeasible with feedback and feedforward control. Implications of this will be briefly covered here and will be more extensively explained in Chapter 6.

3-1 Linear System String Stability

In [20, 28] Jeroen Ploeg presents a definition for string stability based on linear system analysis. This mathematical definition finds its basis in $\mathcal{L}_2$ and $\mathcal{L}_p$ string stability conditions. A string of systems can be represented by the following cascaded system

$$\dot{x}_0 = f_r(x_r, u_r), \tag{3-1a}$$
$$\dot{x}_i = f(x_i, x_{i-1}), \quad i \in \mathcal{S}_m \tag{3-1b}$$
$$y_i = h(x_i). \qquad i \in \mathcal{S}_m \tag{3-1c}$$

Here the set $\mathcal{S}_m = \{i \in \mathcal{N} | 1 \leq i \leq m\}$ is the set containing all m vehicles in the platoon. Furthermore, $u_r \in \mathcal{R}^q$ is the external input for the host vehicle, $x_i \in \mathcal{R}^n$, $i \in \mathcal{S}_m$, is the vector containing all the states and finally $y_i \in \mathcal{R}^l$, $i \in \mathcal{S}_m$ is the chosen output of the system. For the system in equation 3-1 it is said to be $\mathcal{L}_p$ string stable if there exists a class $\mathcal{K}$ functions ν and σ such that

$$||y_i(t) - h(\bar{x}_0)||_{\mathcal{L}_p} \leq \nu(||u_r(t)||_{\mathcal{L}_p}) + \sigma(||x(0) - \bar{x}||) \tag{3-2}$$

for any initial state $x(0)$ and external control input u_r. Class $\mathcal{K}$ functions are functions that are continuous in a domain $[0, a) \to [0, \infty)$ and the function is strictly increasing and zero at zero. A simple example of a class $\mathcal{K}$ function is $f(x) = x^2$.

This definition is better suited than Swaroops as it also includes the external disturbance u_r as well as initial condition perturbations. The definition in equation 3-2 is generalized for linear and non linear systems. For purely linear system analysis, where it is assumed that the system is homogeneous, meaning that each agent shares the same dynamics, equation 3-1 can be written as

$$\begin{bmatrix} \dot{x}_0 \\ \dot{x}_1 \\ \vdots \\ \dot{x}_m \end{bmatrix} = \begin{bmatrix} A_r & & & O \\ A_1 & A_0 & & \\ & \ddots & \ddots & \\ O & & A_1 & A_0 \end{bmatrix} \begin{bmatrix} x_0 \\ x_1 \\ \vdots \\ x_m \end{bmatrix} + \begin{bmatrix} B_r \\ 0 \\ \vdots \\ 0 \end{bmatrix} u_r. \tag{3-3}$$

The matrices A_r, A_1, A_0 denote the dynamics of the host vehicle and following vehicles respectively. The matrix B_r is the input matrix for the host vehicle. Because of the homogeneity assumption the states can be lumped together into a single state vector as $x = \begin{bmatrix} x_0^T & x_1^T & \dots & x_m^T \end{bmatrix}^T$ and in extension the system can be written as

$$\dot{x} = Ax + Bu_r. \tag{3-4}$$

Additionally taking the output also as a linear equation, then

$$y_i = C_i x. \tag{3-5}$$

Using this description it is then possible to also write the model of (3-4) and (3-5) in the Laplace domain as follows

$$y_i(s) = P_i(s)u_r(s) + O_i(s)x(0), \tag{3-6}$$

where $P_i(s) = C_i \left(sI - A\right)^{-1} B$, the transfer function from external input to chosen output, and $O_i = C_i \left(sI - A\right)^{-1}$ the transfer function from any initial condition error to chosen

output. From equation 3-6 it follows that the input output relation for $y_i(s)$, when assuming that $x(0) = 0$, can be written as

$$y_i(s) = \Gamma_i(s) y_{i-1}(s), \tag{3-7}$$

with $\Gamma_i(s)$ the so-called string stability complementary sensitivity function defined as

$$\Gamma_i(s) = P_i(s) P_{i-1}^{-1}(s). \tag{3-8}$$

From [29] we can then define $\mathcal{L}_2$ string stability in H_∞ sense. It states that a platoon is considered strictly $\mathcal{L}_2$ string stable with respect to its input u_i if and only if

$$||P_1(s)||_{\mathcal{H}_\infty} < \infty \tag{3-9}$$

$$||\Gamma_i(s)||_{\mathcal{H}_\infty} \leq 1 \quad \forall i \in \mathbb{N} \setminus \{1\}, \tag{3-10}$$

where $P_1(s)$ in equation (3-9) is the transfer function of the system in (3-4) with output matrix C_1 chosen such that the unstable and marginally stable modes of the system are unobservable [29, 28]. This framework can also be used concerning lateral string stability.

3-2 Lateral String Stability

In this section the model of (2-53) will be used to find the string stability complementary sensitivity function, as given in equation 3-10, for a lateral platoon of vehicles. Consider now a platoon with a leader vehicle. The dynamics for this lead vehicle is given by

$$\begin{bmatrix} \dot{v}_{y,0} \\ \ddot{\psi}_0 \\ \dot{y}_{e,0} \\ \dot{\psi}_{e,0} \\ \dot{\delta}_0 \\ \ddot{\delta}_0 \end{bmatrix} = \begin{bmatrix} -\left(\frac{C_{\alpha_f}+C_{\alpha_r}}{m v_{x,0}}\right) & \left(-v_{x,0} + \frac{bC_{\alpha_r}-aC_{\alpha_f}}{m v_{x,1}}\right) & 0 & 0 & \frac{C_{\alpha_f}}{m} & 0 \\ \left(\frac{bC_{\alpha_r}-aC_{\alpha_f}}{I_z v_{x,0}}\right) & \left(-\frac{a^2C_{\alpha_f}+b^2C_{\alpha_r}}{I_z v_{x,0}}\right) & 0 & 0 & \frac{aC_{\alpha_f}}{I_z} & 0 \\ 0 & 0 & 0 & 0 & 0 & 0 \\ 0 & 0 & 0 & 0 & 0 & 0 \\ 0 & 0 & 0 & 0 & 0 & 1 \\ 0 & 0 & 0 & 0 & -\omega_n^2 & -2\zeta\omega_n \end{bmatrix} \begin{bmatrix} v_{y,0} \\ \dot{\psi}_0 \\ y_{e,0} \\ \psi_{e,0} \\ \delta_0 \\ \dot{\delta}_0 \end{bmatrix} + \begin{bmatrix} 0 \\ 0 \\ 0 \\ 0 \\ 0 \\ \omega_n^2 \end{bmatrix} \delta_{0,ref}, \tag{3-11}$$

which is written in short hand notation as

$$\dot{x}_0 = A_r x_0 + B_r \delta_{0,ref}. \tag{3-12}$$

Control input $\delta_{0,ref}$ comes from a pre-programmed steering command on the vehicle. Steering of the lead vehicle can also be done by a human operator. This however, would require a different model description as the steering model includes actuator dynamics. Although the error states are still included, they have no dynamics. The lead vehicle is completely

independent of the rest of the platoon. From (2-53), the closed loop dynamics of any of the trailing vehicles can be written as

$$\dot{x}_i = A_i x_i + A_{i-1} x_{i-1} (t - \Delta t) . \tag{3-13}$$

As the control action directly depends on the preceding vehicles states, in closed loop, The dynamics of vehicle i depend on its own dynamics and that of the preceding vehicle. In spirit of equation 3-1, the cascade of the lateral system is then written as

$$\dot{x}_0 = A_r x_0 + B_r \delta_{0,ref}, \tag{3-14a}$$
$$\dot{x}_i = A_i x_i + A_{i-1} x_{i-1} (t - \Delta t) , \qquad i \in \mathcal{S}_m \tag{3-14b}$$
$$y_i = C_i x_i. \qquad i \in \mathcal{S}_m \tag{3-14c}$$

A difference between (3-14) and (3-1) is the time delay Δt. In longitudinal platooning control action is applied immediate upon change in acceleration. This can not be done for lateral platooning, as the trailing vehicle first needs to arrive at the correct location before starting to steer. If this is not the case, then the vehicles would drive completely different paths. In [21] it is shown that this delay does not influence the string stability analysis of the system, and the same transfer functions can be used as those derived in [20] and section 3-1.

3-3 Platoon Block Scheme

Figure 3-1 shows the block scheme of the interconnected vehicle platoon as given in (2-53).

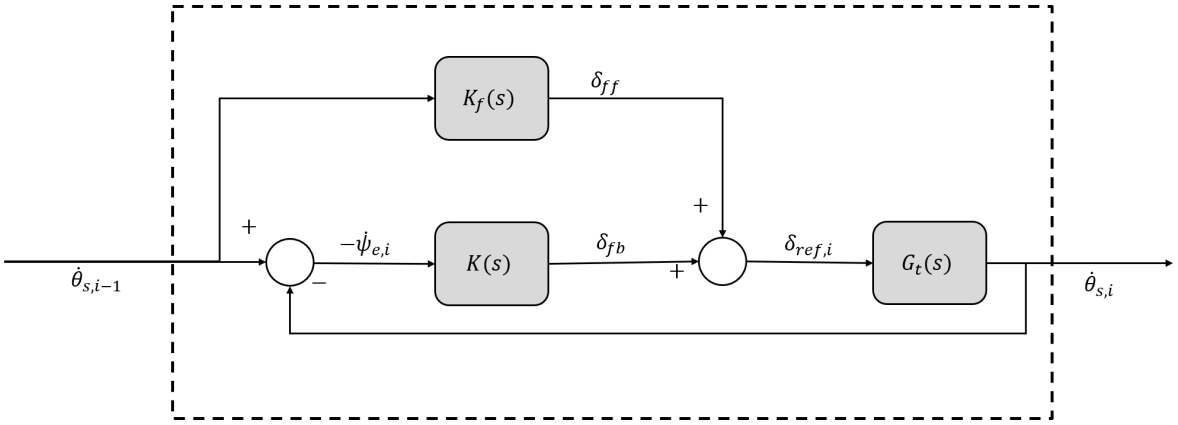

Figure 3-1: Block Scheme of a vehicle in the platoon.

In figure 3-1, the block $K_f(s)$ denotes a feed forward controller, to be designed on the signal $\dot{\theta}_{s,i-1}$. The block $K(s)$ contains the controller structure, which will be elaborated in section 3-4. Finally the block $G_t(s)$ is the transfer function from control input $\delta_{i,ref}$ to output $\dot{\theta}_{s,i}$. Neither $K_f(s)$, $K(s)$ nor $G_t(s)$ carry index i as homogeneity is assumed for the platoon, meaning the dynamics and in extend the controllers will all be the same. To arrive at transfer function $G_t(s)$ the output matrix C_i is taken as

$$C_i = \begin{bmatrix} -\left(\frac{C_{\alpha_f}+C_{\alpha_r}}{m v_{x,i}^2}\right) & \left(\frac{bC_{\alpha_r}-aC_{\alpha_f}}{m v_{x,i}^2}\right) & 0 & 0 & \frac{C_{\alpha_f}}{m v_{x,i}^2} & 0 \end{bmatrix}, \tag{3-15}$$

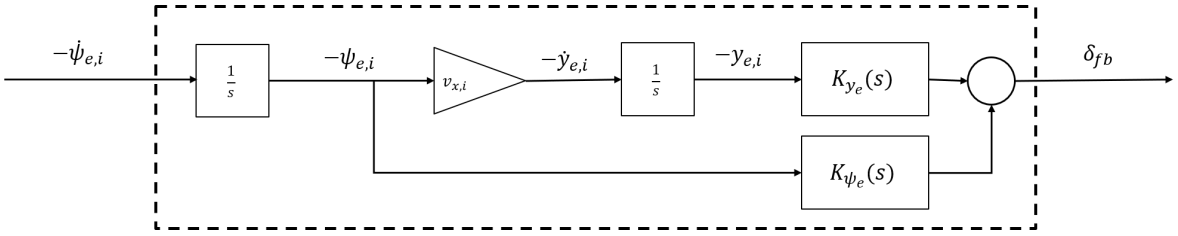

Figure 3-2: Control block scheme internal structure.

for the state space system in (2-47). Further analysis of the state space system in (2-47) shows that both heading and lateral offset error follows in the Laplace domain:

$$\psi_{e,i} = \frac{1}{s}\dot{\psi}_{e,i} = \frac{1}{s}\left(\dot{\theta}_{s,i} - \dot{\theta}_{s,i-1}\right), \tag{3-16a}$$

$$y_{e,i} = \frac{v_{x,i}}{s^2}\dot{\psi}_{e,i} = \frac{v_{x,i}}{s^2}\left(\dot{\theta}_{s,i} - \dot{\theta}_{s,i-1}\right). \tag{3-16b}$$

The vehicle interconnection becomes apparent by the fact that the $\dot{\theta}_{s,i-1}$ signal from the preceding vehicle can be interpreted as a reference signal for the trailing vehicle. The error between the reference and the vehicle output is then the error defined as $\dot{\psi}_{e,i}$. Note that the block scheme in figure 3-1 excludes any form of delay, one of the assumptions in this thesis. The block $K(s)$ can be further expanded, using the error definitions as in equation 3-16, into the block scheme in Figure 3-2. Although ultimately the system will also have an observer included in the closed loop, control design is done with the idea that both error states $y_{e,i}$ and $\psi_{e,i}$ are accessible. Because the system is observable this is the case. Therefore, there is no reference to the observer in the following analysis.

The blocks $K_{y,e}(s)$ and $K_{\psi,e}$ denote the individual feedback controllers to be developed. The structure is based on the definitions given in (3-16). From the block scheme in Figure 3-1 the string stability complementary sensitivity function can be deduced. It is given by (where the (s) notation is dropped for convenience)

$$\Gamma_i = \frac{G_t K_f + G_t K}{1 + G_t K} = \frac{G_t K_f}{1 + G_t K} + \frac{G_t K}{1 + G_t K}. \tag{3-17}$$

In equation 3-17 two classical closed loop transfer functions can be found. Equation 3-17 can also be written as

$$\Gamma_i = \frac{G_t K_f + G_t K}{1 + G_t K} = G_t K_f S + T \tag{3-18}$$

where $S = \frac{1}{1+L}$ is the sensitivity function for a typical feedback system, and $T = \frac{L}{1+L}$ the complementary sensitivity function. In both these functions L is the loop-gain of the open-loop, defined as $L = KG_t$. Using well established properties for these transfer functions, limitations on the string stability of the system will be explored.

3-4 Analysis of String Stability Properties

Given the string stability equation for the interconnected vehicle system depicted in figure 3-1, we now show that string stability cannot be achieved for this system when using only

feedback control. Before giving the proof, first Bode's integral theorem will be introduced in this section 3-5-1. It forms the basis on which the proof is given. Section 3-5-2 will evaluate the system given in figure 3-1 in terms of excess poles in the system to determine which form of the Bode integral has to be used. Section 3-5-3 will show infeasibility for a system with only feedback controllers. Section 3-5-4 will show that with a feedforward - feedback structure it might be possible to achieve string stability for this system, but that the gain of the individual feedback controllers has to be so large, that in practice it is an infeasible solution. From this analysis it is concluded that, although theoretically possible, practically speaking the system cannot be made string stable.

3-4-1 Bode's Integral Theorem

Bode's integral theorem developed for feedback design can be stated as [30]

$$\int_0^\infty \ln|S(j\omega)|\,d\omega = \int_0^\infty \ln\left|\frac{1}{1+L(j\omega)}\right| d\omega = \pi \sum \mathfrak{Re}(p_k), \tag{3-19}$$

where $S(j\omega)$ is the sensitivity function, and $L(j\omega) = C(j\omega)G(j\omega)$ is the loop gain. Appendix B goes into greater detail and gives the derivation for Bode's Integral. In Equation 3-19 p_k denotes any of the unstable poles in the loop gain, $L(j\omega)$. For a system with only stable poles, the integral will be equal to zero. The integral defines a conservation law and it quantifies the waterbed effect. The waterbed effect is a term that is used to describe that attenuation in one frequency range results in amplification in another frequency range. In similar fashion we can write a Bode integral for the complementary sensitivity function as [31]

$$\int_0^\infty \frac{1}{\omega^2}\ln|T(j\omega)|\,d\omega = \int_0^\infty \frac{1}{\omega^2}\ln\left|\frac{L(j\omega)}{1+L(j\omega)}\right| d\omega = \pi\sum_{i=1}^{n_{uz}}\frac{1}{z_i} + \frac{\pi\tau}{2}. \tag{3-20}$$

In Equation 3-20 n_{uz} is the total number of unstable zeros in the complenetary sensitivity function, z_i is the i^{th} unstable zero and τ is the time delay. Recall that in this work time delay is assumed to be zero. Like Bode's integral, the integral over the complementary sensitivity function is conservative if there are no unstable zeros in the loop gain and time delay is not present in the model,

$$\int_0^\infty \frac{1}{\omega^2}\ln|T(j\omega)|\,d\omega = \int_0^\infty \frac{1}{\omega^2}\ln\left|\frac{L(j\omega)}{1+L(j\omega)}\right| d\omega = 0. \tag{3-21}$$

The integrals in Equation 3-20 and 3-21 are conservative integrals. They form the basis of one of the fundamental trade-offs that has to be made in classical feedback control design.

3-4-2 Bode's Integral Theorem Applied for String Stability Analysis

We will now analyse the transfer function in equation 3-17 using Bode's Integral applied to the complementary sensitivity function. First the pole excess of the loop gain $L(s) = G_t(s)K(s)$ is analysed. The transfer function $G_t(s)$ is given by

$$G_t(s) = C_i\left(sI - A\right)^{-1}B + D \tag{3-22}$$

with the matrices as defined in equation 2-47 and output matrix C_i as in equation 3-15. Transfer function G_t has two free integrators in its transfer function, and $D = 0$. Controller $K(s)$ can be written as

$$\delta_{i,ref} = \left(\frac{u_i}{s^2}K_{y_{e,i}}(s) + \frac{1}{s}K_{\psi_{e,i}}(s)\right)\dot{\psi}_{e,i} = \left(\frac{v_{x,i}K_{y_{e,i}}(s) + sK_{\psi_{e,i}}(s)}{s^2}\right)\dot{\psi}_{e,i}. \tag{3-23}$$

Both controllers in $K(s)$, $K_{y_{e,i}}(s)$ and $K_{\psi_{e,i}}(s)$, are proper transfer functions. This means that they will have at least an equal amount of poles and zeros in their transfer function, or more poles than zeros. Because the transfer function $K(s)$ already has two free integrators, regardless of controllers $K_{y_{e,i}}(s)$ and $K_{\psi_{e,i}}(s)$, the overall loop gain $L(s)$ will have $4 + x$ free integrators. Another two free integrators are added by $G_t(s)$ and x is the number of integrators the controller $u_iK_{y_{e,i}}(s) + sK_{\psi_{e,i}}(s)$ adds. Hence equation 3-20 can be used to analyse the system.

3-4-3 System with Only Feedback

Consider now the closed loop system in figure 3-1 without any feedforward control, i.e. $K_f = 0$, then the string stability complementary sensitivity function reduces to

$$\Gamma_i = \frac{G_tK}{1 + G_tK} = \frac{L}{1 + L}. \tag{3-24}$$

From the analysis in section 3-4-1, and the integral given in equation 3-20 we know that for this system this integral has to be equal to zero, as it has at least two free integrators, and thus the following integral

$$\int_0^\infty \ln|\Gamma_i|\, d\omega = \int_0^\infty \ln\left|\frac{G_tK}{1 + G_tK}\right| d\omega = \int_0^\infty \ln\left|\frac{L}{1 + L}\right| d\omega = 0. \tag{3-25}$$

From the requirements we desire good tracking performance. Good tracking performance requires $|S(j\omega)|$ to be small for low frequencies. From linear system theory we know that $|S(j\omega) + T(j\omega)| = 1$, so if $|S(j\omega)|$ is small at low frequencies, then $|T(j\omega)| = 1$, such that the equality holds. From equation 3-19 we deduced that the area under $|S(j\omega)|$ is equal to zero, the integral is conservative. At high frequencies it is desired that $|T(j\omega)| << 1$, for noise suppression. This inherently means that $|S(j\omega)| \approx 1$. Becauase both the Bode integral over $|S(j\omega)|$ and $|T(j\omega)|$ are conservative integrals, their negative area in low and high frequency domain, respectively, needs to be counter by positive area. It means that at some frequency both $|S(j\omega)| > 1$ and $|T(j\omega)| > 1$ for the integral to hold.

The string stability complementary sensitivity function is the frequency response function from the disturbance input $\dot{\theta}_{s,i-1}$ to $\dot{\theta}_{s,i}$. If this transfer function has no high frequency roll-off, any small disturbance, or noise, in signal $\dot{\theta}_{s,i-1}$ will be present in the signal of $\dot{\theta}_{s,i}$. To counteract this it is also desired to have high frequency roll-off in the string stability complementary senstivity function. The complementary sensitivity function and string stability complementary sensitivity function are the same when using only feedback controllers. Since for both functions it is desired to have high frequency roll-off, i.e., $|T(j\omega)| << 1$, it must mean that $|T(j\omega)|$ has to be larger than 1 at some frequency. This contradicts our requirement on string stability. From this it is concluded that when using the vehicle-road error model from chapter 2 with only a feedback controller, no matter what the system will never be string stable.

3-4-4 System with Feedback and Feedforward

Before starting this section, the author feels the need for a disclaimer. A large part of this thesis was spent investigating the properties of the string stability properties of the same system, but with both a feedback and feedforward controller. Several thought experiments can be used to to explain why it might be also impossible to achieve string stability when a feedforward controller is present in the system. The author acknowledges that this, however, is not a formal proof. Finally it was decided to make the argument based on the analysis in given in this section. Appendix B gives an alternative derivation based on Bode's integral, by which it can also be proven that string stability is not achievable using both feedforward and feedback controllers. *It could well be that one of the, or both arguments, can be disproven. They are nevertheless included in the thesis to serve as starting point for anyone else doing research in this area.*

Starting now with the actual derivation, in Chapter 4 the use of an H_∞ synthesis is motivated. In H_∞ synthesis the goal is to minimize the norm of a transfer function that can be found by doing the lower fractional expansion for the optimization set-up. The full details can be found in Chapter 4. For now it serves to give the lower fractional expansion as function of the earlier introduced transfer functions G_t, K_f, $k_{y_{e,i}}$ and $K_{\psi_{e,i}}$. Doing this gives insight in potential controller solutions that make the system string stable. For this optimization process the lower fractional expansion is given by

$$N = \left(\frac{s^2\Big(G_t(s)K_f(s) - 1\Big)}{-s^2 + G_t(s)K_{\psi_{e,i}}(s)s + G_t(s)K_{y_{e,i}}(s)} \right). \tag{3-26}$$

The goal of an H_∞ optimized controller is to minimize the infinity norm of (3-26) as a function of the controllers. Given that weight $W_T = 1$, the optimization can be written as

$$\begin{aligned}
\min_K ||N||_\infty &= \min_K \max_s \left| \frac{s^2\Big(G_t(s)K_f(s) - 1\Big)}{-s^2 + G_t(s)K_{\psi_{e,i}}(s)s + G_t(s)K_{y_{e,i}}(s)} \right| \leq 1 \\
&= \min_K \sup_\omega \left| \frac{-\omega^2\Big(G_t(j\omega)K_f(j\omega) - 1\Big)}{\omega^2 + G_t(j\omega)K_{\psi_{e,i}}(j\omega)j\omega + G_t(j\omega)K_{y_{e,i}}(j\omega)} \right| \\
&= \min_K \sup_\omega \frac{\left|-\omega^2\Big(G_t(j\omega)K_f(j\omega) - 1\Big)\right|}{\left|\Big(\omega^2 + G_t(j\omega)K_{\psi_{e,i}}(j\omega)j\omega + G_t(j\omega)K_{y_{e,i}}(j\omega)\Big)\right|} \\
&= \min_K \sup_\omega \frac{\omega^2\left|\Big(G_t(j\omega)K_f(j\omega) - 1\Big)\right|}{\left|\Big(\omega^2 + G_t(j\omega)K_{\psi_{e,i}}(j\omega)j\omega + G_t(j\omega)K_{y_{e,i}}(j\omega)\Big)\right|} \leq 1
\end{aligned} \tag{3-27}$$

Writing out the absolute values in (3-27) allows us to gain insight in the magnitude of controller gains required to make the system string stable. Using the triangle inequality it is

possible to find an upper bound the maximum absolute value of the denominator of (3-27) can attain. The triangle inequality states that $|a+b| \leq |a| + |b|$. Dropping the $j\omega$ notation for clarity, we can obtain

$$\begin{aligned}\left|\left(\omega^2 + G_t K_{\psi_{e,i}} j\omega + G_t K_{y_{e,i}}\right)\right| &= \omega^2 + |G_t| \left|K_{\psi_{e,i}} j\omega + K_{y_{e,i}}\right| \\ &= \omega^2 + |G_t| \sqrt{\left(K_{\psi_{e,i}} j\omega + K_{y_{e,i}}\right)\left(K_{\psi_{e,i}} j\omega + K_{y_{e,i}}\right)^*},\end{aligned} \tag{3-28}$$

where the * denotes the complex conjugate. Continuing the equality yields that

$$\begin{aligned}\left|\left(\omega^2 + G_t K_{\psi_{e,i}} j\omega + G_t K_{y_{e,i}}\right)\right| &= \omega^2 + |G_t| \sqrt{\left(K_{\psi_{e,i}} j\omega + K_{y_{e,i}}\right)\left(K_{\psi_{e,i}} j\omega + K_{y_{e,i}}\right)^*} \\ &= \omega^2 + |G_t| \sqrt{\omega^2 \left|K_{\psi_{e,i}}\right|^2 + \left|K_{y_{e,i}}\right|^2 - K_{y_{e,i}} K^*_{\psi_{e,i}} j\omega + K^*_{y_{e,i}} K_{\psi_{e,i}} j\omega} \\ &= \omega^2 + |G_t| \sqrt{\omega^2 \left|K_{\psi_{e,i}}\right|^2 + \left|K_{y_{e,i}}\right|^2 + j\omega\left(-K_{y_{e,i}} K^*_{\psi_{e,i}} + K^*_{y_{e,i}} K_{\psi_{e,i}}\right)}.\end{aligned} \tag{3-29}$$

Evaluating the square root at the end of equation 3-29

$$\sqrt{\omega^2 \left|K_{\psi_{e,i}}\right|^2 + \left|K_{y_{e,i}}\right|^2 + j\omega\left(-K_{y_{e,i}} K^*_{\psi_{e,i}} + K^*_{y_{e,i}} K_{\psi_{e,i}}\right)}, \tag{3-30}$$

it can be written as

$$\sqrt{\omega^2 \left|K_{\psi_{e,i}}\right|^2 + \left|K_{y_{e,i}}\right|^2 + j\omega\left(-K_{y_{e,i}} K^*_{\psi_{e,i}} + \left(K_{y_{e,i}} K^*_{\psi_{e,i}}\right)^*\right)}. \tag{3-31}$$

For any ω the multiplication $K_{y_{e,i}} K^*_{\psi_{e,i}}$ will yield a number of the form $a + bj$, where either a or b can be, but not necessarily are, equal to 0. Then

$$\left(-K_{y_{e,i}} K^*_{\psi_{e,i}} + \left(K_{y_{e,i}} K^*_{\psi_{e,i}}\right)^*\right) = -(a+bj) + (a+bj)^* = -2bj. \tag{3-32}$$

Inserting it into the equation gives

$$\sqrt{\omega^2 \left|K_{\psi_{e,i}}\right|^2 + \left|K_{y_{e,i}}\right|^2 + 2b\omega}, \tag{3-33}$$

thus

$$\begin{aligned}\left|\left(\omega^2 + G_t K_{\psi_{e,i}} j\omega + G_t K_{y_{e,i}}\right)\right| &= \omega^2 + |G_t| \sqrt{\left(K_{\psi_{e,i}} j\omega + K_{y_{e,i}}\right)\left(K_{\psi_{e,i}} j\omega + K_{y_{e,i}}\right)^*} \\ &= \omega^2 + |G_t| \sqrt{\omega^2 \left|K_{\psi_{e,i}}\right|^2 + \left|K_{y_{e,i}}\right|^2 - K_{y_{e,i}} K^*_{\psi_{e,i}} j\omega + K^*_{y_{e,i}} K_{\psi_{e,i}} j\omega} \\ &= \omega^2 + |G_t| \sqrt{\omega^2 \left|K_{\psi_{e,i}}\right|^2 + \left|K_{y_{e,i}}\right|^2 + 2b\omega}.\end{aligned} \tag{3-34}$$

Having found an expression for the maximum of the denominator of (3-27) let us consider the numerator of (3-27). The absolute value of in the numerator of (3-27) can be written as

$$\begin{aligned}\omega^2 \left|\left(G_t K_f - 1\right)\right| &= \omega^2 \sqrt{\left(G_t K_f - 1\right)\left(G_t K_f - 1\right)^*} \\ &= \omega^2 \sqrt{|G_t|^2 |K_f|^2 - \left(G_t K_f\right) - \left(G_t K_f\right)^* + 1}\end{aligned}. \tag{3-35}$$

Saying again, that for a frequency ω_m, $G_t(j\omega_m)K_f(j\omega_m) = c + dj$, where again c and/or d can be, but are not necessarily, equal to 0. Then the absolute value is given by

$$\omega^2 \left| \left(G_t K_f - 1 \right) \right| = \omega^2 \sqrt{|G_t|^2 |K_f|^2 - 2c + 1}. \tag{3-36}$$

Because $|G_t(j\omega)|$, and $G_t(j\omega)$ approach zero as frequency increases the absolute value converges to 1 (the value c will also vanish because it is dependant on $G_t(j\omega)$).

Writing out the supremum that needs to be minimized for a general feedforward controller $K_f(j\omega)$ gives that

$$\omega^2 + |G_t| \sqrt{\omega^2 \left| K_{\psi_{e,i}} \right|^2 + \left| K_{y_{e,i}} \right|^2 + 2b\omega} \geq \omega^2 \sqrt{|G_t|^2 |K_f|^2 - 2c + 1}, \tag{3-37}$$

has to hold for $||N||_\infty \leq 1$.The norm on the right hand side will go towards infinity as frequency increases. To make sure the inequality holds, the square root $|G_t| \sqrt{\omega^2 \left| K_{\psi_{e,i}} \right|^2 + \left| K_{y_{e,i}} \right|^2 + 2b\omega}$ has to go to infinity faster than the right hand side of (3-37). However, $|G_t|$ goes to zero as frequency increases. To have the inequality hold, controller gains of $K_{\psi_{e,i}}$ and/or $K_{y_{e,i}}$ then have to go to infinity. This is an infeasible result, and in stark contrast to the desire to have real world implementable controllers. It is from this result that it is concluded that string stability is very difficult or impossible to achieve.

3-5 Short Discussion

In this chapter string stability was introduced. Based on the analysis for a longitudinal platoon, a mathematical definition for lateral string stability can be found. Based on the analysis of how the errors are defined in Chapter 2 it is shown that there are limitations when it comes to achieving string stability. When employing only feedback controllers it turn out to be a fundamental limitation, based on the conservation properties of Bode's integral. The argument for the feedforward-feedback structure is a bit weaker. The inequality in (3-37) can be met for low frequencies. It becomes difficult, however, when the value of $|G_t|$ starts becoming smaller, something that happens when frequencies increases. To keep the inequality intact the gains of the controllers $K_{\psi_{e,i}}$ and/or $K_{y_{e,i}}$ have to rise, something which is undesired from an actuation and noise sensitivity limitation. High frequency roll-off is still expected in the system. In the square root $\sqrt{\omega^2 \left| K_{\psi_{e,i}} \right|^2 + \left| K_{y_{e,i}} \right|^2 + 2b\omega}$, $\omega^2 + 2b\omega$ will continue to grow as frequency increases. At a certain frequency, $\omega^2 + |G_t| \sqrt{\omega^2 \left| K_{\psi_{e,i}} \right|^2 + \left| K_{y_{e,i}} \right|^2 + 2b\omega}$ is expected to overtake $\omega^2 \sqrt{|G_t|^2 |K_f|^2 - 2c + 1}$ again. It is in the area where ω is still too small to have this happen, that high controller gains are needed to have the inequality hold.

Chapter 4

Control Design

Controllers designed for lateral control in autonomous driving aim to generate a steering such that a reference path or preceding vehicle can be followed. In this chapter a control design method will be proposed such that string instability can be minimized whilst also assuring that the tracking requirements are met. In Chapter 3 several notions of string stability were explored, where one was based on an infinity norm, as seen in equation 3-10. This motivates the development of an H_∞ based controller. This is further motivated by the desire to minimize the lateral overshoot caused by the string instability. Using the platoon framework developed in Chapter 3, a generalized plant can be formulated to be used in H_∞ control optimization.

Section 4-1 will further explore the control targets set for the controllers. Section 4-2 explains the theory behind H_∞ control optimization. Building upon that, section 4-3 covers how the platoon model from section 3-3 can be adapted for the controller optimization. It will further explain how the weights can be designed to meet the control requirements. Finally the results from the optimization will be evaluated in section 4-4.

4-1 Control Targets

The goal for the controller is to minimize the positional errors of the vehicle with respect to a certain path. A two degree of freedom controller will be designed, comprising of a feedforward and feedback controller. The feedback controller will consist of two individual feedback controllers, one for each road error state. The vehicles will be indirectly steered through a reference steering command. The controllers need to be able to

- Follow a path asymptotically, the path errors need to go to zero as time goes to infinity and external input is constant, or

$$\lim_{t\to\infty} y_{e,i}(t) = 0 \quad \forall \ddot{\theta}_{s,i-1} = 0, \tag{4-1a}$$

$$\lim_{t\to\infty} \psi_{e,i}(t) = 0 \quad \forall \ddot{\theta}_{s,i-1} = 0, \tag{4-1b}$$

- The controllers should generate a reference command such that a vehicle is physically capable of following it, i.e, the controllers are constrained by the hardware available on the vehicles.
- Minimize overshoot caused by string instability.

Based on these three requirements one can formulate weights for the H_∞ control design. Before analysing how the H_∞ optimization is implemented for the platoon controller, first H_∞ optimization is briefly introduced.

4-2 H_∞ Control Optimization

Any classical feedback control loop, as for example the one in Figure 3-1 can also be represented in a generalized plant structure, as in Figure 4-1.

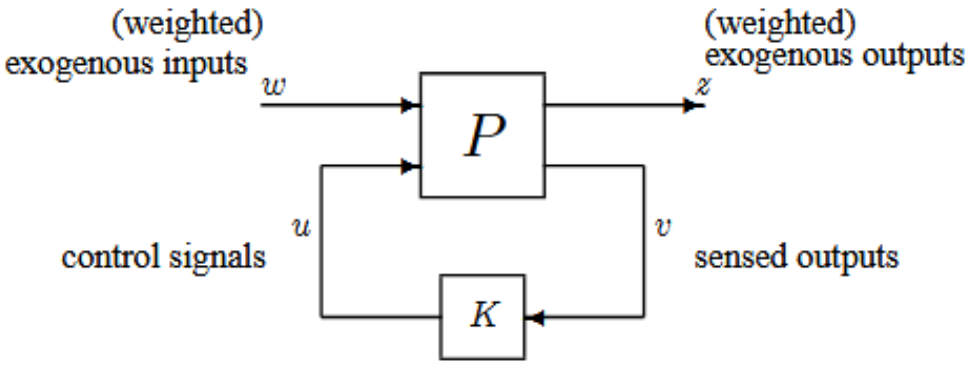

Figure 4-1: General Feedback/Forward control configuration [32].

In figure 4-1 the block P represents the plant. The plant contains all the dynamics, and where applied weights used in the optimization. The plant has two inputs, namely w, a so-called exogenous input and the control input u. The input w can, but doesn't necessarily have to, comprise of the reference, input disturbance and output disturbance signals. Two outputs can also be defined, z the exogenous outputs and v the sensed outputs. The output z contains signals that are weighted and to be used in the optimization process. The output v contains all measurements used for the controller.

The plant P represents then the collection of transfer functions from the two inputs to the two outputs and in general is comprised of the following four blocks:

$$\begin{bmatrix} z \\ v \end{bmatrix} = \begin{bmatrix} P_{11} & P_{12} \\ P_{21} & P_{22} \end{bmatrix} \begin{bmatrix} w \\ u \end{bmatrix}. \tag{4-2}$$

The size of the blocks $P_{i,j}$ $i, j \in [1, 2]$ is dependant on the size of their respective inputs and outputs. The goal of an H_∞ optimized controller K is to minimize the H_∞ norm of the

transfer function from w to z as a function of controller(s) K and with weights W. Without going into too much detail, from [33] this closed-loop transfer function reads

$$N = P_{11} + P_{12}K\left(I - P_{22}K\right)^{-1}P_{21}, \tag{4-3}$$

where N can be found by performing the lower fractional expansion of the Equation 4-2. The controllers are then designed solving the following minimization problem:

$$\min_K ||N||_\infty . \tag{4-4}$$

The optimization can be reformulated through the use of weights. These can be scalar values, or transfer functions that are to be designed. The next section will explain the use of weights in H_∞ optimization.

4-2-1 Transfer Function Weights

The generalized plant in Figure 4-1 can also be depicted as in Figure 4-2

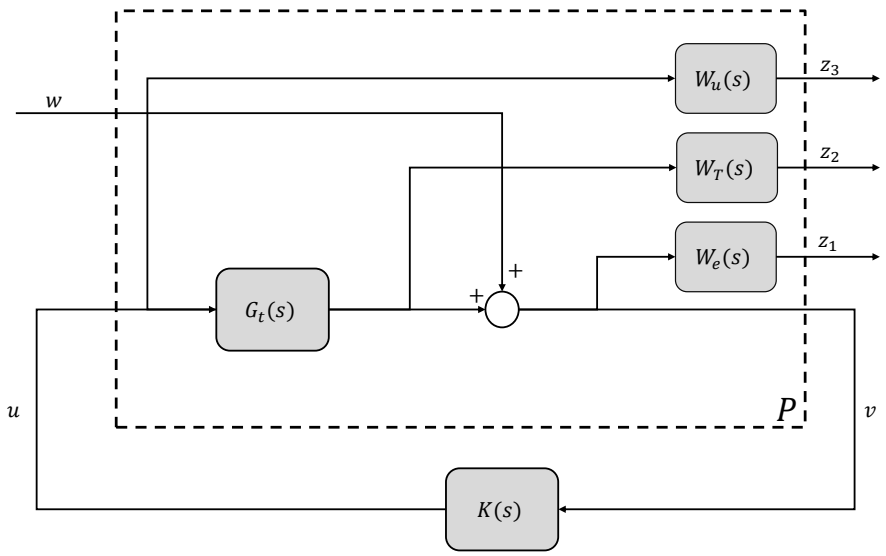

Figure 4-2: Generalized plant with weights.

Here it is assumed that there are no disturbances present in the system and hence only the reference signal is an exogenous input. Included in the generalized plant, P, are now three weights. More (or less) weights can be implemented, as many as the designer desires, but typically three weights are chosen. Weight W_u weights the control action and can be used to limit controller action. Weight W_T weights the complementary sensitivity function, and can be used to weight the system performance and finally weight W_e weights the error signal and can be used to regulate the amount of steady state error the system will have. The next

section shows how the platoon model can be adapted to this framework and what weights will be used.

The generalized plant P, for the system in Figure 4-2 is given by

$$P = \left[\begin{array}{c|c} W_e & W_e G_t \\ 0 & W_T G_t \\ 0 & W_u \\ \hline I & G \end{array}\right] = \left[\begin{array}{c|c} P_{11} & P_{12} \\ \hline P_{21} & P_{22} \end{array}\right]. \tag{4-5}$$

Taking the LFT of (4-5) gives for the following N that has to be minimized

$$N = \begin{bmatrix} W_e S \\ W_T T \\ W_u K S \end{bmatrix}, \tag{4-6}$$

where S and T are again the complementary sensitivity functions as defined in Chapter 3. When $||N||_\infty = \gamma$, with $\gamma > 0$, then

$$\left|\left|\begin{bmatrix} S \\ T \\ KS \end{bmatrix}\right|\right|_\infty \leq \gamma \left|\left|\begin{bmatrix} W_e^{-1} \\ \frac{1}{W_T} \\ \frac{1}{W_u} \end{bmatrix}\right|\right|_\infty. \tag{4-7}$$

The following minimization

$$\min_K \left|\left|\begin{bmatrix} W_e S \\ W_T T \\ W_u K S \end{bmatrix}\right|\right|_\infty. \tag{4-8}$$

searches for an optimal controller K such that,

$$\left|\left|\begin{bmatrix} S \\ T \\ KS \end{bmatrix}\right|\right|_\infty \leq \gamma \left|\left|\begin{bmatrix} W_e^{-1} \\ \frac{1}{W_T} \\ \frac{1}{W_u} \end{bmatrix}\right|\right|_\infty, \tag{4-9}$$

and thus the weights can be used to shape the transfer functions. In this way performance can be tuned much the same way it is done using manual loop shaping. The form of these weights is then up to the user to decide and is based on performance requirements.

4-3 H_∞ Control Optimization for Platoon Model

The platoon model for a single vehicle in the platoon, as shown in Figure 3-1, can also be adapted to be suited for use in H_∞ optimization. To that end the model is adapted, such that a generalized plant can be found. This can be seen in Figure 4-3

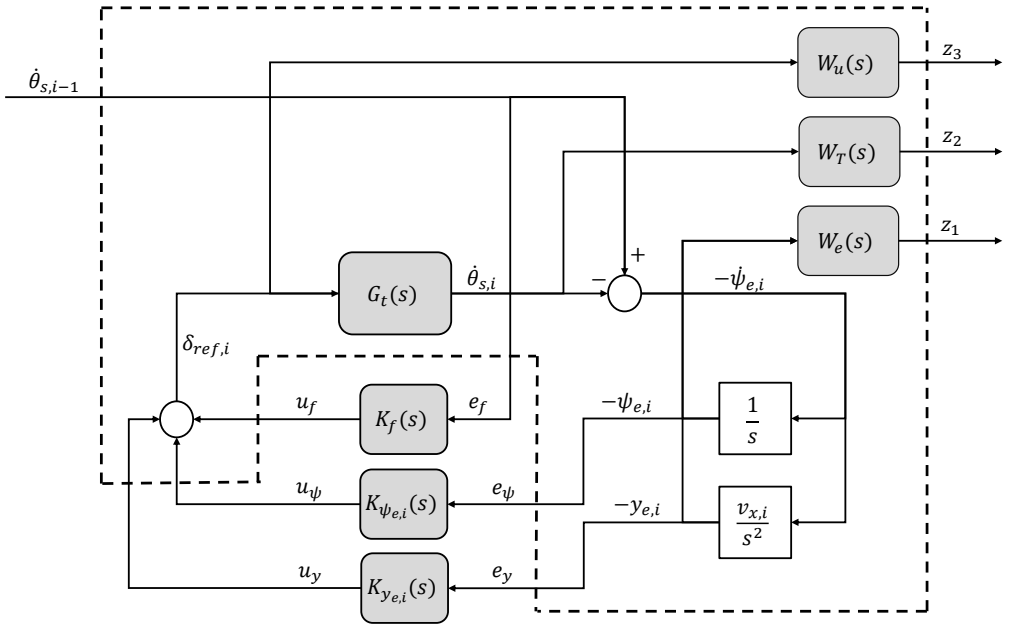

Figure 4-3: Generalized plant with implemented weights for the platoon model. Adapted from Figure 3-1.

The dashed line indicates everything contained in the generalized plant. The plant has 4 inputs, the exogenous input being the rotation of the curvature of the road caused by the preceding vehicle, $\dot{\theta}_{s,i-1}$, and three control inputs u_f, u_ψ and u_y, each for the individual controllers. As with the example in the preceding section it was opted to go with three weights. Their use and design will be explained. These weights are responsible for 3 of the 6 outputs, namely the three performance outputs, $z_i,\ i \in [1,2,3]$. The other three signals e_f, e_ψ and e_y are the errors signals for which each of the individual controllers will be designed. The generalized plant is given by

$$\begin{bmatrix} z_1 \\ z_2 \\ z_3 \\ e_f \\ e_\psi \\ e_y \end{bmatrix} = \begin{bmatrix} W_eE & -G_tW_eE & -G_tW_eE & -G_tW_eE \\ 0 & W_TG_t & W_TG_t & W_TG_t \\ 0 & W_u & W_u & W_u \\ 1 & 0 & 0 & 0 \\ \frac{1}{s} & \frac{-G_t}{s} & \frac{-G_t}{s} & \frac{-G_t}{s} \\ \frac{v_{x,i}}{s^2} & \frac{-v_{x,i}}{s^2}G_t & \frac{-v_{x,i}}{s^2}G_t & \frac{-v_{x,i}}{s^2}G_t \end{bmatrix} \begin{bmatrix} \dot{\theta}_{s,i-1} \\ u_f \\ u_\psi \\ u_y \end{bmatrix}. \tag{4-10}$$

In (4-10) the matrix E is a diagonal matrix given by

$$E = \begin{bmatrix} \psi_{e,i} & 0 \\ 0 & y_{e,i}, \end{bmatrix} \tag{4-11}$$

and its accompanying weight is given by

$$W_e = \begin{bmatrix} W_{e_{1,1}} & 0 \\ 0 & W_{e_{2,2}}, \end{bmatrix}. \tag{4-12}$$

To better understand how to design the weights, each output z_i can be written as a function of exogenous input $\dot{\theta}_{s,i-1}$. Starting with output z_1, it can be written as

$$z_1 = W_e \left(I - G_t K_{fb}\right)^{-1} \left(I - G_t K_f\right) \dot{\theta}_{s,i-1}, \tag{4-13}$$

and z_2 as

$$z_2 = W_T \Gamma_i \dot{\theta}_{s,i-1}, \tag{4-14}$$

with Γ_i as in equation 3-17. Finally, performance signal z_3 can be written as

$$z_3 = W_u S \left(K_f + K_{fb}\right). \tag{4-15}$$

In Equations 4-13 and 4-15, K_{fb}, denotes the feedback controllers. This is done to distinguish them from the feedforward controller. Of the three performance signals, z_2 is deemed most interesting, as it can be seen that the weight W_T directly weights the string stability complementary sensitivity function. Hence with weight W_T it is possible to force the optimization to find a solution that meets string stability requirements. Further of interest is the signal z_1. Given a certain boundary on rate of change of the curvature of the road $\dot{\theta}_{s,i-1}$, it is possible to translate how much steady state error in both $\psi_{e,i}$ and $y_{e,i}$ can occur (if any at all). Having defined the generalized plant with weights, and their according performance signals, the weights have to be designed. The following three subsections will deal with each of the weights.

4-3-1 Weight $W_T(s)$

It is desired that, up to a certain frequency, the path driven by each of the vehicles is the same. Effectively this means that for $\Gamma_i(s)$ a DC gain of 1 up to a said frequency is desired. This desired frequency can be taken from a typical highway steering manoeuvre. The steering behaviour for a highway lane change can be approximated as a sinusoidal input on the steering wheel. Typical frequencies for such an input are around 0.1 Hz [34].

From this it is possible to determine the weight on throughput from $\dot{\theta}_{s,i-1}$ to $\dot{\theta}_{s,i}$, weighted by W_T. This relation has to be as close as possible to 1 for up to a bandwidth of 0.1 Hz as it means vehicle following is achieved with minimal corner cutting. Any component of higher frequency is regarded as noise or external input that is not relevant for the vehicle following task and should be ignored. The weight on $\Gamma_i(s)$ is then taken as

$$W_t(s) = \frac{6\pi}{s + 6\pi}. \tag{4-16}$$

The filter frequency is set at 3 Hz such that the -3 dB point is not too close to the desired tracking frequency. The driving factor behind the choice of this weight, comes from the analysis in Chapter 3, section 3-4. If there exists a conservation law for the string stability complementary sensitivity function with both feedforward and feedback controller the system can not be string stable, and have noise rejection. By choosing weight W_T as in (4-16) we open up the frequency area after 3 Hz for this overshoot to occur.

4-3-2 Design of $W_u(s)$

For the weight on the control action the inverse of the steering dynamics is used given in (2-23). The steering dynamics attenuates high-frequency signals. For this reason it is desired that the steering reference is generated in such a manner that it does not contain high-frequency components. The weight is given by

$$W_u(s) = \frac{s^2 + \zeta\omega_n s + \omega_n^2}{\omega_n^2 \cdot (s + 200\pi) \cdot (s + 201\pi)}, \tag{4-17}$$

where the two poles are required to make the transfer function proper.

4-3-3 Design of $W_e(s)$

The design of the error weights is based on the allowable steady state error of the error states. The average turn radius on a Dutch highway is around 750 metres. If this is navigated at a velocity of 80 km/h, then the vehicle has a yaw rate of approximately 0.03 rad/s. From Equation 4-15 the relation between the incoming curvature/yaw-rate and the outgoing error signals is deduced. Using this upper limits for the DC gain of the weights can be designed.

As it was seen that lateral offset error was solely dependant on heading error, having zero steady state error in heading error translates to no further accumulation of lateral offset error. It was found during controller design that using the other weights as is this occurred naturally and that the weight on ψ_{e_i} was not a limiting factor. Furthermore, making the weight less restrictive improved overall controller performance without hampering the steady state error of ψ_{e_i}. The weight is given by

$$W_e(2,2) = \frac{3 + 0.01 \cdot s}{2 + s} \tag{4-18}$$

A similar approach is taken to determine the weight on y_{e_i}. A maximum desired steady state offset is set at 30 cm, approximately a tyres width. Since the maximum expected yaw rate is taken at 0.03 rad/s, it can be calculated what the DC-gain of this transfer function needs to be. This translates to a DC-gain on the yaw rate of maximum 20 dB. Here it was also found that the transfer function of (4-13) is not a limiting factor in the control synthesis. Lowering the weight's DC gain resulted in an equal decrease of DC gain for the transfer function of $\dot{\theta}_{s,i-1}$ to y_{e_i}. Hence the weight given has a DC gain higher than originally designed, but it yields the desired results. It is given by

$$W_e(1,1) = \frac{0.0075 \cdot s + 0.3}{60 \cdot s + \pi}. \tag{4-19}$$

The complete weight matrix is given by

$$W_e(s) = \begin{bmatrix} \frac{0.0075 \cdot s + 0.3}{60 \cdot s + \pi} & 0 \\ 0 & \frac{3 + 0.01 \cdot s}{2 + s} \end{bmatrix}. \tag{4-20}$$

4-4 H_∞ Controller Results

For the actual synthesis the following table shows the vehicle parameters used for the vehicle model of (3-11). This model will be used in the controller synthesis. As the system in (3-11)

Table 4-1: Values for vehicle parameters used in optimization.

Parameter	Value	Description
a	1.1 m	Distance front axle to CoG.
b	1.6 m	Distance rear axle to CoG.
C_{α_f}	117000 Nrad^{-1}	Front tyre Cornering Stiffness.
C_{α_r}	143000 Nrad^{-1}	Rear tyre Cornering Stiffness.
m	1650 kg	Vehicle mass
I_z	2900 kg m^2	Vehicle Inertia
$v_{x,i}$	80 km/h	Design Velocity
ω_n	17.5 rad s^{-1}	Natural frequency steering system
ζ	0.7 [-]	Damping ratio steering system

is of order 6, and the weights are all of order 2, an 8^{th}-order state space controller will be the result from the optimization. Although higher order controllers are generally not preferred because of their complexity, or difficulty for implementation, given the way W_u is designed it ensures that the controllers won't contain any fast modes. Figure 4-4 shows the Bode diagrams of each of the individual controllers, given in black. The horizontal blue lines are the gains of the controllers currently implemented for vehicle following. They are static gains based on steady state vehicle dynamics. More information can be found in [13].

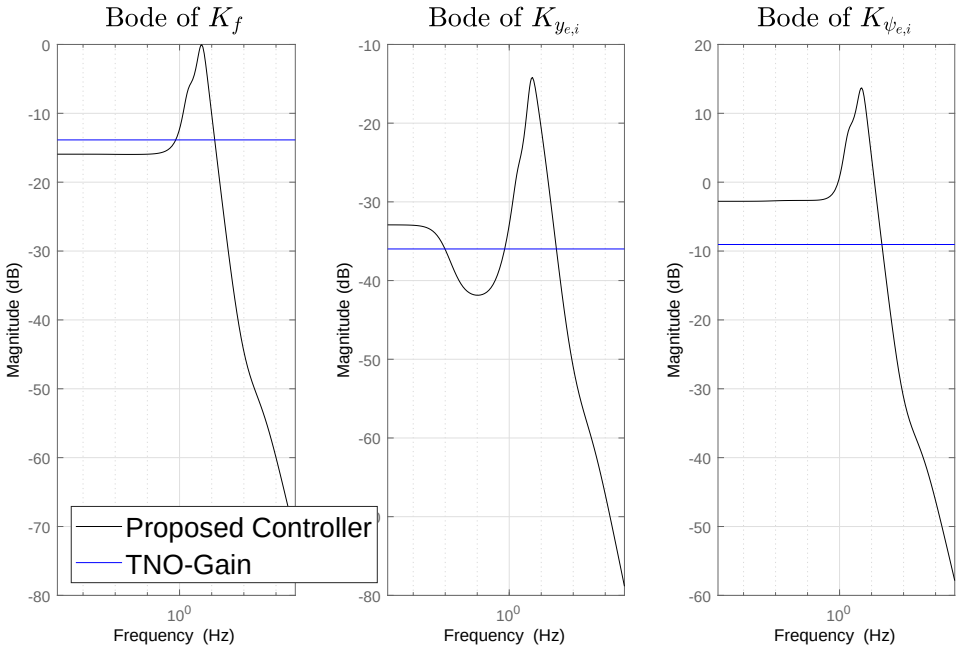

Figure 4-4: Bode diagrams of the synthesized controllers. From left to right $|K_f(s)|$, $|K_{y_{e,i}}|$ and $|K_{\psi_{e,i}}|$.

The optimized controllers in Figure 4-4 have similar steady state gains as those based on

the linear vehicle dynamics. This is to be expected as synthesis is done for a linear model, and at low frequencies the steady state gains provide an accurate description for the relation between steering and vehicle rotation. At higher frequencies differentiator action is desired, after which there is high frequency roll-off, a consequence of the design of weight W_u. Figure 4-5 shows the transfer functions given in (4-13), (4-14) and (4-15) and compares them to their appropriate weight.

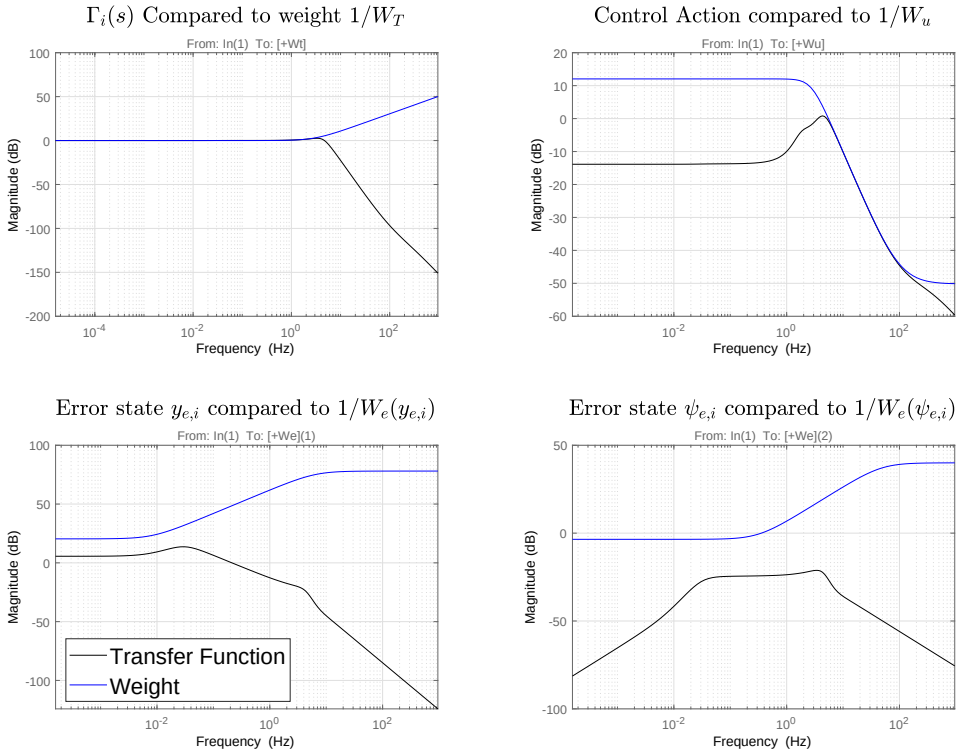

Figure 4-5: Bode diagrams of the transfer functions z_1, z_2 and z_3. Top left shows the comparison between z_2 and its weight W_T. Top right shows the comparison between z_3 and its weight W_u. The bottom left and right shows the comparison for the weight W_e on $y_{e,i}$ and $\psi_{e,i}$ respectively.

As desired the steady state errors on both error states is within bounds, where $\psi_{e,i}$ will have zero steady state error. From Figure 4-5 it can be further seen that both the string stability and control action requirement are the limiting factor. The reason for this was explained in section 3-4. Closer inspection of the string stability complementary sensitivity function in relation to its weights, as seen in Figure 4-6 shows that system is not fully string stable, although the maximum overshoot is around ≈ 1.05.

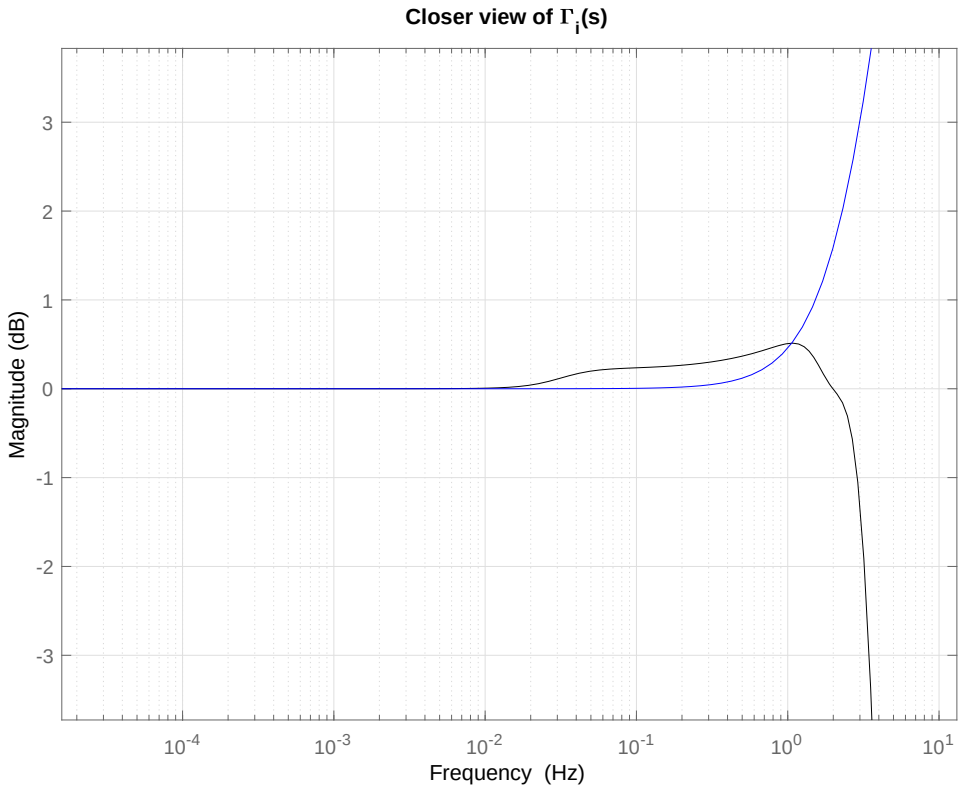

Figure 4-6: Reducing the y-axis scale reveals that with these optimized controllers the system is not string stable, as $||\Gamma_i||_\infty > 1$. It is thought that with this system description the system can never be string stable.

The big downside of this result is that amplification occurs across the frequency range of interest. Nevertheless, this amplification is small. Depending on the amount of vehicles in the platoon, and the type of manoeuvre the total amplification can be limited. A way to analyse this is given in Chapter 6, section 6-2. Unconstraining the weights on the control action does reduce the overshoot, but the optimization will not be able to find feasible controllers that render the system string stable. The analysis in Chapter 3 has shown this in much greater detail. Nevertheless the overshoot was deemed small enough to proceed with simulation.

4-5 Observer Design

Using the fact that the combined error $y_{e,i}+d_i\psi_{e,i}$ is available for measurement when the road error, ε_i, is included in the transmission an observer can be designed to allow access to the individual road error states. In the previous section it was assumed that $y_{e,i}$ and $\psi_{e,i}$ are both accessible. Without access to the states the proposed controllers can not be implemented. For this the observer is requirement. Consider the state space system of (2-47) but with the output matrix chosen as

$$C_{obs} = \begin{bmatrix} 0 & 0 & 1 & d_i & 0 & 0 \end{bmatrix}, \tag{4-21}$$

The observability matrix

$$\begin{bmatrix} C_{obs} \\ C_{obs}A \\ C_{obs}A^2 \\ \vdots \\ C_{obs}A^{n-1} \end{bmatrix} \tag{4-22}$$

has full column rank, thus the system is observable with this output. For this thesis it was chosen to use a Luenberger type observer, using pole placement. Although the output as in Equation 4-21 is sufficient, i.e., the system is observeable with this output matrix, it was chosen to also include the vehicles yaw rate in the output. As the yaw rate is easily accessible during driving, it can be used to improve convergence speed and accuracy of the estimated states $\hat{x}$. The actual output matrix then is

$$C_{obs} = \begin{bmatrix} 0 & 0 & 1 & d_i & 0 & 0 \\ 0 & 1 & 0 & 0 & 0 & 0 \end{bmatrix}, \tag{4-23}$$

for which the system is also observable. Given the output in (4-23) the goal is to then find a output injection gain F, such that the matrix

$$A_{obs} = A - FC_{obs}, \tag{4-24}$$

results in a Hurwitz matrix. For this matrix A_{obs} it is required that the dynamics are faster than that of the controlled system. The last requirement is important such that the estimated states $\hat{x}$ converge to the actual states x. As it is difficult to predict where the H_∞ optimized controllers places the poles, choosing a pole location for A_{obs} often was a matter of manual tuning. Although workable results were found, it remained a rather cumbersome process, and far from optimal. It also turned out that taking the output matrix as in (4-23), the gains of the output injection gain would be so large that the system would turn unstable. Restricting the output matrix to (4-21) solved this issue. In Chapter 6, section 6-3 a solution to better integrate this observer into the design will be suggested.

Chapter 5

Simulation Results

This chapter will cover the results of the synthesized controller when a platoon of vehicles performs a lane change. The synthesized controllers will be tested in a situation where it is assumed both path errors are available and one where the observer is employed. The synthesized controllers will also be compared, in both cases, to the currently implemented controllers, considered to be state of the art. Originally it was also intended to implement the controllers on an actual platoon of vehicles, i.e., real world experiments. Unfortunately the outbreak of the COVID-19 virus prevented this from happening, hence the results are limited to simulation case studies only.

Section 5-1 will show the manoeuvre to be used in simulation. It is based on an overtaking manoeuvre one would normally execute on a highway. Section 5-2 will detail the simulation set-up, and explain how the direct vehicle following measurement is implemented. Section 5-3 covers the simulation results, and shows a comparison with the current state of the art controller.

5-1 Simulation Manoeuvre

Figure 5-1 shows the lane change manoeuvre executed by a single vehicle. For every simulation the velocity is 80 km/h, the same as the used for the controller synthesis. The distance between the vehicles is calculated as in [29], $d_i = r_i + h_i v_{x,i}$, where r_i is the stand still distance, set to be 5 metres. This distance is mainly based on [29], and has little influence on the final results. The headway time , h_i, is the time gap between vehicles, which is set to 1 second. Given this stand still-distance, velocity and headway time, the following distance becomes $d_i = 27.2$ metres. A platoon of 4 vehicles, where vehicle 1 is the leader and independent, is considered, where each vehicle is initialized a distance $nd_i,\ n \in \{2, 3, 4\}$, behind the preceding vehicle. As the focus of this thesis lies on the development of a lateral controller there is no CACC controller implemented (the model also doesn't include longitudinal dynamics for that matter) and thus the velocity is kept at 80 km/h using constant number generator.

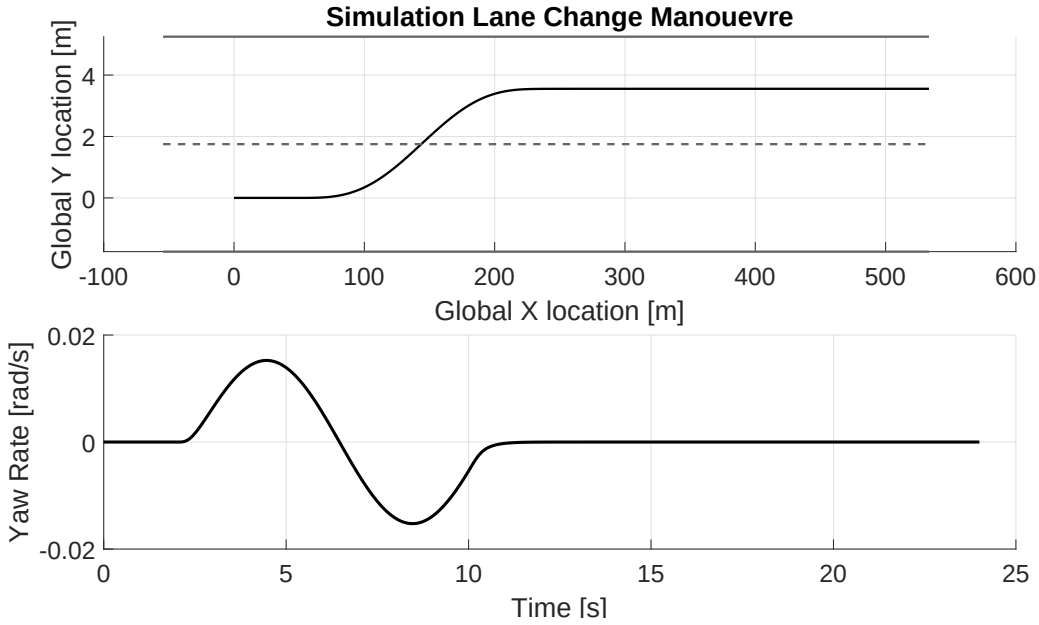

Figure 5-1: Lane change manoeuvre on a two-lane Dutch highway used for simulation.

The top figure in figure 5-1 shows the path of the vehicle in the global coordinates. The host vehicle is initialized at location $(X_1, Y_1) = (0, 0)$. The solid greyed out lines denote the edges of the highway, the dotted grey line denotes the boundary between two lanes, and is the location where in the real world the white road markings would be applied [35]. After two seconds a single sinusoid as steering input makes the vehicle change lanes. This sinusoid has a frequency of 0.125 Hz and an amplitude of 3 degrees. Using this input it takes the vehicle 8 seconds to complete the lane change. The corresponding yaw rate can be seen in the lower graph, in figure 5-1. On the steering signal a first-order filter of the form

$$F(s) = \frac{\pi}{s + \pi}, \tag{5-1}$$

is used to smooth out the abrupt start and end of the sinusoid. This way the input represents human-like dynamics. This prevents excitation of a large range of frequencies in the system, which might cause undesired effects in the simulation.

5-2 Simulation Set-up

Unfortunately it is not possible to directly 1-on-1 reconstruct the camera measurements and other data the vehicle receives when driving in the real world. Therefore, this section will cover how the direct vehicle following measurement can be mimicked in simulation environment as well as go into detail as to how the distance ε_i is calculated. The calculation for ε_i represents the most accurate way to determine this value, as it uses the global coordinates. It represents a method where, in real life, the vehicles would use GPS coordinates to calculate this value. Vehicle states, accessible using on board sensors, can also be used, but given noise when using internal measurements it is likely a less accurate method to determine ε_i.

5-2-1 Direct Vehicle Following Measurement

The $y_{tot,i}$ measurement used in direct vehicle following has to be calculated using the current vehicle locations with respect to the global axis system. Consider for this the situation in figure 5-2.

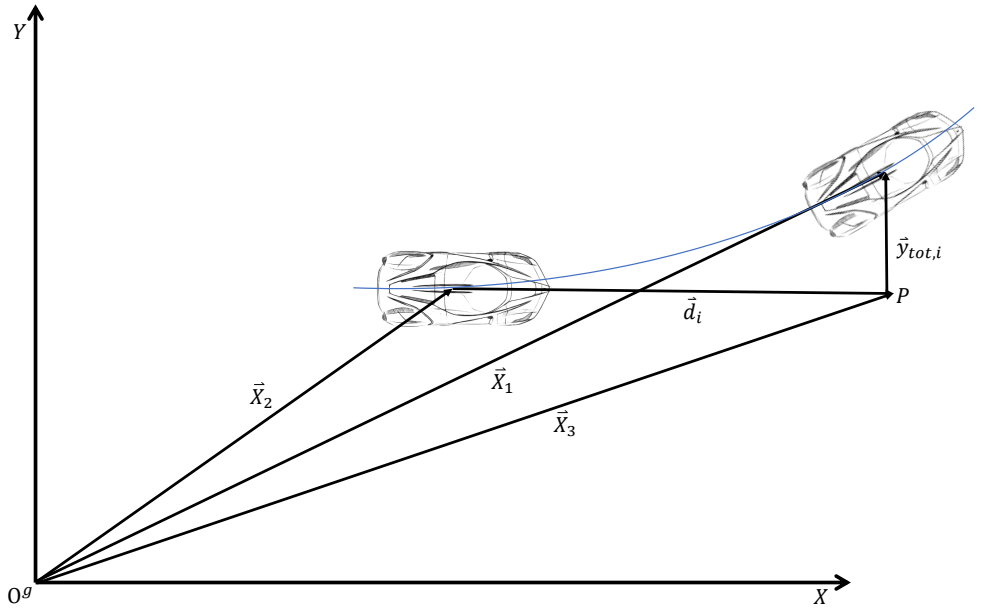

Figure 5-2: Vectors required to calculate the distance $y_{tot,i}$.

Figure 5-2 shows two vehicles in a platoon, and 5 vectors needed to calculate the distance as measured using direct vehicle following. Vectors $\vec{X}_1$, $\vec{X}_2$ and $\vec{X}_3$ are vectors that connect the origin of the global axis system to the centre of the lead vehicle, centre of the trailing vehicle and point P respectively. Point P denotes the end of the look-ahead distance. Vector $\vec{d}_i$ connects the centre of trailing vehicle to point P, and can be interpreted as the look-ahead distance vector. Vector $\vec{y}_{tot,i}$, is the vector of interest. The length of vector $\vec{y}_{tot,i}$ is equivalent to the direct vehicle following measurement. It is given by

$$|\vec{y}_{tot,i}| = \left|\vec{X}_1 - \vec{X}_3\right|, \tag{5-2}$$

where $\vec{X}_3$ can be written as

$$\vec{X}_3 = \vec{X}_2 + \vec{d}_i. \tag{5-3}$$

Vector $\vec{d}_i$ lies in the centre line of the trailing vehicle. As the vehicle rotates, it will also be rotated. In order to calculate (5-3) this rotation needs to be taken into account. This can be done by rotating vector $\vec{d}_i^T$ with a rotation matrix $\mathcal{R}(\psi_i(t))$. This rotation matrix is dependant on the yaw angle ψ_i of vehicle i at any given time t. The coordinates of $\vec{d}_i$ are given by

$$\begin{bmatrix} d_{i,x}(t) \\ d_{i,y}(t) \end{bmatrix} = \begin{bmatrix} \cos(\psi_i(t)) & -\sin(\psi_i(t)) \\ \sin(\psi_i(t)) & \cos(\psi_i(t)) \end{bmatrix} \begin{bmatrix} d_{i,x}(0) \\ d_{i,y}(0) \end{bmatrix}. \tag{5-4}$$

As each of the vehicles will be initialized driving behind another, travelling purely in the X direction, $\vec{d}_i$ at time $t = 0$ equals $\vec{d}_i(0)^T = \begin{bmatrix} d_i & 0 \end{bmatrix}^T$. It must be noted that due to the fact that CACC is not implemented, the following distance will vary ever so slightly, and the point P will not be directly in line with the CoG of the preceding vehicle. The variation in distance is minimal, hence, it can be neglected.

5-2-2 Road Error ε_i

In section 2-4 a method of calculating the distance measured induced by the rotation of the path was introduced. Using this extra calculation, and including it in the transmission between two vehicles, allowed the trailing vehicle to deduce the individual road errors through use of the observer. This distance, denoted by ε_i, can be calculated using a vehicle's current position and its position at time t_{la} ago. As in section 2-4, time t_{la} is the time it takes a vehicle to drive following distance d_i, with velocity $v_{x,i}$. Figure 5-3 shows all the angles and vectors required for calculating the distance ε_i.

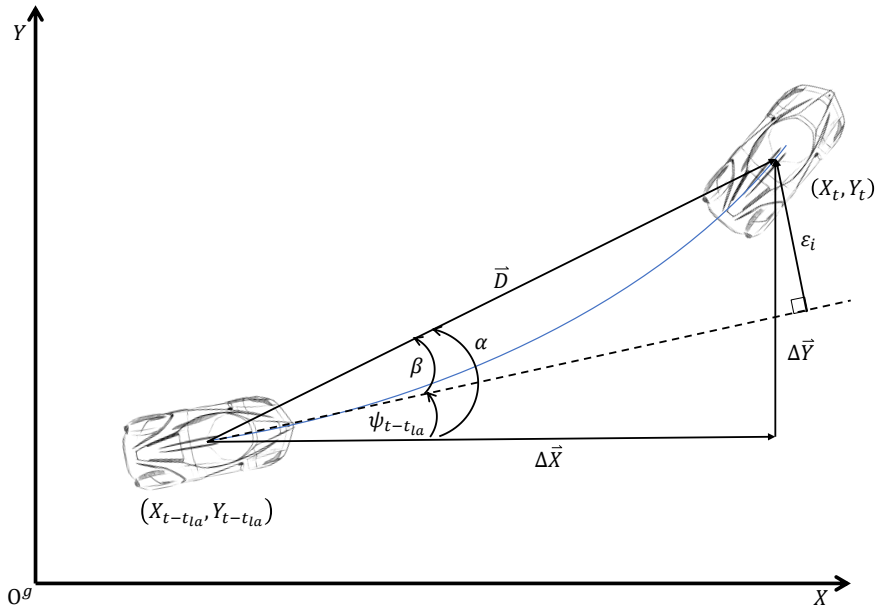

Figure 5-3: Vectors and angles required to calculate the distance ε_i.

From figure 5-3 it can easily be seen that distance ε_i is calculated as

$$\varepsilon_i = \sin(\beta)|\vec{D}|, \tag{5-5}$$

where angle β is the angle between the centre line of the position of the vehicle at time t_{la} ago, and $|\vec{D}|$ is the length of the vector connecting the two vehicles. Vector $\vec{D}$ can be calculated using the current and preceding position of the vehicle and is defined as

$$\vec{D}^T = \begin{bmatrix} X_t - X_{t-t_{la}} \\ Y_t - Y_{t-t_{la}} \end{bmatrix} = \begin{bmatrix} \Delta X \\ \Delta Y \end{bmatrix}. \tag{5-6}$$

Angle β is the difference between angles α and $\psi_{t-t_{la}}$. Angle α is the angle between vector $\Delta\vec{X}$ and vector $\vec{D}$. It is calculated as

$$\alpha = \cos^{-1}\left(\frac{\Delta\vec{X}\cdot\vec{D}}{||\Delta\vec{X}||||\vec{D}||}\right), \tag{5-7}$$

where the $||\cdot||$ notation denotes the vector norm. Angle $\psi_{t-t_{la}}$ is the rotation of the vehicle with respect to the global X-axis. In the simulation it is implemented by integrating the yaw rate of the vehicle. Combining this leads to an expression for angle β as

$$\beta = \cos^{-1}\left(\frac{\Delta\vec{X}\cdot\vec{D}}{||\Delta\vec{X}||||\vec{D}||}\right) - \psi_{t-t_{la}}, \tag{5-8}$$

and in extension for ε_i

$$\varepsilon_i = \sin\left(\cos^{-1}\left(\frac{\Delta\vec{X}\cdot\vec{D}}{||\Delta\vec{X}||||\vec{D}||}\right) - \psi_{t-t_{la}}\right)|\vec{D}|. \tag{5-9}$$

5-3 Simulation Results

This section will cover the simulation results. First the simulation with full state measurement will be discussed, after which the simulation using the observer will be used to compare. In the case of full state information, the errors $y_{e,i}$ and $\psi_{e,i}$ are generated using an exact representation of (3-11). Figure 5-4 shows the results of the four vehicle platoon, where the trailing 3 vehicles are equipped with the proposed controller from chapter 4.

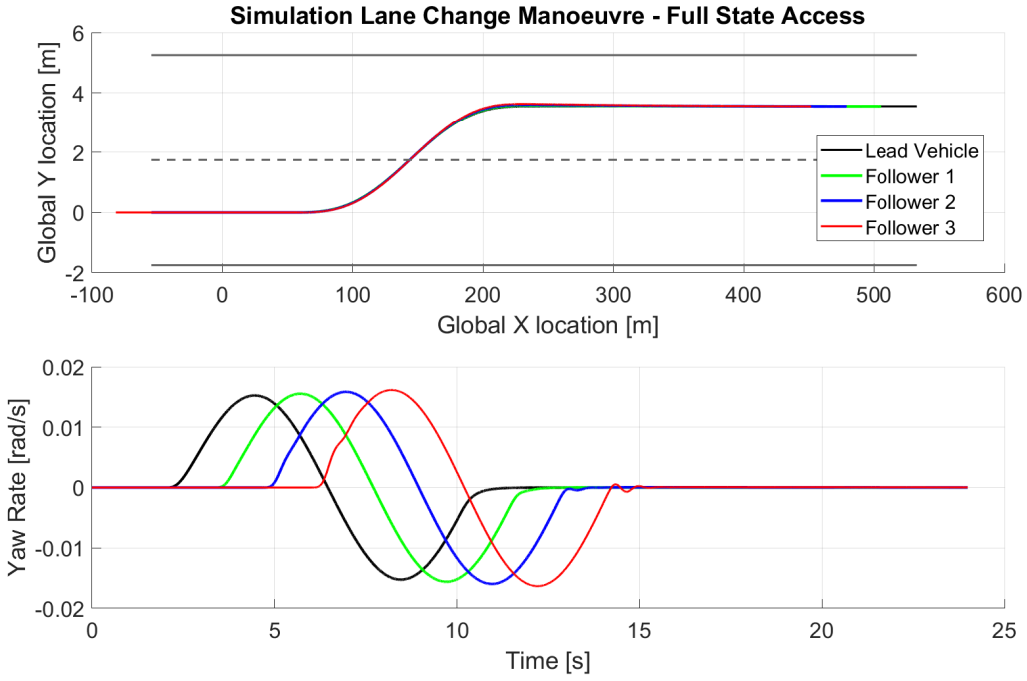

Figure 5-4: Four vehicle platoon executing line change, whilst having access to all state information.

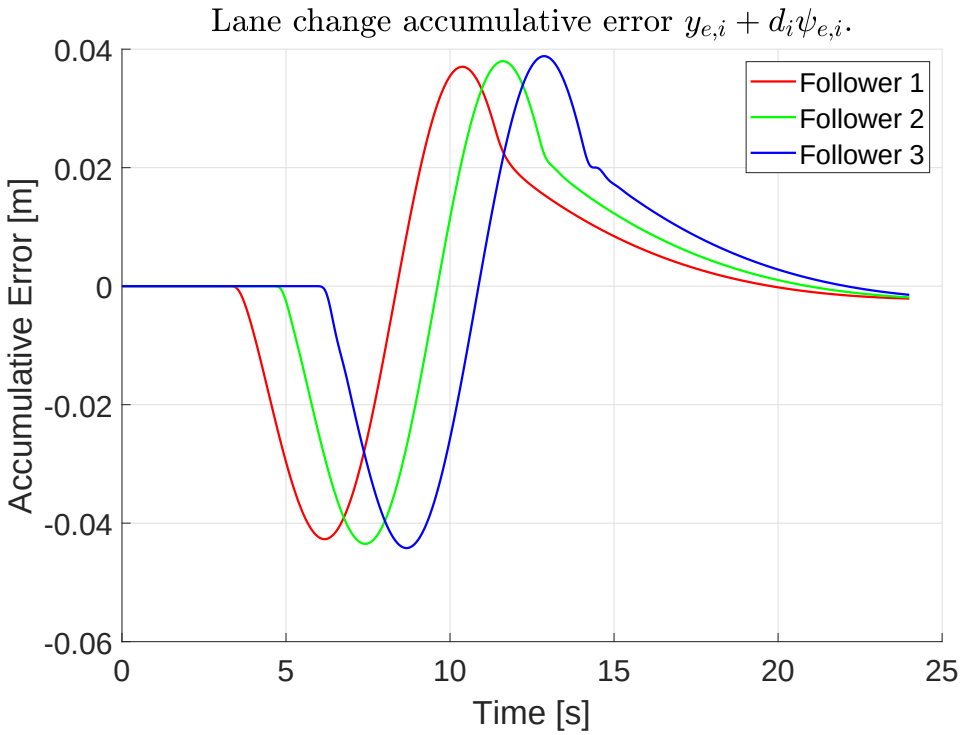

Figure 5-5: Cumulative error $y_{e,i} + d_i\psi_{e,i}$ for each of the trailing vehicles. Notice how the small growth of the distance at the peak indicates string instability.

From the results in figure 5-4 the lack of string stability is barely noticeable, although when observing the paths travelled the small overshoot when settling back to driving straight ahead in the other lane indicates there is some form of string instability (it must be noted that when having string stability, having no overshoot is not guaranteed.). Figure 5-5 shows the cumulative error $y_{e,i} + d_i\psi_{e,i}$ for each of the trailing vehicles From Figure 5-5 the small increase in the peak error measurement is a result of the string instability of the system. An alternative way to see this, is depicted in Figure 5-6. It shows exactly the same manoeuvre, but the bottom graph is zoomed in on the peak yaw rates. From figure 5-6 it becomes clearer that there is amplification present in the yaw rate of each of the vehicles. This is in line with the results from section 4-4. Furthermore, the maximum amplification is expected to be around 1 Hz, as can be seen in figure 4-6. The steering input is restricted to 0.125 Hz, so the frequency content won't excite all frequencies where the gain is higher than 0 dB. If this were to be the case, then the overshoot would be worse.

Figure 5-7 shows the same lane change manoeuvre, but then with the observer providing the states. As explained in section 4-5 the pole locations were chosen manually, with only the measurement $y_{e,i} + d_i\psi_{e,i}$ used in the output. The poles are placed at

$$p_{obs} = \begin{bmatrix} -14.5 & -14.6 & -14.2 & -14.25 & -14.3 & -14.4 \end{bmatrix}. \tag{5-10}$$

This leads to an observer gain

$$F = \begin{bmatrix} -8.3494 & -2.6215 & -354.1313 & 14.7266 & 1.1775 & -10.9761 \end{bmatrix}. \tag{5-11}$$

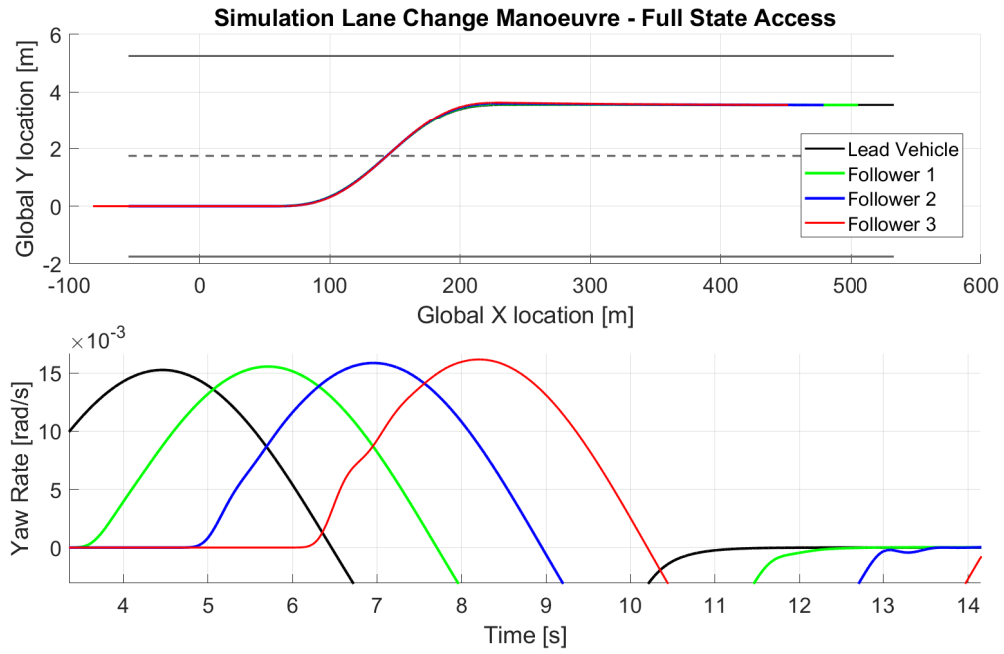

Figure 5-6: Four vehicle platoon executing line change, whilst having access to all state information. The peak yaw rate of each of the vehicles is enhanced to show the minor overshoot due to string instability.

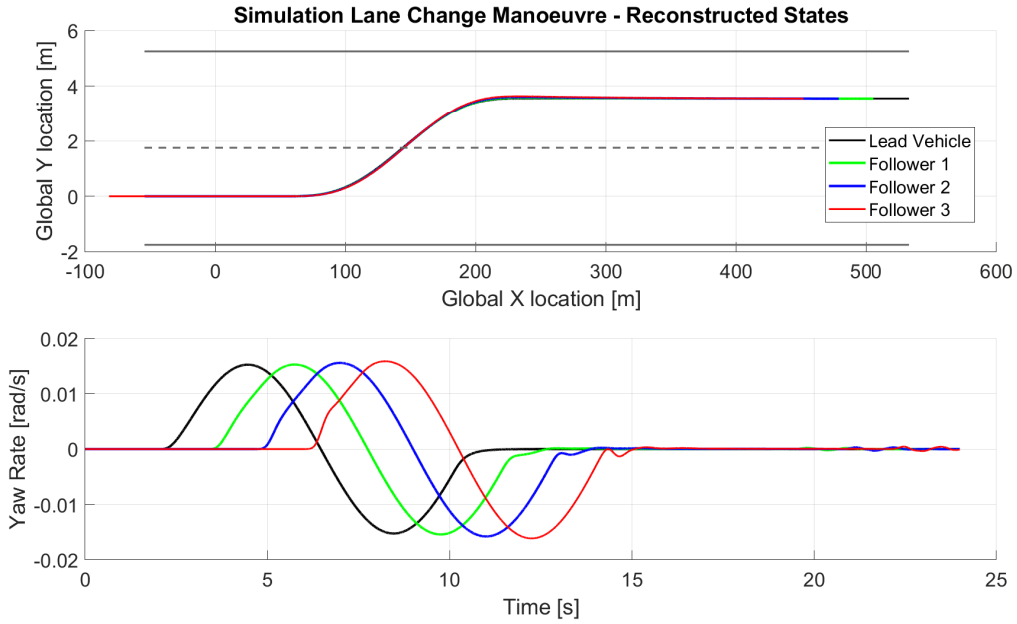

Figure 5-7: Four vehicle platoon executing line change, whilst using reconstructed states.

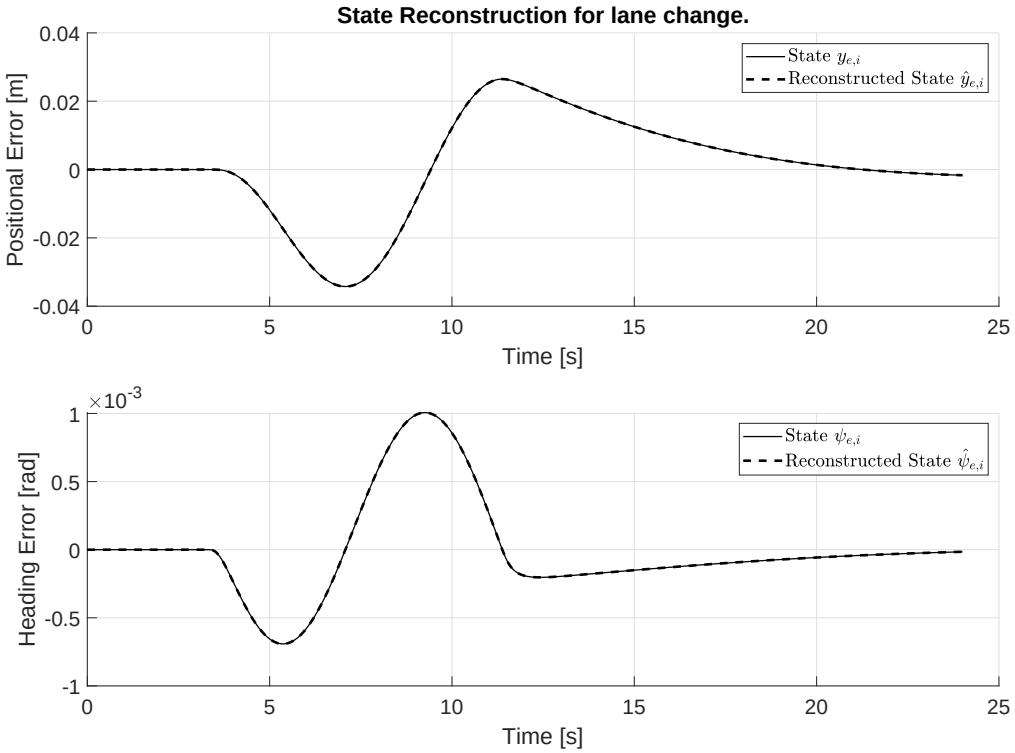

Figure 5-8: Reconstructed states for the lane change.

One of the issues with this observer design is the high gain on the error state $y_{e,i}$. This is also the reason why the yaw rate $\dot{\psi}_i$ was excluded from the observer output, as it drove the feedback gain even higher. One of the reasons thought to cause this is the large difference in magnitude of the various states. For example, $y_{e,i}$ is expected to be in the region of $\approx 1e^{-1}$, where as yaw rate is expected in the region of $\approx 1e^{-3}$. Nevertheless, because the yaw rate of the preceding vehicle is assumed to be available in the transmission the state reconstruction will be near perfect, as all inputs in (2-47) are available, see Figure 5-8.

Furthermore, when the measurement of $y_{tot,i}$ flips in sign from positive to negative, or negative to positive, it causes a small step in the simulation. This is inherent in how Simulink simulates certain functions required in calculation. It is believed it lies in the fact that one of the trigonometric functions switches domain. A shift in domain would mean a loss of directionality in the error, i.e. the error would always be positive or negative. This is also undesired.

This small step is similar to a step input on the system, exciting all frequencies. This causes a small oscillation in the system that slowly gets amplified over the vehicle platoon. This is best seen in the yaw rate of the third vehicle when driving in a straight line after the lane change has happened. A small oscillation persists as the measurement jumps between positive and negative.

5-3-1 Comparison to Benchmark Controllers

Having shown that the proposed controllers work in simulation, they are now compared to a set of benchmark controllers. These controllers are currently used in vehicle or lane following applications and explained in detail in [13]. When forward velocity v_x is constant the controllers consist of two static feedback gains, one for each road error state and a static feed forward gain. The proposed controllers will further be compared to the controllers from [21]. In that work the same problem is also solved using H_∞ synthesis, however due to the choice of weights in that work, the control action isn't limited. This makes the control solution converge to taking the feedforward controller as $K_f = G_t^{-1}$, with two poles at high frequency to make the system proper. Without any noise in the system, that solution outperforms the proposed solution. However, when noise is introduced in the system the performance severely deteriorates, as will be shown after the comparison with the currently implemented controller.

Current Path Following solution.

The feedforward gain is based on steady state vehicle dynamics analysis that links how a steering input can be translated to a yaw rate in steady state. From [36], this gain is given by

$$G_\psi = \frac{\dot{\psi}_i}{\delta_i} = \frac{v_{x,i}}{L + \frac{K_{us} v_{x,i}^2}{g}}, \tag{5-12}$$

where $L = a + b$, g is the gravitational acceleration and K_{us} is the understeer coefficient given by

$$K_{us} = \frac{mg}{L}\left(\frac{b}{C_{\alpha_f}} - \frac{a}{C_{\alpha_r}}\right). \tag{5-13}$$

Given the fact that the yaw rate of the preceding vehicle is included in the transmission between two vehicles, the feedforward gain is then given by $k_f = 1/G_\psi$. The feedback gain on $y_{e,i}$ is given by

$$k_{y_{e,i}} = \frac{2\left(L + K_{us} v_{x,i}^2\right)}{d_i^2}, \tag{5-14}$$

and for $\psi_{e,i}$ it is given by

$$k_{\psi_{e,i}} = k_{y_{e,i}} \cdot v_{x,i} t_{la}. \tag{5-15}$$

The steering command is given by

$$\delta_{i,ref} = k_{y_{e,i}} y_{e,i} + k_{\psi_{e,i}} \psi_{e,i} + k_f \dot{\psi}_{i-1}. \tag{5-16}$$

Figure 5-9 shows the same lane change, but now with two platoons of three vehicles. The amount of vehicles is reduced by one to keep the figure clear.

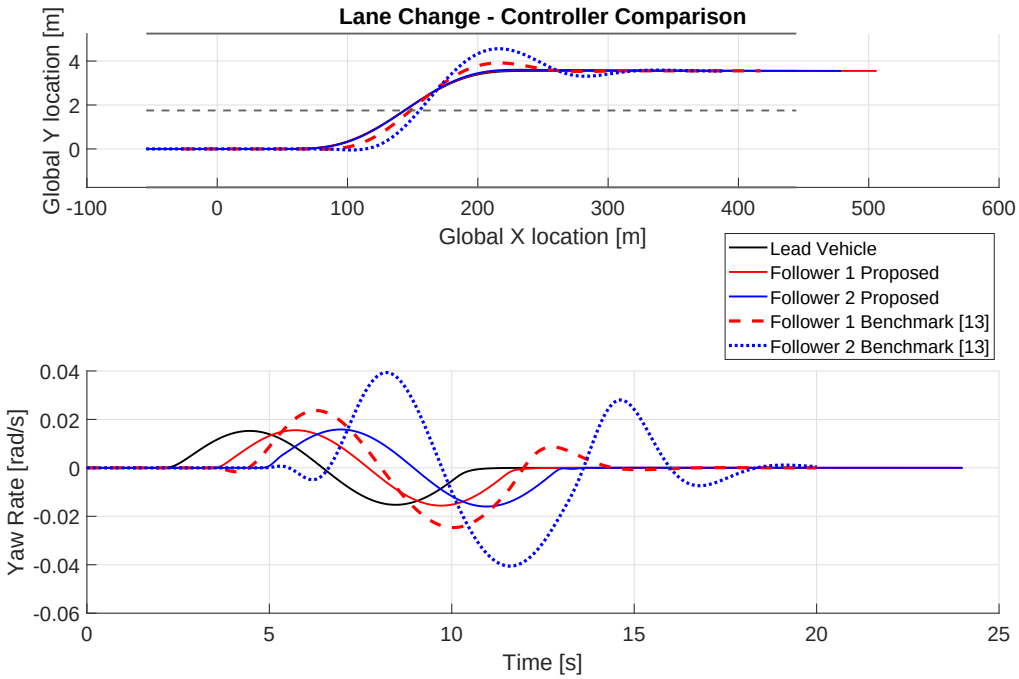

Figure 5-9: Comparison between benchmark controllers and the proposed controllers. Both controllers are using the reconstructed states using an observer. The difference in string instability is clearly visible.

The results shown in figure 5-9 show that the new proposed controller outperform the currently used solution by a good margin. Although the benchmark controllers do end up on the correct path, they do so with severe amplification of the yaw rate, which in extend also causes deviation from the path. Even though the proposed controllers are not string stable, their performance is better than that of those currently used. More importantly, although the proposed controllers do overshoot the yaw-rate, it has such a minor knock-on effect on the position of the vehicles, that the trailing vehicles remain far from the bounds of the highway, something that cannot be said for the benchmark controllers.

Comparison to Controllers from [21]

In [21] a similar method of control design is proposed as used in this thesis. The main differences between this work and [21] can be found in the weighting design, and the new method proposed for vehicle following. In the literature reference it is assumed path information is available. The main difference in weighting design in this thesis compared to [21], is that there is heavy focus on real world applicability. To show case this, the lane change is again simulated, both times with direct state access to prevent the observer from having any influence, as the work in [21] doesn't use an observer. The difference is that on the yaw rate signal, required to construct the road error states, noise is added. Figure 5-10 shows the noise added to the signal.

The noise in figure 5-10 is not necessarily representative of the noise expected in real world applications. However, it was chosen as such to better showcase the differences between the

control solutions. In [21] it can be read that when trying experimental testing the original controllers had to be tuned down significantly such that they didn't amplify the noise too much. The results for lane change simulation with the controllers from [21] can be seen in 5-11.

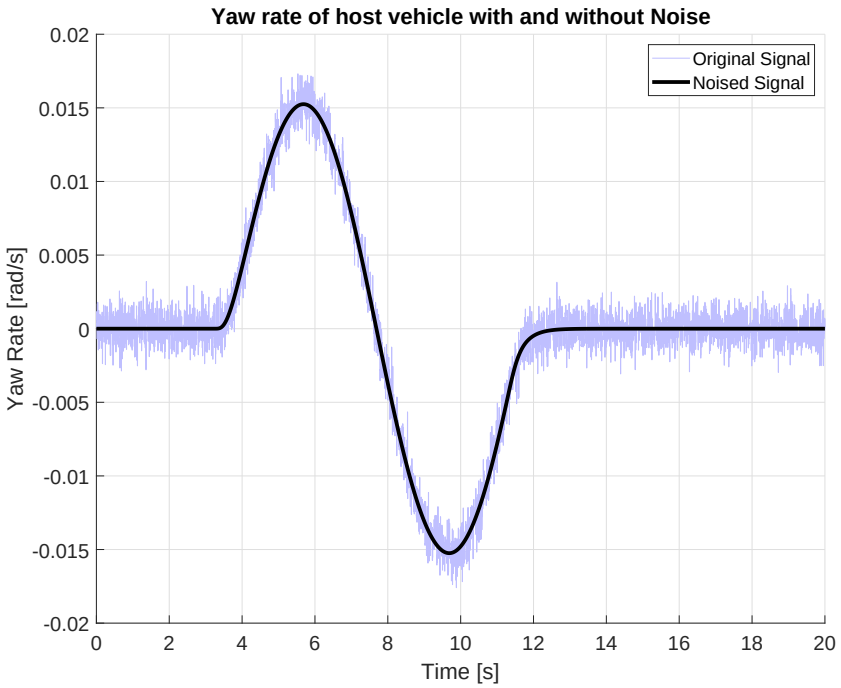

Figure 5-10: Comparison of noised and original used in comparison.

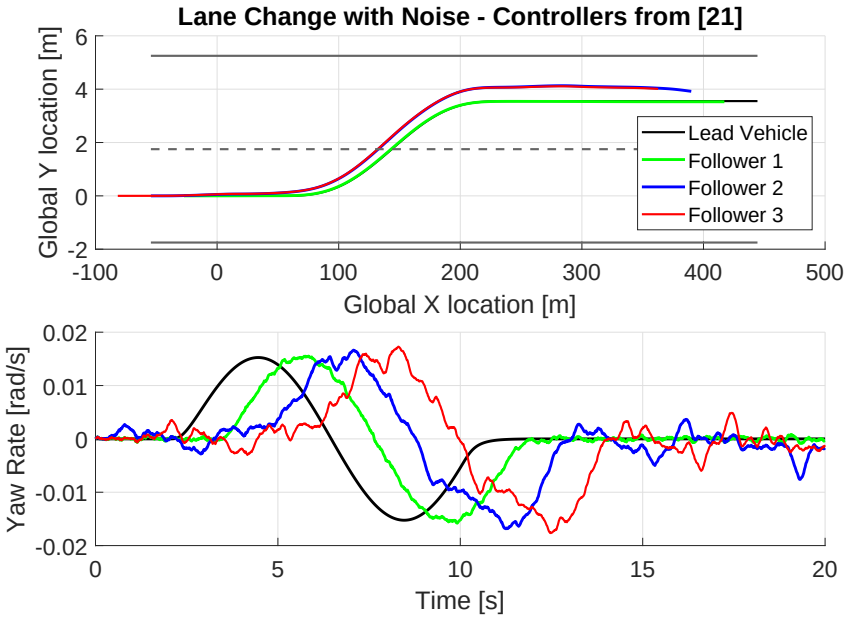

Figure 5-11: Results for lane change with controllers from [21].

Although the first vehicle is able to converge to the correct path, the second and third vehicle are thrown off the path due to the noise in the system. Eventually they will converge to the correct path, but this behaviour is highly undesired. Any string stability property is also breached because of the noise sensitivity. Comparing these results with the results when using the proposed controller, figure 5-12, it becomes clear that the proposed controllers are much less sensitive to noise. Furthermore, the vehicles still drive on the correct path, as desired.

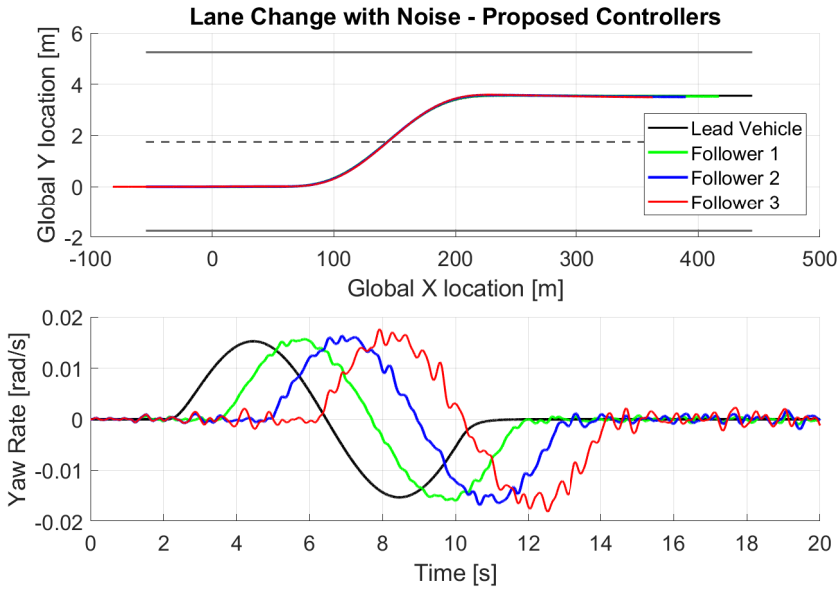

Figure 5-12: Results for lane change with proposed controllers.

The primary reason for this is put down to the fact that when the optimization is left unconstrained on the control action it converges to a solution with an inverse plant as feed forward controller. This can lead to large noise amplification if the original plant has high frequency roll-off. Because in this work the control action is weighted in accordance with what the steering system can achieve, the controllers designed such that their roll-off starts much earlier. This greatly reduces their sensitivity to noise. It is important to note that no other form of filtering besides that off the controllers or the plant is implemented in the system, so the results in figure 5-12 can still be further improved.

5-3-2 Initial Condition Errors

As was stated, when the yaw rate of the preceding vehicle is available as a measurement, then the reconstruction of the states is trivial. Under the assumption that all vehicle operations are well within the boundaries that guarantee high accuracy of the linear model, one can perfectly reconstruct the states. Obviously in real world applications this is not the case, and solely relying on the preceding vehicle yaw rate measurement would compound to steady state errors.

Such a system would best be comparable to a yaw rate controller. The vehicle might be able to match the yaw rate of the preceding vehicle, but there is no guarantee that it will also end

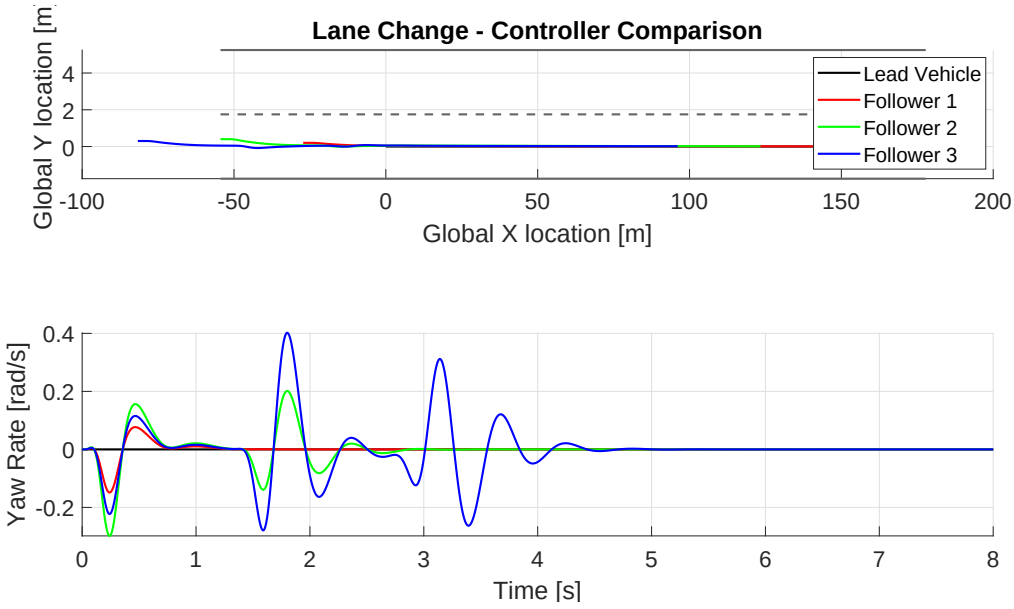

Figure 5-13: Simulation where the three trailing vehicles are initialized with initial conditions errors.

up on the correct path. For this reason path information is required. When using the direct vehicle following method, however, it is impossible to know if a measured error is caused by $\psi_{e,i}$, $y_{e,i}$ or a combination of both. This is where the observer is required. Further use of the observer is whenever the vehicle experiences an disturbance from the outside. An example could be a gust of side wind displacing one of the vehicles. In such a situation the observer is also required to correctly reconstruct the states and steer the vehicle back to the correct path.

To showcase this the platoon of 4 vehicles is initialized with initial condition errors. These are given by

$$y_{0,0} = 0 \tag{5-17a}$$
$$y_{0,1} = 0.2 \tag{5-17b}$$
$$y_{0,2} = 0.4 \tag{5-17c}$$
$$y_{0,3} = 0.3 \tag{5-17d}$$
$$\tag{5-17e}$$

Figure 5-13 shows the results of the initial condition error simulation. Each of the vehicles converges to the correct location. The behaviour of the vehicles is after initialization is not achievable in practice. The way the initial condition error is implemented is similar to applying an impulse input to the steering system, which will cause large variations in yaw rate, due to the assumption of linear tyres. This behaviour happens a few times during the simulation. It is put down to the high gains in the observer gain (5-11). In the real world, steering inputs like this can never produce this kind of output due to how the tyres will either saturate or dampen out the response which can be put down to a phenomenon called tyre relaxation length [22]. The positional errors used as initial condition in this simulation are

also exaggerated. This is mainly done to better show the influence the observer has on the system. The reconstructed state evolution is shown in Figure 5-14.

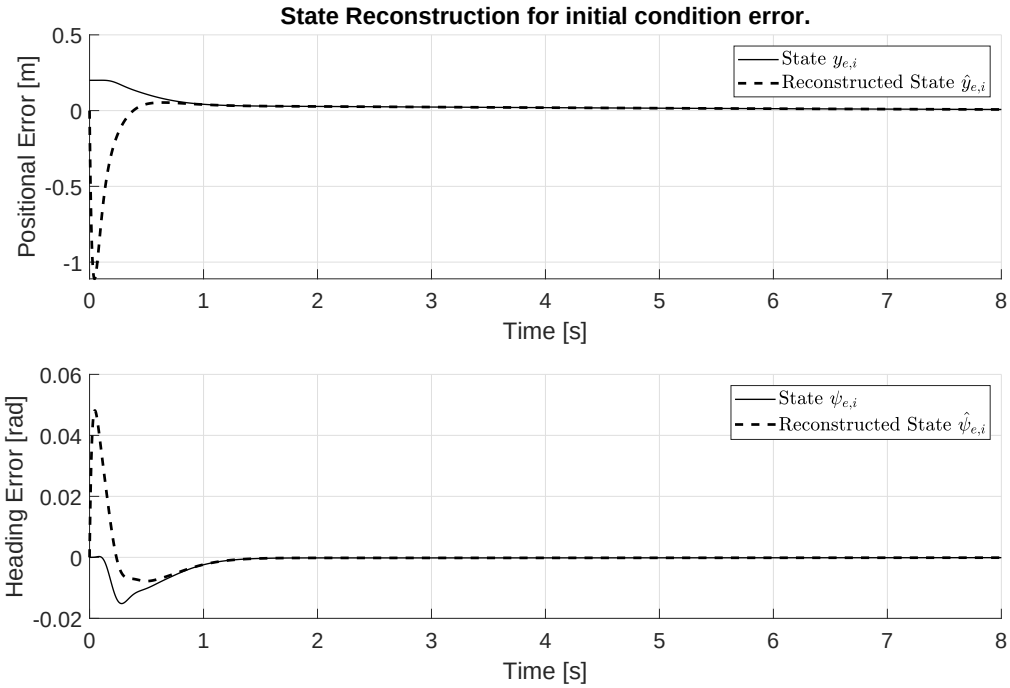

Figure 5-14: Individual graphs for each of the error states of the first vehicle, showing how the reconstructed states converge to their actual states. At around 0.5 second they are close to converging

From Figure 5-14 it can be seen the states converge to their correct values, but before doing that they both diverge away from the value they are supposed to have. As was discussed for the yaw rate response, this large spike is put down to the high gain of the observer gain. Although both reconstructed states first diverge, it does cause the vehicle to converge to the correct path. This means that the sum of the steering input is still correct. Once the vehicle starts steering the states also start converging towards their actual states. This showcases the added value of the observer, being able to accurately reconstruct the states $y_{e,i}$ and $\psi_{e,i}$ whilst not relying on often difficult and inaccurate path reconstruction techniques.

Another aspect where the observer can be of value is when the internal vehicle model does not match the actual dynamics of the vehicle. These can differ due to many reasons, but chief among them are a change in velocity and the tyre cornering stiffness. The observer will still be able to reconstruct the states. Even though it might not be the true actual states, it will make the vehicle converge to the right path. This makes the observer useful even when the model doesn't match the actual situation. Section 6-3 in Chapter 6 will discuss the observer further.

Chapter 6

Discussion

The work in this thesis presents a novel solution to vehicle following and using simulation shown to work. Nevertheless, the primary goal of string stability was not achieved. Rather, a proof that string stability is impossible to achieve was given for a system with only feedback control. For a system where feedback and feedforward control is implemented, it turned out to require infeasibly high gain on the feedback controllers to achieve string stability, something that contradicts the real world application requirement. In this chapter we discuss the implications of these results by comparing them to the solution used in longitudinal platooning. It must also be said, that as a formal mathematical proof still lacks for guaranteed string instability, it is highly advised to look deeper into this problem before attempting any form of control design.

6-1 Discussion on the String Stability Results

In [37] a conclusive proof is given that, for any system using only relative position measurements, string stability is impossible to achieve. In that article, no linearity assumptions are made with regards to controllers, and the controller structure is completely left open. Furthermore, it is generalized for any form of interconnected system.

Interestingly, the same problem originally existed for the longitudinal platooning case, as is explained in [38]. The argument made for string instability is identical between lateral and longitudinal platooning, although in [38] analysis where feedforward is included is lacking. The basis, nonetheless, finds itself in the fact that the system has two free integrators coming from the error definition based on position. As shown in this thesis this results in at least two free integrators in the loop gain. Using Bode's integral relation it is shown that the string stability cannot be achieved when noise suppression is desired. The fact that the system could not be made string stable is in line with work presented in [11, 21], where the same model is used. The difference between the work presented in this thesis and [21] is that in this work the control action is constrained. When left unconstrained, the optimization will move towards the solution as presented in section 3-4, where high gain controllers are necessary to achieve string stability, which is prevented by the weight on control action.

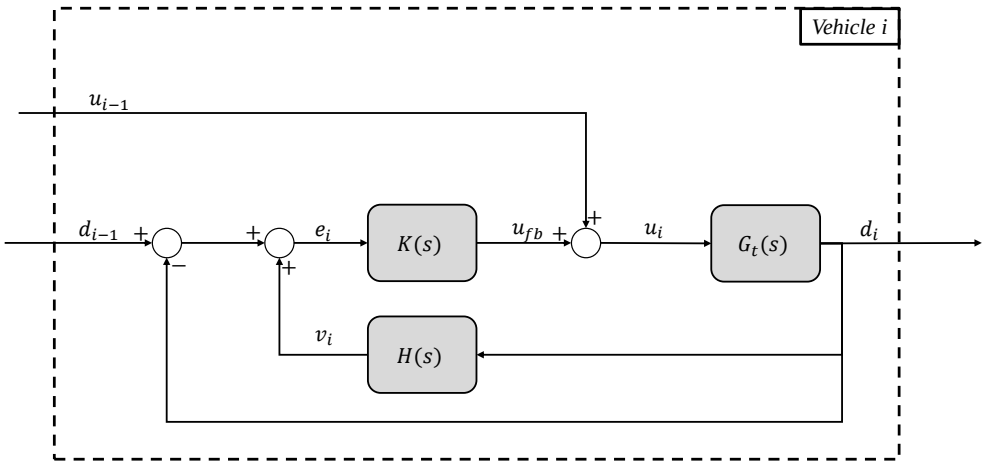

Figure 6-1: Block scheme for a single vehicle in the platoon.

6-1-1 Study of Longitudinal Platoon Solution

The analysis in this thesis, supported by several sources, shows that string stability cannot, or is very difficult to, be achieved with this model. This calls for an alternate approach to the entire lateral vehicle following problem, such that a different model can be found where this issue is not present. A potential solution can be found by a closer study the longitudinal control problem and the solutions used in that to make the system string stable. The solution used in longitudinal platooning is to adaptively change the reference, based on absolute velocity. The error is now not only dependant on a relative position, but also on an absolute measurement from the vehicle itself. The adaptive positional error for longitudinal platooning is defined as

$$e_i(t) = d_i(t) - d_{r,i}(t), \tag{6-1}$$

where $d_i(t)$ is the measured distance between two vehicles, and $d_{r,i}(t)$ the reference difference, also time dependant. This distance reference is in turn given by

$$d_{r,i}(t) = r_i + hv_i(t), \tag{6-2}$$

where r_i is the stand still distance, and h is the headway time. The error as defined in equation 6-1 is actively altered by the velocity of the trailing vehicle. The velocity of the trailing vehicle is also the first time derivative of the measured inter-vehicular distance d_i, which is a state of the longitudinal vehicle model. In a very similar fashion to the block scheme of a vehicle in a lateral platoon (Figure 3-1), the block scheme for a vehicle in a CACC platoon is given in figure 6-1. It is assumed there are no communication delays present in the system. In [6] it is shown that communication delay only worsens the string stability properties of the platoon, hence assuming no delay presents an ideal scenario. In figure 6-1 the block G_t denotes the transfer function from acceleration input u_i to a change in inter vehicular distance d_i.

The block K has the feedback controllers and finally $H(s)$ is the transfer function from the constant time headway policy. $H(s)$ is given by $H(s) = hs$, where h is the headway time. The string stability complementary sensitivity function is given by

$$\Gamma_i = \frac{G_t K}{1 + G_t K - G_t K H}. \tag{6-3}$$

For the function in (6-3) we recognize the complementary sensitivity function, but an extra term has appeared due to the inclusion of $H(s)$. The loop gain for the longitudinal problem also has two free integrators, and thus with $H(s) = 0$, the system will be string unstable. Because $H(s)$ is a pure differentiator, the number of free integrators in $1+G_tK-G_tKH$ is no longer guaranteed to be two or more. Because of this, Bode's integral does not necessarily have to equal 0, and thus this mathematical constraint is removed. This opens up the possibility to design controllers such that the system is string stable.

The implication of altering the reference distance is that during an acceleration change the distance between vehicles is not preserved. In the longitudinal case this is far less an issue than for lateral platooning as the vehicles are driving on the same path, and the stand still distance prevents them from hitting one-another.

6-1-2 Proposal for Lateral Platooning

Let us now consider applying a similar solution for the lateral platooning case. Recall that the error for the lateral vehicle following case is given by

$$\dot{\psi}_{e,i} = \dot{\theta}_{s,i} - \dot{\theta}_{s,i-1}. \tag{6-4}$$

The rate of change for the heading angle is the difference between the rate of change of the curvature of the path of the preceding and following vehicle. The lateral off-set error plays no part in the initial error definition and is only dependant on the accumulation of the heading error. Unlike the case for longitudinal platooning, there is no reference distance which is velocity dependant. Let us assume that there would exist a reference yaw rate, $\dot{\psi}_{r,i}$, then the error would be defined as

$$\dot{\psi}_{e,i} = \dot{\theta}_{s,i} - \dot{\theta}_{s,i-1} + \dot{\psi}_{r,i}. \tag{6-5}$$

When $\dot{\psi}_{r,i} = 0$, we arrive at the original error definition. However if we take $\dot{\psi}_{r,i}$ such that it

$$\dot{\psi}_{r,i} \neq 0, \tag{6-6}$$

it would imply that when both $\psi_{e,i} = 0$ and $y_{e,i} = 0$, then

$$\dot{\psi}_{e,i} = \dot{\psi}_{r,i}. \tag{6-7}$$

This implies the trailing vehicle will still measure an error, even though it has no actual road errors. As it generates control action based on this error it will then creates both positional as well as heading error. In turn this will be counteracted again by the controller and the system will swing back and forth between having actual error and the reference induced error. It might be possible to find a control solution that negates this, but it will mean that the vehicle will be driving with both $\psi_{e,i} \neq 0$ and $y_{e,i} \neq 0$. This can be interpreted as the vehicle having steady state error with respect to the path that it should be travelling on. Remember

that this is identical to the longitudinal case, the trailing vehicles are not driving on the same path as their respective preceding vehicle, but because the path is 1-dimensional, this is much less of a problem.

It seems that a solution whereby the path of the preceding vehicle is followed during both transient and steady state is not feasible. This was not a requirement in the first place, but the way the errors are defined in combination with the string stability requirement does push the closed loop system to converge to this. Figure 6-2 shows an alternative error definition, that could possibly yield a system that is string stable. In [12] it is shown that when the vehicle platoon is modelled as an off-hook trailer system, where the connection point is in the middle of the two vehicles the platoon will be string stable. In Figure 6-2 this set-up is depicted. The off-hook set-up is constructed by dividing the following distance d_i in two equal sized parts.

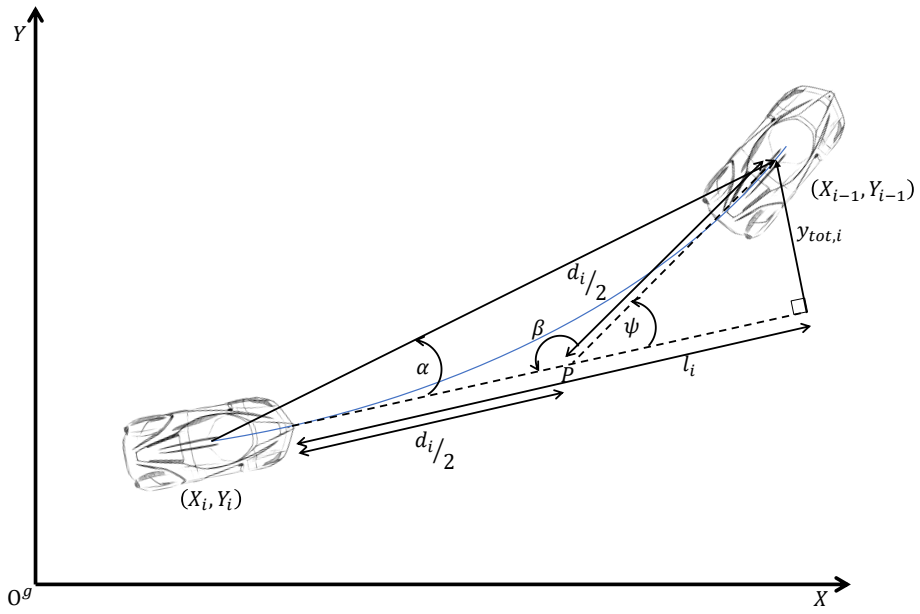

Figure 6-2: Alternate error definition .

Triangle $((X_i, Y_i)P(X_{i-1}, Y_{i-1}))$ is an equilateral triangle, thus

$$2\alpha + \beta = 180^\circ, \tag{6-8}$$

and also

$$\psi + \beta = 180^\circ. \tag{6-9}$$

In steady state, α can then be calculated as

$$\alpha = \frac{\psi}{2} = \frac{\sin^{-1}\left(\frac{2y_{tot,i}}{d_i}\right)}{2}. \tag{6-10}$$

During highway driving the radii of the corners is large, which in turn means that $y_{tot,i}$ is small and $d_i >> y_{tot,i}$. Angle α can be approximated using a small angle approximation as

$$\alpha_{ref} \approx \frac{y_{tot,i}}{d_i}. \tag{6-11}$$

We call (6-11) α_{ref}, as it serves as a reference angle. Triangle $((X_i, Y_i)P(X_{i-1}, Y_{i-1}))$ is only an equilateral triangle when both vehicles are driving on the same radius (see [12]). The definition for α given in (6-11) can be seen as an angle reference the trailing vehicle has to aim for. It can do this by measuring both $y_{tot,i}$ as well as l_i, a distance defined between the front of the trailing vehicle to the measurement point for $y_{tot,i}$. Then the error is defined as

$$e_\alpha = \alpha_{ref} - \alpha = \frac{y_{tot,i}}{d_i} - \frac{y_{tot,i}}{l_i}. \tag{6-12}$$

From [12] it is known that this method does corner cut in transients, but in steady state has no steady state error. Furthermore, it is also shown that for a two vehicle platoon the system is string stable. The proposed solution poses an interesting trade-off, not present in longitudinal platooning. The work in this thesis shows that string stability is possible, but the solution does not corner cut, rather it overshoots the path. As the system is string unstable this overshoot will steadily increase over the platoon which was deemed unsafe. Alternatively, if a solution is found where the vehicles undercuts the path, each of the following vehicles will undercut their respective preceding vehicle. It can be argued that this is also unsafe. Finding the right trade-off depends on what the designer deems preferable.

6-2 Discussion on Control Design

The optimized controllers are, as expected, capable of reducing the H_∞ norm of the string stability complementary sensitivity function. However, the goal of string stability was never achieved, regardless of weighting design. The main limitation comes from the weight on the control action. Entirely removing the weight improves the result, but the system remains string unstable, the overshoot being negligible however. The overshoot, given the synthesized controllers, is around 5% in terms of yaw rate per vehicle.

As an alternative to the definition given in (3-10), a practical definition for string stability can be taken. This practical definition will then allow for overshoot to occur, but limits the yaw rate of the i'th vehicle to a certain bound. Say that the system is designed for a platoon of ten vehicles. At the peak amplification of the yaw rate, the vehicle is furthest away from the path it has to travel in terms of position. This means that $y_{e,i}$ at that point is maximum. Recall that the transfer function

$$\Gamma_e = (I - G_t K_{fb})^{-1} (I - G_t K_f) \dot{\psi}_{i-1}, \tag{6-13}$$

relates the road errors to the rate of change of the curvature. The transfer function for $\dot{\psi}_{i-1}$ to $y_{e,i}$ will have a maximum at a certain frequency, which relates the maximum $y_{e,i}$ the vehicle will have given a certain input. In the bottom left figure of figure 4-5, this peak can also be clearly seen. It is this transfer function that then translates the curvature of the road in rad/s to a potential maximum lateral error $y_{e,i}$. It is a potential maximum, as it highly depends on the frequency content and value of $\dot{\psi}_{i-1}$.

In the same way that we restrict the frequency of the steering input of the host vehicle, we can also restrict the maximum steering angle the vehicle can attain. The maximum steering angle is highly dependant on the type of vehicles in the platoon. However, with this value known,

from this maximum steering angle, a peak yaw rate of the host vehicle can be determined. The total lateral offset of the 10^{th} vehicle is then given by

$$\left|\left|\Gamma_{y_{e,i}}\right|\right|_{\infty}^{10} = \sup\left\{\frac{||y_{e,10}||_2}{\left|\left|\dot{\psi}_0\right|\right|_2} \;:\; \dot{\psi}_0 \neq 0\right\}, \tag{6-14}$$

where with a slight abuse of notation $\Gamma_{y_{e,i}}$ is used to denote the transfer function. If the designer has a certain design case, for which the maxima for $y_{e,10}$ and $\dot{\psi}_0$ can easily be defined, then a bound, γ, on $\left|\left|\Gamma_{y_{e,i}}\right|\right|_{\infty}^{10}$ can be set. The system can then be said to be 'practically string stable' when

$$\left|\left|\Gamma_{y_{e,i}}\right|\right|_{\infty}^{10} \leq \gamma. \tag{6-15}$$

The definition in equation 6-15 is much weaker than that of (3-10), as it is heavily dependant on what requirements the designer has for the system. Nevertheless, if overshoot is indeed an inherent part of the system, and the system will always be string unstable regardless of controller choice, then a definition such as (6-15) at least ensures safety for a certain length of platoon.

6-2-1 Proposal for Observer Design

The observer forms an integral part of the control design as its pole locations are dependant on where the closed loop poles are of the actual system. In this thesis the pole locations of the observer are found by manual tuning because there is no influence on where the H_∞ optimization places the poles. In [39] a novel way of using an H_∞ optimization is proposed. In this work but then the pole locations can be also used as an input. It can be further extended by also including an observer in the optimization. This way two feedback gains for the both the controller and observer can be found, subject to the same constraints. An alternative approach also using state feedback with integral action is presented in [40]. It is expected that the performance of the entire system will be improved if either of these approaches, where possible, is adapted for the platooning system.

6-3 Discussion on Simulation Results

The simulations show that the proposed method for vehicle following in combination with the observer works as well as a system that has direct access to the road error states. This is mainly due to the fact that the dynamics of the system are slow, given the low frequency content of the lead vehicle manoeuvre. It is expected that if one of the vehicles somehow displays behaviour with high frequency content, the observer will lag behind a system with direct state access. Nevertheless, either system displays the expected string instability in each of the vehicles respective yaw rates.

A difference between the system with observer and the system with direct access to vehicle states is that due to the way the $y_{tot,i}$ measurement is implemented in Simulink it tends to oscillate around the the preceding vehicle when driving in a straight line behind it. This problem is purely down to the Simulink implementation and is not expected to occur in the

real world. The use of the observer when all the signals are available without any noise is limited. It is useful in situations if a vehicle, or multiple vehicles, have an initial condition error. The observer can then asymptotically reconstruct the road errors. The convergence of the states does take a significant time compared to the settling time. Nevertheless the vehicles converges to the correct path without first driving away from it.

One of the big drawbacks with the way the observer is implemented in this thesis is that the feedback and feedforward control design is without taking the observer into regard. Having no real control on where the poles will be located by the controller synthesis makes it difficult to determine where the poles of observer have to be located. This leads to high feedback gains, especially on the observer gain for $y_{e,i}$. This makes it difficult to have an observer that has fast convergence as well as be stable. This can clearly be seen in the initial condition error simulation.

Chapter 7

Conclusion

The increase in road usage over the past 20 years has called for smart solutions for driving. Platooning is one such solution. Platooning has both the potential to safely allow for a reduction in inter-vehicular distance as well increase overall road safety. The first allows for more efficient use of the existing road network, the latter is a welcome extra benefit. Furthermore, platooning has also shown to decrease fuel usage and thus decrease emissions as well. An important, or arguably the most important, property for a platoon of vehicles was argued to be string stability. Without it, platoons would inherently be able to reach an unsafe state of operation. One of the challenges with lateral vehicle platooning, besides achieving string stability, is having accurate path information, especially in close vehicle following. In Chapter 1 two methods of vehicle following were introduced, each having their own strengths and weaknesses.

The main contribution of this thesis is that it proposes a method which combines the strengths of two vehicle following methods. By using the positional information of the preceding vehicle, the road induced error can be calculated. Alternatively the vehicle could use its onboard sensors to approximate this distance. Including this road error in the communication between two vehicles allows the trailing vehicle to deduce a compound distance error consisting of both positional as well as heading error. Using an observer it is further possible to reconstruct the individual road error states using the linear vehicle-road error model. The theoretical background for this is shown in Chapter 2.

Chapter 3 shows that using this vehicle-road error model makes achieving string stability infeasible. Nevertheless, the overshoot caused by the lack of string stability can be minimized using some form of optimal control, where optimality is defined as a minimization of the overshoot. The mathematical definition for string stability developed in Chapter 3 based on an infinity norm pairs well with an optimal H_∞ type controller. Using weights as form of soft constraints the controllers can be pushed towards minimizing string instability over a frequency range of interest.

As seen in Chapter 4 the platoon model can easily be adapted for use in an H_∞ controller synthesis. Besides directly weighting the complementary sensitivity function, both errors can

also be weighted, allowing for freedom in the permissible amount of steady state error. It is shown that allowing steady state error on the lateral offset increased overall controller performance. Because the controllers were designed with the goal to be real-time implementable another weight was added to limit control action within what the power steering of the vehicle is capable of. The results from the optimization indicate that both the string stability weight and controller weight are the limiting factor when it comes to the controller synthesis.

The simulations in Chapter 5 show that the system in combination with the observer can perform a typical lane change without any issues. The string instability also becomes clear in the form of a small amplification of the yaw rate of each of the vehicles in the platoon. This in turn leads to a small overshoot, of several centimetres per vehicle. As was discussed in Chapter 6, it could be argued that this can be deemed safe. Nevertheless, the platoon is string unstable. The use of the observer when it comes to dealing with initial condition errors is also shown.

For future research re-evaluating the string stability properties for this system is highly recommended. It is not definitively proven, but there are a lot of indications that it is very difficult to achieve. An alternative vehicle-following model is proposed in Chapter 6. Furthermore, an alternative for the observer design to better integrate it into the control design is proposed. The manual tuning used in this thesis work gives for a non-ideal observer gain, with high gains as a result. By better aligning the pole locations of the H_∞ synthesis and the observer, the necessity for high observer gains to have state converge can be relaxed.

Appendix A

On Signal and System Norms

A-1 The $\mathcal{L}_2$ Norm

For a scalar signal $x(t)$ defined for $t \geq 0$, the $\mathcal{L}_2$ norm is defined as

$$||x||_2 = \left(\int_0^\infty x(t)^2 dt \right)^{1/2}. \tag{A-1}$$

The Laplace transform of signal $x(t)$ is given by

$$\hat{x}(s) = \int_0^\infty x(t) e^{-st} dt, \tag{A-2}$$

where s is the Laplace variable defined as $s = j\omega$. In accordance with equation A-1, the $\mathcal{L}_2$ norm for the signal $\hat{x}(s)$ is given by

$$||\hat{x}||_2 = \left(\frac{1}{2\pi} \int_{-\infty}^\infty |\hat{x}(s)|^2 d\omega \right)^{1/2}, \tag{A-3}$$

where the factor $1/2\pi$ is introduced for convenience. By Parseval's theorem the induced 2 norm of in both the time and frequency domain are equal

$$||x||_2 = ||\hat{x}||_2 . \tag{A-4}$$

A-2 The H_2 Norm

For any stable SISO linear system with transfer function $G(s)$, the H_2 norm is defined as

$$||G||_2 = \left(\frac{1}{2\pi} \int_{-\infty}^\infty |G(j\omega)|^2 d\omega \right)^{1/2}. \tag{A-5}$$

The H_2 norm can also be calculated from the state space representation of $G(s)$. Take a state space system of the form

$$\dot{x}(t) = Ax(t) + Bu(t), \tag{A-6a}$$
$$y(t) = Cx(t), \tag{A-6b}$$

so that

$$G(s) = C\left(sI - A\right)^{-1} B. \tag{A-7}$$

For a given input $u(t)$, the output $y(t)$ can be written as

$$y(t) = Ce^{At}x(0) + \int_0^t \left[Ce^{A(t-\tau)}B\right] u(\tau)d\tau, \tag{A-8}$$

where e^{At} is the matrix exponential, and $x(0)$ represents the initial conditions of the system. To gather information about the system we can subject it to either a step signal or an impulse, when the system has zero initial condition. The impulse response function is given by

$$H(t) = \begin{cases} Ce^{At}B, & \text{if } t \geq 0 \\ 0, & \text{if } t < 0. \end{cases} \tag{A-9}$$

Furthermore, the transfer function $G(s)$ is simply the Laplace transform of the impulse response function $H(t)$,

$$G(s) = \int_0^\infty H(t)e^{-st}dt = C\int_0^\infty e^{(A-sI)t}dtB = C\left(sI - A\right)^{-1} B\left[e^{(A-sI)t}\right]_0^\infty = C\left(sI - A\right)^{-1} B, \tag{A-10}$$

because A is Hurwitz and its matrix exponential converges to zero as $t \to \infty$. Applying Parseval's theorem again to the time signal $H(t)$ and its Laplace transform $G(s)$, it follows that

$$||G||_2 = ||H||_2 . \tag{A-11}$$

For a continuous time system we can write $||H||_2$ as [41]

$$||H||_2 = \left(\int_0^\infty H(t)^T H(t)dt\right)^{1/2} = \left(\int_0^\infty Ce^{At}BB^T e^{A^T t}C^T dt\right)^{1/2} = ||G||_2 . \tag{A-12}$$

Taking the square yields that

$$||H||_2^2 = ||G||_2^2 = \int_0^\infty Ce^{At}BB^T e^{A^T t}C^T dt. \tag{A-13}$$

A-3 The H_∞ Norm

The H_∞ norm for a stable SISO linear system with transfer function $G(s)$ is given by

$$||G||_\infty = \sup_\omega |G(j\omega)|. \tag{A-14}$$

The H_∞ norm is a measure of the largest amplification of any sinusoid introduced to the system $G(s)$. The H_∞ norm can also be interpreted as the effect $G(s)$ has on the space of inputs with bounded $\mathcal{L}_2$ norms. For the transfer function in equation A-7 we can write that

$$\hat{y}(s) = G(s)\hat{u}(s). \tag{A-15}$$

The $\mathcal{L}_2$ norm of $G(s)\hat{u}(s)$ is given by

$$\begin{aligned} ||G\hat{u}||_2 &= \left(\frac{1}{2\pi}\int_{-\infty}^{\infty} |G(j\omega)\hat{u}(j\omega)|^2 d\omega\right)^{1/2} \\ &= \left(\frac{1}{2\pi}\int_{-\infty}^{\infty} |G(j\omega)|^2 |\hat{u}(j\omega)|^2 d\omega\right)^{1/2} \\ &\leq \sup_{\omega} |G(j\omega)| \left(\frac{1}{2\pi}\int_{-\infty}^{\infty} |\hat{u}(j\omega)|^2 d\omega\right)^{1/2} \\ &= ||G||_\infty \, ||\hat{u}||_2 \,. \end{aligned} \tag{A-16}$$

Hence

$$||G||_\infty \geq \frac{||G\hat{u}||_2}{||\hat{u}||_2}, \ \forall \ \hat{u} \neq 0. \tag{A-17}$$

Taking $\hat{u}(s) = 1$, the Laplace transform of the impulse input, and the square on either side yields

$$||G||_\infty^2 \geq ||G||_2^2 \,. \tag{A-18}$$

The result in equation A-18 can be interpreted in the following way. The H_∞ norm acts as an upperbound on the 2-norm of a system. If that signal is the impulse input, which excites all frequencies equally, then the infinity norm is an upperbound of the maximum amount of energy that gets added to the outgoing signal by the system G.

A-3-1 State-Space computation of the H_∞ Norm

The H_∞ norm can also be calculated using state space methods. Let the transfer function $G(s)$ again have a state space representation of the following form

$$\dot{x}(t) = Ax(t) + Bu(t), \tag{A-19a}$$
$$y(t) = Cx(t). \tag{A-19b}$$

It follows from equation A-17, the H_∞ norm can also be characterized as

$$||G||_\infty = \sup\left\{\frac{||y||_2}{||u||_2} \ : \ u \neq 0\right\} \tag{A-20}$$

Let us introduce scalar value γ. For any $\gamma > 0$, $||G||_\infty < \gamma$ if and only if

$$\begin{aligned} J_\infty(G,\gamma) &\equiv \max_u \left[||y||_2^2 - \gamma^2 ||u||_2^2\right] \\ &= \max_u \int_0^\infty \left[y^T(t)y(t) - \gamma^2 u^T(t)u(t)\right] dt \\ &< \infty \end{aligned} \tag{A-21}$$

The maximization problem in equation A-21 can be solved using LQR techniques. If the following ARE

$$A^T P_\infty + P_\infty A + \frac{1}{\gamma^2} P_\infty B B^T P_\infty + C^T C = 0, \tag{A-22}$$

has a bounded positive semidefinite solution P_∞, then $||G||_\infty < \gamma$. If the ARE in (A-22) has no solution, then $||G||_\infty > \gamma$. Checking whether the ARE has a solution can be done using its associated Hamiltonian matrix

$$H_\infty = \begin{bmatrix} A & \frac{-1}{\gamma^2} BB^T \\ C^T C & -A^T \end{bmatrix}. \tag{A-23}$$

Equation A-22 has a solution when (A-23) has no eigenvalues of the imaginary axis. Alternatively (A-22) has a stabilizing solution if and only if (A, B) is stabilizable and $(A^T, C^T C)$ has no uncontrollable modes on the imaginary axis. In practice one often just verifies whether the pair $(A^T, C^T C)$, or (A^T, C^T) is stabilizable.

Appendix B

Bode's Integral

This appendix will go into the details behind the derivation that led to the well known results from Bode's work into feedback systems. The proof that system with two or more free integrators having both a feedback and feedforward controller can not be string stable has remained rather elusive. In the actual thesis the argument is made by logical induction on the lower fractional expansion used by the controller optimization. At a later stage it was found that evaluating Bode's derivation that arrives at the well known integral

$$\int_0^\infty \log|S(j\omega)|\,d\omega = \int_0^\infty \log\left|\frac{1}{1+L(j\omega)}\right| d\omega = \pi \sum \mathfrak{Re}(p_k), \tag{B-1}$$

and applying the same mathematical steps to the string stability complementary sensitivity function,

$$\Gamma_i = \frac{G_t K_f + G_t K}{1 + G_t K} = \frac{G_t K_f}{1 + G_t K} + \frac{G_t K}{1 + G_t K}, \tag{B-2}$$

it is possible to formulate an integral constrain similar to the one in (B-1), but then for $\Gamma_i(s)$. All of the work in this document is based off from the book [42] chapters 2 and 3.

B-1 Bode's Integral Derivation

Bode's integral theorem is developed from a relation between the real and imaginary components of analytic functions. It provides an expression of how the imaginary part of a function behaves at high frequency, in terms of the integral of the real part, for a function H that satisfies the following conditions

1. $H(j\omega) = P(\omega) + jQ(\omega) = \overline{H(-j\omega)}$, with P and Q real valued functions of ω
2. $H(s)$ is analytic at $s = \infty$ and in the closed right half plane except for possible singularities $s_0 = j\omega_0$ on the finite imaginary axis which satisfy $\lim_{s\to s_0}(s - s_0)H(s) = 0$

In his original work Bode called P the attenuation part and Q the phase part. Hence the integral relation is often called Bode's Attenuation Integral Theorem.

Theorem 1 (Bode's Attenuation Integral Theorem). Let H be a function satisfying conditions 1 and 2. Then for $H(j\omega) = P(\omega) + jQ(\omega)$,

$$\int_0^\infty [P(\omega) - P(\infty)]\, d\omega = \frac{-\pi}{2} \operatorname*{Res}_{s=\infty} H(s) \tag{B-3}$$

where $\operatorname*{Res}_{s=\infty} H(s)$ is the residual of transfer function $H(s)$ at $s = \infty$.

Proof. Since H is analytic at infinity, there exists a so-called Laurent series expansion of H as

$$H(s) = \ldots + \frac{c_{-k}}{s^k} + \ldots + \frac{c_{-1}}{s} + c_0 \tag{B-4}$$

which is convergent. From assumption 1 it follows that the coefficients c_k are real, and that $c_0 = P(\infty)$. To see that H can be written as this series expansion consider the following example.

Say that a function f is analytic at $x = \infty$. Then the function $g(y) = f(1/y)$ is analytic at $y = 0$. Any analytic function has a Taylor series expansion of the form

$$g(y) = \sum_{k=0}^{\infty} a_k y^k \tag{B-5}$$

that converges in $|y| \leq b$ for some $b > 0$. Ergo, the function f is represented in $|x| \geq 1/b$ by the series expansion

$$f(x) = \sum_{k=-\infty}^{0} c_k s^k \tag{B-6}$$

where $c_{-k} = a_k$. Consider we now do a contour integration over the contour given in figure B-1.

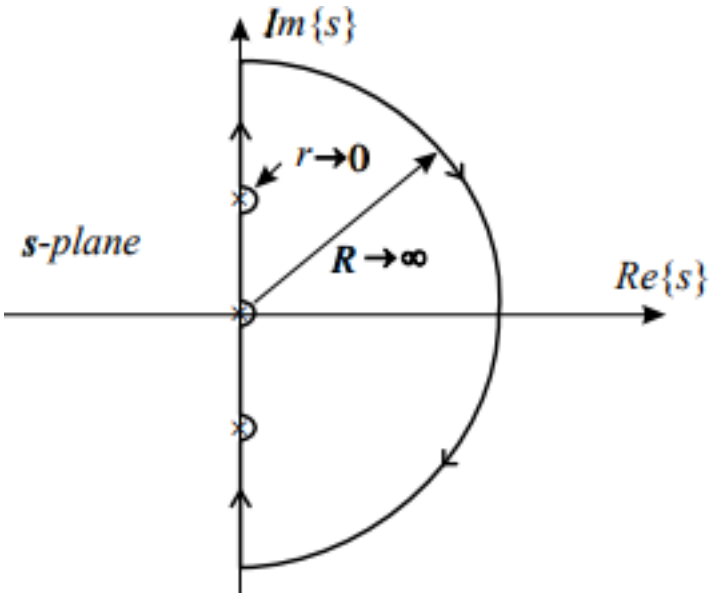

Figure B-1: Nyquist Contour

where the small semicircles on the imaginary axis denote possible singularities of H on the imaginary axis. According to Cauchy's integral theorem this integral is given by

$$\oint_C (H(s) - P(\infty))\, \mathrm{d}s = 0 \tag{B-7}$$

The contribution of the integral on the semicircles on the imaginary axis can be shown to go to zero. The integral over the large semicircle of the terms in $s^k, k \leq -2$ tends to zero as the radius becomes infinite. Taking the limit, as depicted in figure B-1, as $R \to \infty$ (B-7) reduces to

$$\int_{-\infty}^{\infty} [P(\omega) + jQ(\omega) - P(\infty)]\, jd\omega + \lim_{R\to\infty} \int_{C_R} \frac{c_{-1}}{s} ds = 0. \tag{B-8}$$

Using the symmetric properties of P and Q, from assumption 1, this reduces to

$$2j \int_0^{\infty} [P(\omega) - P(\infty)]\, d\omega - j\pi c_{-1} = 0, \tag{B-9}$$

or

$$\int_0^{\infty} [P(\omega) - P(\infty)]\, d\omega = \frac{\pi}{2} c_{-1} \tag{B-10}$$

From this we see that $\operatorname{Res}_{s=\infty} H(s) = -c_{-1}$. The Laurent series expansion in (B-4) can be written as, using the fact that $Q(\omega) = \mathfrak{Im} H(j\omega) = \frac{-c_{-1}}{\omega} + \frac{-c_{-3}}{\omega^3} + \ldots$. From this equation B-10 can be written as

$$\int_0^{\infty} [P(\omega) - P(\infty)]\, d\omega = -\frac{\pi}{2} \lim_{w\to\infty} \omega Q(\omega) = -\frac{\pi}{2} \operatorname*{Res}_{s=\infty} H(s) \tag{B-11}$$

This concludes the proof.

Theorem 2 (Bode's Attenuation Integral Theorem at zero Frequency). A formula equivalent to (B-11) at zero frequency can also easily be obtained. Let H be a function such that $H(1/\lambda)$ also satisfies conditions 1 and 2. Then

$$\int_0^{\infty} \frac{[P(\omega) - P(0)]}{\omega^2} d\omega = \frac{\pi}{2} \lim_{s\to 0} \frac{dH(s)}{ds} \tag{B-12}$$

Proof. Since H is chosen such that it is analytic at zero, it has a Taylor series expansion of the form

$$H(s) = a_0 + a_1 s + \ldots + a_k s^k + \ldots \tag{B-13}$$

which is convergent for some $|s| \leq r$ for some $r > 0$. Consider the function $H(1/\lambda)$ which has Laurent series expansion as in (B-4), where the coefficients $c_{-k} = a_k$. Using (B-3) we arrive at

$$\int_0^{\infty} [P(1/\lambda) - P(0)]\, d\lambda = \frac{\pi}{2} \lim_{s\to 0} \frac{dH(s)}{ds} \tag{B-14}$$

The proof is completed by taking the change of variables of integration as $\omega = 1/\lambda$.

B-1-1 Bode's Integral for the Sensitivity Function

Let us now evaluate (B-11) for the sensitivity function. Take $H(s) = \log S(j\omega)$, and that S is a proper rational transfer function without poles or zeros in the ORHP. This transfer function satisfies the assumptions 1 and 2. Thus we can apply (B-11), where $\log|S(j\omega)|$ equals the real part of $S(j\omega)$, to obtain

$$\int_0^\infty \left[\log|S(j\omega)| - \log|S(j\infty)|\right] d\omega = -\frac{\pi}{2} \operatorname*{Res}_{s=\infty} \log S(j\omega). \tag{B-15}$$

If $S(s)$ is a transfer function with relative degree two or higher, the Laurent expansion is given by

$$S(s) = \frac{c_{-2}}{s^2} + \frac{c_{-3}}{s^3} + \dots, \tag{B-16}$$

from which we see that $c_{-1} = 0$. The residual $\operatorname*{Res}_{s=\infty} \log S(j\omega) = 0$. Likewise $S(j\infty) = 1$, as $L(j\infty) = 0$. Equation B-15 then reduces to

$$\int_0^\infty \left[\log|S(j\omega)| - \log|1|\right] d\omega = \int_0^\infty \log|S(j\omega)|\, d\omega = 0, \tag{B-17}$$

which is the well known bode integral as presented in (3-19).

B-1-2 Bode's Integral for Γ_i

Let us now take $H(s) = \log \Gamma_i(j\omega)$, with Γ_i as in equation B-2. For this analysis it is easier to use the definition of Bode's integral given in (B-14). This becomes

$$\int_0^\infty \left[\log|\Gamma_i(\omega)| - \log|\Gamma_i(0)|\right] \frac{1}{\omega^2} d\omega = \frac{\pi}{2} \lim_{s\to 0} \frac{d \log \Gamma_i(s)}{ds} \tag{B-18}$$

The derivative of $\log \Gamma_i(s)$ with respect to s when $s \to 0$ is zero. Because the system has two free integrators, it will have zero steady state error, giving for a 'flat' line at zero frequency. In turn this means that the integral also has to equal zero,

$$\int_0^\infty \left[\log|\Gamma_i(\omega)| - \log|\Gamma_i(0)|\right] \frac{1}{\omega^2} d\omega = 0. \tag{B-19}$$

As $\Gamma_i(0) = 1$ by design and requirement the integral can be further reduced to

$$\int_0^\infty \log|\Gamma_i(\omega)| \frac{1}{\omega^2} d\omega = 0. \tag{B-20}$$

This result is identical to the result for the Bode integral over the complementary sensitivity function. It can be interpreted as a conversation of energy integral. It implies that for this form of string stability complementary sensitivity function, with two free integrators in the system, the waterbed effect also exists. This concludes the proof that string stability is impossible to achieve.

Bibliography

[1] CBS. *Helft meer kilometers dan in 1990*. URL: https://www.cbs.nl/nl-nl/nieuws/2019/46/helft-meer-kilometers-dan-in-1990.

[2] CBS. *Personenauto's rijden recordaantal kilometers in 2018*. URL: https://www.cbs.nl/nl-nl/nieuws/2019/38/personenauto-s-rijden-recordaantal-kilometers-in-2018 (Accessed: 13 February 2020).

[3] Kent M Hymel, Kenneth A Small, and Kurt Van Dender. "Induced demand and rebound effects in road transport". In: *Transportation Research Part B: Methodological* 44.10 (2010), pp. 1220–1241.

[4] Stichting BOVAG RAI Mobiliteit. *Mobiliteit in Cijfers Auto's 2019-2020*. Research rep. September 1, 2019.

[5] S. Sheikholeslam and C.A. Desoer. "Longitudinal control of a platoon of vehicles with no communication of lead vehicle information: a system level study". In: *IEEE Transactions on Vehicular Technology* 42.4 (1993), pp. 546–554. DOI: 10.1109/25.260756.

[6] Jeroen Ploeg et al. "Design and experimental evaluation of cooperative adaptive cruise control". In: *2011 14th International IEEE Conference on Intelligent Transportation Systems (ITSC)*. IEEE. 2011, pp. 260–265.

[7] Yuki Sugiyama et al. "Traffic jams without bottlenecks—experimental evidence for the physical mechanism of the formation of a jam". In: *New Journal of Physics* 10.3 (2008), p. 033001. DOI: 10.1088/1367-2630/10/3/033001.

[8] JingHua Guo, YuGong Luo, and KeQiang Li. "Adaptive fuzzy sliding mode control for coordinated longitudinal and lateral motions of multiple autonomous vehicles in a platoon". In: *Science China Technological Sciences* 60.4 (2016), pp. 576–586. DOI: 10.1007/s11431-016-0606-1.

[9] Roozbeh Kianfar et al. "Combined longitudinal and lateral control design for string stable vehicle platooning within a designated lane". In: *17th International IEEE Conference on Intelligent Transportation Systems (ITSC)*. IEEE. 2014, pp. 1003–1008.

[10] Anggera Bayuwindra et al. "Combined lateral and longitudinal CACC for a unicycle-type platoon". In: *2016 IEEE Intelligent Vehicles Symposium (IV)*. IEEE. 2016, pp. 527–532.

[11] WL Jansen. "Lateral Path-Following Control of Automated Vehicle Platoons." In: *Master Thesis* (2016).

[12] Teck Chew Ng, Javier Ibanez Guzman, and Martin David Adams. "Autonomous vehicle-following systems: A virtual trailer link model". In: *2005 IEEE/RSJ international conference on intelligent robots and systems*. IEEE. 2005, pp. 3057–3062.

[13] Antoine Schmeitz et al. "Towards a generic lateral control concept for cooperative automated driving theoretical and experimental evaluation". In: *2017 5th IEEE International Conference on Models and Technologies for Intelligent Transportation Systems (MT-ITS)*. IEEE. 2017, pp. 134–139.

[14] Manolis Tsogas, Aris Polychronopoulos, and Angelos Amditis. "Using digital maps to enhance lane keeping support systems". In: *2007 IEEE Intelligent Vehicles Symposium*. IEEE, 2007. DOI: 10.1109/ivs.2007.4290106.

[15] Louay Saleh, Philippe Chevrel, and Jean-François Lafay. "Optimal Control with Preview for Lateral Steering of a Passenger Car: Design and Test on a Driving Simulator". In: *Time Delay Systems: Methods, Applications and New Trends*. Springer Berlin Heidelberg, 2012, pp. 173–185. DOI: 10.1007/978-3-642-25221-1_13.

[16] Louay Saleh et al. "Shared Steering Control Between a Driver and an Automation: Stability in the Presence of Driver Behavior Uncertainty". In: *IEEE Transactions on Intelligent Transportation Systems* 14.2 (2013), pp. 974–983. DOI: 10.1109/tits.2013.2248363.

[17] Shantanu Ingle and Madhuri Phute. "Tesla autopilot: semi autonomous driving, an uptick for future autonomy". In: *International Research Journal of Engineering and Technology* 3.9 (2016).

[18] Stefan Solyom, Arash Idelchi, and Badr Bin Salamah. "Lateral control of vehicle platoons". In: *2013 IEEE International Conference on Systems, Man, and Cybernetics*. IEEE. 2013, pp. 4561–4565.

[19] Weihai Chen et al. "A partially flexible virtual trailer link model for vehicle-following systems". In: *Transactions of the Institute of Measurement and Control* 37.2 (2014), pp. 273–281. DOI: 10.1177/0142331214539990.

[20] J Jeroen Ploeg. *Analysis and design of controllers for cooperative and automated driving*. en. 2014. DOI: 10.6100/IR772224.

[21] Omar Hassanain. "String-stable automated steering in cooperative driving applications". In: *Master Thesis* (2017).

[22] Hans Pacejka. *Tire and vehicle dynamics*. Elsevier, 2005.

[23] *Vehicle Dynamics Terminology*. 2008. DOI: https://doi.org/10.4271/J670_200801. URL: https://doi.org/10.4271/J670_200801.

[24] J. Craens and N. Das. *Taking over the steering of a toyota prius using the electric steering motor*. Hoge School Fontys, 2014.

[25] G. Burnham, Jinbom Seo, and G. Bekey. "Identification of human driver models in car following". In: *IEEE Transactions on Automatic Control* 19.6 (1974), pp. 911–915. DOI: 10.1109/tac.1974.1100740.

[26] P.A. Ioannou and C.C. Chien. "Autonomous intelligent cruise control". In: *IEEE Transactions on Vehicular Technology* 42.4 (1993), pp. 657–672. DOI: 10.1109/25.260745.

[27] D Swaroop and J Karl Hedrick. "String stability of interconnected systems". In: *IEEE transactions on automatic control* 41.3 (1996), pp. 349–357.

[28] Jeroen Ploeg, Nathan Van De Wouw, and Henk Nijmeijer. "Lp string stability of cascaded systems: Application to vehicle platooning". In: *IEEE Transactions on Control Systems Technology* 22.2 (2013), pp. 786–793.

[29] Jeroen Ploeg et al. "Controller synthesis for string stability of vehicle platoons". In: *IEEE Transactions on Intelligent Transportation Systems* 15.2 (2013), pp. 854–865.

[30] Hendrik W Bode et al. "Network analysis and feedback amplifier design". In: (1945).

[31] Mike Ruth, Kenneth Lebsock, and Cornelius Dennehy. "What's New is What's Old: Use of Bode's Integral Theorem (circa 1945) to Provide Insight for 21st Century Spacecraft Attitude Control System Design Tuning". In: *AIAA Guidance, Navigation, and Control Conference*. American Institute of Aeronautics and Astronautics, 2010. DOI: 10.2514/6.2010-8428.

[32] Postlethwaite Skogestad. *Multivariable Feedback Control 2e*. John Wiley & Sons, October 26, 2005. 592 pp. ISBN: 047001167X. URL: https://www.ebook.de/de/product/4018240/skogestad_postlethwaite_multivariable_feedback_control_2e.html.

[33] Sigurd Skogestad and Ian Postlethwaite. *Multivariable feedback control: analysis and design*. Vol. 2. Wiley New York, 2007.

[34] John R. McLean and Errol R. Hoffmann. "Analysis of Drivers Control Movements". In: *Human Factors: The Journal of the Human Factors and Ergonomics Society* 13.5 (1971), pp. 407–418. DOI: 10.1177/001872087101300503.

[35] J. Vos. *Richtlijn Ontwerp Autosnelwegen 2017*. Tech. rep. Ministerie van Infrastructuur en Milieu, November 27, 2017.

[36] William F Milliken, Douglas L Milliken, et al. *Race car vehicle dynamics*. Vol. 400. Society of Automotive Engineers Warrendale, PA, 1995.

[37] Arash Farnam and Alain Sarlette. "Towards a comprehensive impossibility result for string stability". In: *IEEE Transactions on Automatic Control* (2019), pp. 1–1. DOI: 10.1109/tac.2019.2929967.

[38] P. Seiler, A. Pant, and K. Hedrick. "Disturbance Propagation in Vehicle Strings". In: *IEEE Transactions on Automatic Control* 49.10 (2004), pp. 1835–1841. DOI: 10.1109/tac.2004.835586.

[39] Richard J. Vaccaro. "An optimization approach to the pole-placement design of robust linear multivariable control systems". In: *2014 American Control Conference*. IEEE, 2014. DOI: 10.1109/acc.2014.6858987.

[40] M. Z. Mohd Tumari et al. "H-infinity with pole placement constraint in LMI region for a buck-converter driven DC motor". In: *2012 IEEE International Conference on Power and Energy (PECon)*. IEEE, 2012. DOI: 10.1109/pecon.2012.6450271.

[41] László Keviczky et al. In: *Control Engineering*. Széchenyi University Press, 2011. Chap. A-16.1, p. 444. ISBN: 978-963-9819-74-0. DOI: 10.1007/978-981-10-8297-9_1.

[42] Julio H. Braslavsky, Graham C. Goodwin, and Maria M. Seron. *Fundamental Limitations in Filtering and Control*. Springer London, September 17, 2011. 388 pp. ISBN: 144711244X. URL: https://www.ebook.de/de/product/19302330/julio_h_braslavsky_graham_c_goodwin_maria_m_seron_fundamental_limitations_in_filtering_and_control.html.